STUDIES IN STRONGLY CORRELATED SYSTEMS

By
SAURABH PRADHAN
PHYS08200805002

Harish-Chandra Research Institute, Allahabad

A thesis submitted to the
Board of Studies in Physical Sciences
In partial fulfillment of requirements
for the Degree of
DOCTOR OF PHILOSOPHY
of
HOMI BHABHA NATIONAL INSTITUTE

September, 2016

Homi Bhabha National Institute[1]

Recommendations of the Viva Voce Committee

As members of the Viva Voce Committee, we certify that we have read the dissertation prepared by Saurabh Pradhan entitled "Studies of Strongly Correlated Electron System" and recommend that it may be accepted as fulfilling the thesis requirement for the award of Degree of Doctor of Philosophy.

Chairman – Prof. Sumathi Rao	**Date:** 20/11/17
Convener – Prof. B. Ramakrishnan	**Date:** 20/11/17
Guide - Dr. G. V. Pai	**Date:** 20-11-2017
Examiner – Prof. Sankalpa Ghosh	**Date:** 20/11/2017
Member 1- Prof. Pinaki Majumdar	**Date:** 20/11/17
Member 2- Dr. Anirban Basu	**Date:** 20/11/17

Final approval and acceptance of this thesis is contingent upon the candidate's submission of the final copies of the thesis to HBNI.

I/We hereby certify that I/we have read this thesis prepared under my/our direction and recommend that it may be accepted as fulfilling the thesis requirement.

Date: 20-11-2017

Place: Allahabad

Dr. G. V. Pai
Guide

[1] This page is to be included only for final submission after successful completion of viva voce.

STATEMENT BY AUTHOR

This dissertation has been submitted in partial fulfillment of requirements for an advanced degree at Homi Bhabha National Institute (HBNI) and is deposited in the Library to be made available to borrowers under rules of the HBNI.

Brief quotations from this dissertation are allowable without special permission, provided that accurate acknowledgement of source is made. Requests for permission for extended quotation from or reproduction of this manuscript in whole or in part may be granted by the Competent Authority of HBNI when in his or her judgment the proposed use of the material is in the interests of scholarship. In all other instances, however, permission must be obtained from the author.

Saurabh Pradhan

Saurabh Pradhan

DECLARATION

I, hereby declare that the investigation presented in the thesis has been carried out by me. The work is original and has not been submitted earlier as a whole or in part for a degree / diploma at this or any other Institution / University.

Saurabh Pradhan

Name: Saurabh Pradhan
Enrolment No.: PHYS08200805002

List of Publications arising from the thesis

Journal

1. "Holstein-Hubbard model at half filling: A static auxiliary field study", Saurabh Pradhan and G. Venkesteswara Pai, *Phys. Rev. B,* **2015**, *92*, 165124

Communicated

1. "Effect of site dilution in the two-dimensional attractive Hubbard model", Saurabh Pradhan and G. Venkesteswara Pai, arXiv: 1511.00380

Other Publications not related to thesis

1. "Proximity induced superconductivity in Weyl semi-metals", Udit Khanna, Arijit Kundu, Saurabh Pradhan, and Sumathi Rao, *Phys. Rev. B*, **2014**, *90*, 195430.

2. "Transport and STM studies of hyperbolic surface states of topological insulators", Udit Khanna, Saurabh Pradhan, and Sumathi Rao, *Phys. Rev. B*, **2013**, *87*, 245411.

3. "Disorder overtakes Order in Information Concentration over Quantum Networks ", R. Prabhu, Saurabh Pradhan, Aditi Sen De, and Ujjwal Sen, *Phys. Rev. A*, **2011**, *84*, 042334.

Saurabh Pradhan

Dedicated to

My Family

ACKNOWLEDGEMENTS

I would like to thank all who supported me during my PhD in HRI. Especially, I want to express my gratitude to G. Venketeswara Pai for supervising this PhD thesis and introducing me to the fascinating field of condensed matter physics. I have greatly benefited from the collaborations with Prof. Pinaki Majumdar and Prof. Sumathi Rao. Additionally I would like to thank both of them for creating a beautiful research environment in HRI. Furthermore I would like to thank the members of the Condensed Matter group for various discussions and providing such a friendly and inspiring atmosphere. I gratefully acknowledge financial support by the Department of Atomic Energy, India.

I want to thank Prof. Asesh Krishna Datta, Prof. Sandhya Choubey,Prof Tapas Kumar Das, Prof. Raj Gandhi, Prof. Dileep Jatkar, Prof. Jasjeet Singh Bagla, Prof. Lakshmanan Sriramkumar, Prof. Ashoke Sen for teaching graduate courses.

I would like to thank all my friends Saurabh Niyogi, Ujjal Dey, Manoj Mandal, Dhiraj Hazra, Sanjoy Biswas, Sanjoy Dutta, Vivekananda Singh, Rajarshee Tiwari, Sourav Mitra, Arjun Bagchi, Arunabha Saha, Animesh Chatterjee, Sabyasachi Tarat, Akansha Singh, Joydeep Chakrabarty, Vikas Chauhan, Udit khanna, Sauri Bhattacharyya, Nabarun Chakrabarty, Titas Chanda, Arijit Dutta, Aritra Gupta, Abhishek Joshi, Samrat Kadge, Ajanta Maity, Mehedi Masud, Avijit Misra, Swapnamay Mondal,Dibya Kanti Mukherjee, Nyayabanta Swain, Atri Bhattacherjee. I would like to thank my family for all their love and encouragement and most of all for my loving, supportive, encouraging, and patient wife Sangeeta whose faithful support during the final stages of Ph.D. is so appreciated. Thank you.

CONTENTS

Synopsis

Strong correlations among active degrees of freedom, for example, electron-electron interaction and/or electron-phonon coupling, are characteristic features of many materials that have been explored in the last couple of decades. They often lead to new ground states and affect the response of the system at nonzero temperatures. Theoretical study of such systems is a difficult task since competing interactions and ordering tendencies are present and conventional perturbative approaches cannot be relied upon. Geometric frustration inherent in certain lattices and disorder that may be present bring in additional complexity. In this thesis we investigate two class of problems that involve correlation effects. The first one explores the competition between repulsive interaction among electrons and their coupling to the underlying lattice degrees of freedom. The second study dwells on the effect of randomly placed attractive centers that promote pairing and hence, superconductivity in an electronic system. After presenting a brief review of the physics of electron correlations, we introduce the models that have been explored and the methodology used in the second chapter. The next four chapters contain the original study carried out in this thesis. The concluding chapter has a critique on the limitations of the method used, suggestions for improvements, and discusses possible extensions of the present study.

Chapter I gives an overview of the physics of correlations and how they alter the physical properties of materials away from the behavior expected within "the non-interacting picture". The conventional framework of understanding electrons in solids relies on the appearance of energy bands and the notion of "renormalized quasiparticles" as described by the Fermi liquid theory. However, strong local Coulomb interactions present in narrow band metals can make the system insulating, for example, in a single-band model at half filling, freezing out the charge fluctuations. The resulting local moments develop effective interactions that can promote long-ranged magnetic order at low temperatures in most cases. On the contrary, an electron deforms the lattice it resides in and gets self-trapped in the resulting potential, thus forming a polaron. The electron-phonon coupling can also lead to insulating phases by promoting charge density modulations at certain commensurate fillings. An obvious question of interest is the compe-

tition between these two and how it affects the ground state and finite-temperature properties of the system. Certain lattices are geometrically frustrated, which affect the charge or spin order at low temperatures. Attractive interaction arising from electron-lattice coupling leads to a superconducting ground state that is well described, in the weak coupling regime, by the Bardeen-Cooper-Schrieffer (BCS) theory. However, as the strength of interaction increases, there is a striking separation between the pairing and superconducting energy scales resulting in a BCS-BEC crossover. The latter is a Bose-Einstein Condensate (BEC) of local fermion pairs. The Zeeman coupling of a magnetic field to spins promotes a modulated superconducting state, known in the literature as Fulde-Ferrel-Larkin-Ovchinnikov (FFLO) state. Further, the impurities present in materials alter the property of the superconducting state. The mean field BCS state survives at weak disorder. However, as disorder increases, the system becomes highly inhomogeneous and phase fluctuations play a dominant role. Often, a superconductor-insulator transition occurs especially in low dimensions. We discuss these broad notions and briefly review the existing theoretical work in these areas.

Chapter II introduces the models used in the present work to study two class of problems mentioned above. The repulsive Hubbard model captures the essential physics of strong local Coulomb interaction among electrons. The Holstein model describes the interaction of a single-band electron coupled to a single-mode Einstein phonon. The attractive Hubbard Hamiltonian is an effective model to understand the pairing of electrons, after the phonon degrees of freedom have been "integrated out". All these are many-body problems and understanding the resulting physics requires well-controlled methods that often have limitations. We introduce an approach in which electronic interaction is rewritten in terms of auxiliary fields coupled to electrons using the Hubbard-Stratanovich (HS) transformation and treat all auxiliary fields, as well as lattice degrees, as static. This results in a problem of investigating the quantum-mechanical dynamics of electrons coupled to classical auxiliary fields that are thermally fluctuating. The former can be explored by exactly diagonalizing the electron problem in a given classical background and classical configurations can be statistically sampled using the Monte Carlo estimation of their relative weights. A traveling cluster algorithm is used for computational efficiency and to extend the study to larger system sizes. The results obtained for these three models on a two-dimensional square lattice are used as benchmarks. They capture the weak-to-strong-coupling regimes of these models and incorporate thermal fluctuations which significantly modify the finite-temperature responses, both in spectral and transport properties. The method is intrinsically real-space based, which helps us visualize the nature of the phases and transitions among them.

In **Chapter III**, we study the Holstein-Hubbard model at half filling on a two-dimensional square lattice using the method mentioned in the previous chapter. This model captures the essential physics of strong local Coulomb interactions among electrons in a single-band system that are also coupled to a single-mode Einstein phonon. When the former interaction dom-

inates, the ground state transforms from a spin density wave arising due to Slater instability to a Mott insulating Néel state, while at higher temperatures above the magnetic transition, from a paramagnetic metal to a paramagnetic Mott insulator. When the latter dominates, the ground state crosses over from a charge density wave resulting from Peierls instability to a charge-ordered state that evolves to a bipolaron-ordered insulator at strong couplings. Above the ordering temperature, there is a metal-to-insulator transformation with an intervening "pseudogap phase" that originates from short-ranged fluctuations of the relevant degrees of freedom, magnetic moments in the former and charges in the latter. When both interactions are present, a nonmagnetic metallic ground state appears at weak couplings since these interactions frustrate different degrees of freedom, namely, the charge and spin channels, and prohibit exclusive ordering of either of them. Thermodynamics of these phase transformations is presented along with real-space features. Spectral and transport properties are studied in detail; signatures of the pseudogap phase appear as non-Drude response in optical conductivity. **Chapter IV** explores the influence of lattice geometry on the ordered phases in the Holstein-Hubbard model. In particular, as an example of a geometrically frustrated lattice, we consider the two-dimensional triangular lattice. Absence of nesting at half filling gives rise to a metallic ground state at weak couplings, unlike in a square lattice. In the insulating phases, both charge and spin degrees order at a wave vector different from that is observed in the square lattice. We explore the change in ordering wave vector as the square lattice is smoothly transformed to a triangular one. Pseudogap features dominate the finite-temperature phase diagram near the metal-insulator transition. These are also reflected in the momentum dependence of the electronic spectral functions.

.

The next two chapters investigate two-dimensional lattice electron systems that have randomly placed attractive centers, whose density can be tuned to obtain a putative percolation transition to a superconducting ground state. An interplay of interaction, disorder, and phase fluctuations of the superconducting (SC) order parameter is expected to give rise to rich physics. We decompose the attractive interaction into charge and pairing fields coupled to electrons using the HS transformation. At the saddle-point level, this reproduces the Bogoliubov-de Gennes phenomenology. In **Chapter V**, we study the site-diluted attractive Hubbard model with a metallic host. We find that there is a critical density of attractive centers needed to establish globally phase-coherent superconductivity. The critical density appears to saturate as interaction increases. At larger densities that support SC ground state, the system undergoes a BCS-BEC crossover as interaction strength increases. Thermal phase fluctuations play a dominant role in driving the transition at moderate dilution and in the BCS-BEC crossover at low dilution. The finite temperature phase has pseudogap features originating from amplitude inhomogeneities of the SC order parameter and characteristic non-Drude response in optical conductivity. **Chapter VI** presents some preliminary studies on the nature of this percolative transition in an insulating host and a metallic host with imbalanced electron spins. In the former case, there is a charge density wave (CDW) instability both in the limit of perfect dilution and attractive centers present at all sites. Thus, the SC state competes with CDW when all sites have attractive centers, resulting in a charge-modulated insulator, and signaling a BCS-BEC-CDW crossover as dilution reduces.

In the concluding **Chapter VII**, we first discuss the approximations used in the methodology adopted to investigate the problems. While the method takes into account thermal fluctuations of auxiliary fields in both the problems and phonons in the first one, quantum fluctuations are neglected. Thus, the present approach should be considered in the spirit of spin wave theory as applied to magnetic systems. An obvious way of including corrections is to retain fluctua-

tions at the Gaussian level and study the stability of the phases and how these fluctuations affect the low-temperature thermal, spectral, and transport properties. Such a procedure is yet to be explored and we leave it for future work. Possible applications and/or extensions of the study include keeping multiorbital nature of the underlying electron system that, in principle, may be coupled to multiphonon modes, investigating frustrated, three-dimensional systems, and exploring heterostructures or interfaces of correlated systems and correlated phenomena in topological systems.

List of Figures

Chapter 1

Introduction

1.1 Band Theory of Solids

The application quantum mechanics to electrons in solids was first introduced by Sommerfeld[1]. It was assumed that all the valence electrons are free, thereby neglecting both electron-electron and electron lattice interaction in the model. These two interactions are the main subject of this thesis. Free-electron theory successfully explained the small heat capacity and magnetic susceptibility of metals. At finite temperature the number of electrons contributing to thermal or transport properties proportional to k_BT/E_F where E_F is the Fermi energy. Thus, for example, the specific heat is order of k_BT/E_F.

There are many atomic orbitals within a solid and they will overlap with each other. If we start with N number of atomic levels then there will $N/2$ molecular orbitals, half of them having lower energy and the other half a higher energy, compared to the atomic energies. The energy separation between "molecular levels" decrease as atoms come closer and in a solid, these energy levels for a quasi-continuous spectrum. This is called an energy band. Though this is a reasonable assumption, we should keep in mind that there are very narrowly spaced energy

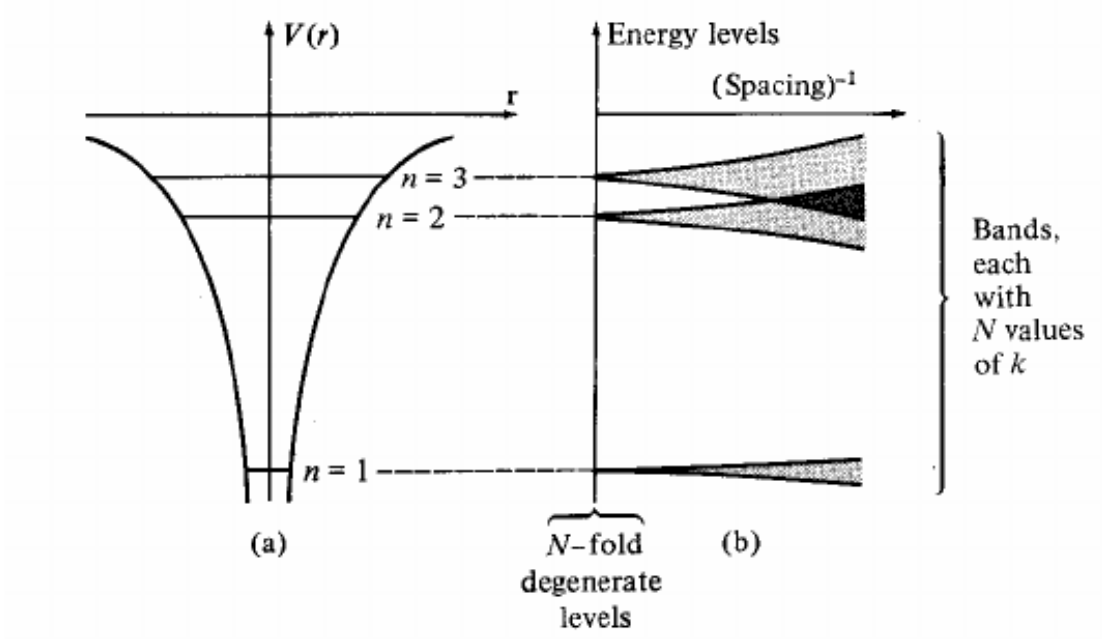

Figure 1.1: (a) Schematic representation of nondegenerate (neglecting spin) electronic levels in an atomic potential. (b) The energy levels of N such atoms in a periodic array, plotted as a function of mean inverse interatomic spacing. Then the atoms are far apart the energy levels are nearly degenerate but when the atoms are closer together, the levels broaden into bands.

levels. The spread between the maximum and minimum energies within a band is called the bandwidth W.

The formation of energy bands is illustrated schematically in Fig[1.1]. There exists a sharp distinction between a metal and an insulator in band theory. A material with one or more partially filled bands becomes metal. At zero temperature electrons are filled up to a maximum energy known as the Fermi energy E_F and the higher energy states are completely empty. Electrons are free to move to the empty higher energy states and conduct across the sample when an electric field is applied. Standard examples are Alkali metals in the periodic table (Li, Na, K, Rb, Cs). However, on the other hand in an insulator (or semiconductor), lower energy bands are completely occupied and other higher energy bands are unoccupied. There is also an energy gap (E_g) between the occupied and unoccupied bands. Hence the density of states $N(E)$ at the Fermi energy is zero. Fig[1.2] shows density of states of a typical metal and

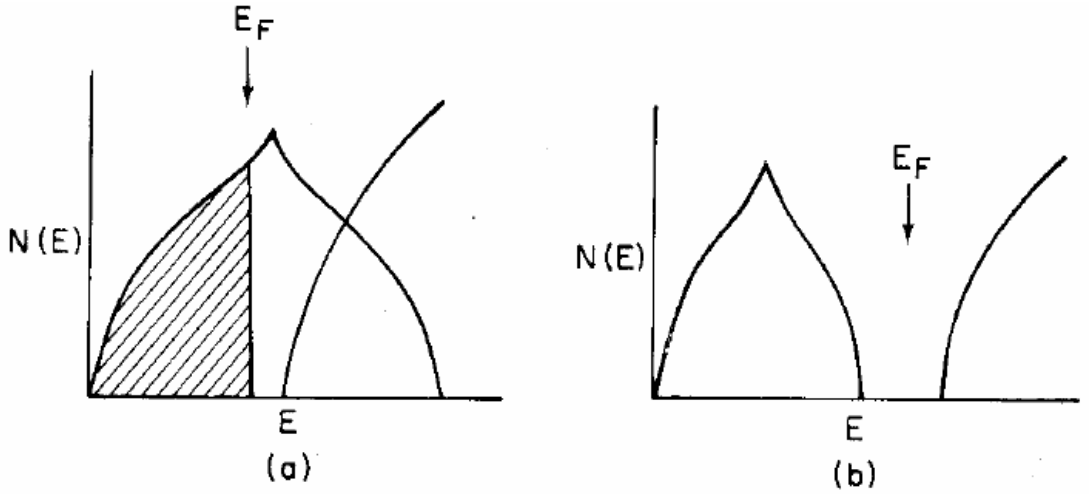

Figure 1.2: The electronic density of states $N(E)$ in a cubic crystalline material where E_F denotes the Fermi energy for (a) a normal metal and (b) an insulator.

an insulator. The highest occupied band is called the *valence band* and lowest empty band is named the *conduction band*. If the band gap (E_g) is much smaller than the bandwidth, conventionally the material is called a semiconductor and when E_g is of the order of W, it is named a band insulator. In both cases, electrical transport is exponentially suppressed for small applied voltage when temperature $T \ll E_g/k_B$. Examples include carbon (in the diamond allotropic form) and *Si* and *Ge* (conventionally called semiconductors). One should keep in mind that the above picture assumes that the lattice is static and provides only a background periodic potential to the electrons. It also assumes that is no interaction among electrons, or at best, is treated in an average way . Band theory of independent electrons fails when there is considerable interaction amongst the electrons.

One of the earliest theory of transport of metal was give by Drude- Sommerfeld model[2], where electrons are assumed to be objects moving, mostly freely, through the lattice of static ionic charges. Conductivity of these system is limited by the scattering of the electrons with imperfections. In a clean system inelastic scattering happens due to the thermal fluctuation of

the lattice vibration. Lattice defects, vacancies, grain boundaries will contribute to the elastic scattering processes. Conductivity within Drude Model is given by

$$\sigma = \frac{ne^2\tau}{m} \tag{1.1}$$

where n m, τ are the carrier density, mass of electrons and the scattering rate. This model applies to many materials even though it assumes that the electron follow classical trajectory and electron-electron interaction is neglected. A rationalisation of this observed behavior underpins in the Landau Fermi liquid theory which proposes that weakly interacting particle states can be mapped on to a system of non-interacting quasiparticles. These quasiparticle have same charge as electron but have a effective mass different from the bare mass of the electron. It is also evident from the above equation that with increasing disorder resistivity increases.

The mean free path of electron is $l = v_F\tau$ where v_F is the Fermi velocity. Carrier density (n) is related to the Fermi velocity and for a three dimensional free electron system it is given by $n = k_F^3/3\pi^2$. We can rewrite the conductivity equation as

$$\sigma_{3D} = \frac{e^2}{3\pi^2\hbar}k_F^2 l \tag{1.2}$$

In the large disorder limit where mean free path approaches lattice spacing, *i. e.,* $k_F l \sim 1$. Due to strong scattering, electrons are not able to travel a full wavelength before they get scattered off. This sets the condition for the applicability of the Drude formula, *i.e.,* $k_F l \gg 1$.

The absence of metallic state in a strongly disordered medium was first proposed by Anderson[3]. The scaling theory of localization [4] successfully gave the theory of disorder induced metal to insulator transition (MIT). This was based on an earlier theoretical advances by Thouless[5]. Let us consider a system composed of hypercubes of size L and dimension D. The mean energy

level spacing (δ_L) of this block is inversely proportional to the density of state $N_L(E)$. The energy scale associated with the lifetime of an electron to stay within a particular block of length L is $E_L = \hbar/\tau_L$. Thouless suggested that electrical conductance can be written as

$$g = \frac{E_L}{\delta_L} \tag{1.3}$$

In a metallic system blocks are well coupled and $g \gg 1$. On the other hand in a insulator states are localized and τ_L become very large so $g \ll 1$. Thouless argued that in infinite 1D systems and in infinite wires with finite thickness electronic states always localise. Abrahams *et al.*[4] studied how g scales with L in the metallic and insulating region. Weakly disordered system is expected to obey the Ohm's law with $(g) \propto L^{D-2}$. Electronic states in a disordered insulator are exponentially localized with $g \propto \exp(-L/\zeta)$ where ζ is the localization length. The universal β function can be defined as

$$\beta = \frac{d\ln g}{d\ln L} = \begin{cases} D-2 & \text{for } g \gg 1 \\ const. + \ln g & \text{for } g \ll 1 \end{cases} \tag{1.4}$$

For large systems, there are two different regimes, namely, $\beta > 0$(metallic) and $\beta < 0$ (insulator). It is evident from the above equation that a metallic state does not exist for $1D$ and $2D$ system. However, in 3D, the system undergoes a metal-insulator transition at critical value of $g = g_c$ as g increases. This is an example of a quantum critical point.

1.1.1 Landau's Theory of Fermi Liquids

Landau Fermi liquid theory is based on the idea of quasiparticles. As the interaction is turned on, single particle free electron states evolve into fully interacting state. Landau assumed that interacting states are adiabatically connected to free electron states, *i.e.,* there is a one-to-one mapping between these states. This implies that each interacting state can be characterized by

momentum **k** and spin σ as it was done for the free electrons.

The momentum distribution of the quasiparticles is given by $n_\sigma(k)$. In the absence of interactions, this momentum distribution is reduced to the Fermi-Dirac distribution. At zero temperature, the Fermi-Dirac distribution is a step-function :

$$n^0_\sigma(k) = \Theta(k_F - k) \tag{1.5}$$

The quasiparticle distribution can be thought of as a small deviation from the noninteracting distribution.

$$n_\sigma(k) = n^0_\sigma(k) + \delta n_\sigma(k) \tag{1.6}$$

In terms of this distribution function we can write energy functional as

$$E = E_0 + \sum_{k,\sigma} \varepsilon_\sigma(k)\delta n_\sigma(k) + \frac{1}{2\Omega}\sum_{k,k',\sigma,\sigma'} f_{\sigma\sigma'}(k,k')\delta n_\sigma(k)\delta n_{\sigma'}(k') \tag{1.7}$$

E_0 is the ground state energy in the absence of interaction. $\varepsilon_\sigma(k)$ and $f_{\sigma\sigma'}(k,k')$ are variational parameters which have to be determined experimentally. The effective energy momentum relation is obtained by taking the variational derivative.

$$\tilde{\varepsilon}_\sigma(k) = \frac{\delta E}{\delta n_\sigma(k)} = \varepsilon_\sigma(k) + \frac{1}{\Omega}\sum_{k',\sigma'} f_{\sigma\sigma'}(k,k')\delta n_{\sigma'}(k') \tag{1.8}$$

The second derivative defines the coupling amongst the quasiparticles ,

$$\frac{\delta^2 E}{\delta n_\sigma(k)\delta n_{\sigma'}(k')} = \frac{1}{\Omega}\sum_{k',\sigma'} f_{\sigma\sigma'}(k,k') \tag{1.9}$$

Further we will assume a spherical symmetry of the Fermi surface and consider quasiparticles very near to the Fermi surface. We can decompose the $f_{\sigma\sigma'}(k,k')$ into a symmetric and an anti-symmetric part and then these can be further expanded using Legendre-polynomials .

$$f_{\sigma\sigma'}(k,k') = f^s(k,k') + \sigma\sigma' f^a(k,k') \tag{1.10}$$

$$f^{s,a}(k,k') = \sum_{l=0}^{\infty} f_l^{s,a} P_l(\cos\theta_{k,k'}) \tag{1.11}$$

$\theta_{k,k'}$ is the angle between momenta k and k'. The density of states at the Fermi surface is defined as

$$N(\varepsilon_F) = \frac{2}{\Omega}\sum_k \delta(\varepsilon(k) - \varepsilon_F) = \frac{k_F^2}{\pi^2\hbar v_F} = \frac{m^* k_F}{\pi^2\hbar^2} \tag{1.12}$$

Near the Fermi surface, variation of $\varepsilon(k)$ can be described by an effective mass (m^*).

$$\nabla_k \varepsilon(k)|_{k_F} = v_F = \frac{\hbar k_F}{m^*} \tag{1.13}$$

We can redefine the Landau parameters as

$$F_l^s = N(\varepsilon_F) f_l^s, \tag{1.14}$$

$$F_l^a = N(\varepsilon_F) f_l^a, \tag{1.15}$$

Now we will relate these Landau parameters to experimentally measurable quantities such as

specific heat. The finite temperature Fermi distribution function is

$$n_\sigma(k) = \frac{1}{e^{[\varepsilon(k)-\varepsilon_F]/k_BT}+1} \tag{1.16}$$

The entropy of Fermi gas can be calculated from the distribution function

$$S = -\frac{k_B}{\Omega}\sum_{k,\sigma}\Big[n_\sigma(k)\ln(n_\sigma(k)) + (1-n_\sigma(k))\ln(1-n_\sigma(k))\Big] \tag{1.17}$$

The specific heat is obtained by

$$C(T) = T\frac{\partial S}{\partial T} \simeq \frac{\pi^2 k_B^2 N(\varepsilon_F)}{3}T \tag{1.18}$$

This is the well known linear behavior of specific heat $C(T) = \gamma T$ with $\gamma = \pi^2 k_B^2 N(\varepsilon_F)/3$. Measuring specific heat would directly give effective mass (m^*) as $N_F = m^* k_F/\pi^2\hbar^2$. Using Galilean invariance we can find

$$\frac{m^*}{m} = 1 + \frac{1}{3}F_1^s \tag{1.19}$$

Similarly we can calculate the compressibility (κ) and spin susceptibility (χ) as

$$\frac{\kappa}{\kappa_0} = \frac{m^*}{m}\frac{1}{1+F_0^s} \tag{1.20}$$

$$\frac{\chi}{\chi_0} = \frac{m^*}{m}\frac{1}{1+F_0^a} \tag{1.21}$$

1.1.2 Failures of the non-interacting theory

Fermi liquid theory gives a quasiparticle theory of interacting electron system. These are weakly interacting quasiparticles characterized by several Landau parameters, as we have described in

the previous section. However, the validity of this theory is not limited to the weak interaction, *per se*. Heavy fermion systems such as $CeAl_3$, UBe_{13} have effective masses of the order of 100 to 1000 times the bare electron mass and the Fermi liquid theory is still found to be valid in the low temperature regime.

Landau theory of Fermi liquid breaks down when physical properties such as specific heat, compressibility and spin susceptibility diverge. In most of the cases degeneracy leads to large low energy fluctuations. These collective modes are characterized by angular momentum l and the condition for the instability is $F_l^{s,a} \leqslant -(2l+1)$. Fermi liquid theory also fails to describe system which have instability at some characteristic wave-vector. Examples of such instability, especially in low dimensions, are charge-density wave (CDW) and spin density wave (SDW). Usually such instabilities are easily captured within RPA and/or $t-$matrix calculation.

There is a temperature scale below which the Fermi liquid theory is valid in strongly correlated metals. The "coherence temperature" T^* below which the theory applies is inversely proportional to the effective mass enhancement (m^*/m). This temperature scale is much smaller than the Fermi energies in a strongly interacting system. A classic example is the Kondo systems having diluted magnetic impurities in a metal, where the coherence temperature is called the Kondo temperature. Above this temperature (T^*) all the physical quantities are dominated by incoherent electron-electron scattering and the quasiparticle description of Fermi liquid theory becomes invalid. In many heavy fermion systems, T^* is of the order of $10-100K$.

Another class of materials where a clear departure from the Fermi liquid theory is seen, are

materials close to Mott transition. These include transition metal oxides $(V_{1-x}Cr_x)_2O_3$, chalcogenides $NiS_{2-x}Se_x$[6], and two dimensional organic materials $\kappa-(BEDT-TTF)_2Cu[N(CN)_2]Cl$[7]. These materials can be driven across the Mott transition by applying pressure. On the metallic side, resistivity shows a T^2 behaviour below a crossover temperature $T^* \approx 50K$. Above this temperature, the system shows an insulating behaviour. This clearly indicates the destruction of quasiparticles by inelastic scattering.

In doped semiconductors, we see a temperature dependence of the form [8, 9]

$$\sigma(T) = \sigma_0 + m\sqrt{T} \tag{1.22}$$

where m and σ_0 depend on the carrier concentration n. As the carrier concentration varies, it shows a metal-insulator transition and near the transition the zero temperature conductivity shows a critical behavior[8–10].

$$\sigma(T \to 0) \approx (n - n_c)^{\mu} \tag{1.23}$$

where the exponent $\mu \approx 0.50$ in most materials.

A Fermi liquid state cannot be adiabatically connected to a Mott insulating state which is the result of strong electron-electron interaction. Electron-phonon interaction could lead to polaron formation or superconductivity which are beyond the scope of Fermi liquid theory.

1.2 Electron-electron interaction

There are many condensed matter systems where single particle approaches fail to describe the underlying physics. Local Coulomb repulsion among the electrons is an important ingredient in these materials. Density Functional Theory is very successful in describing metals which have delocalized bands such as s or p. However, it fails to describe electrons which live in localized

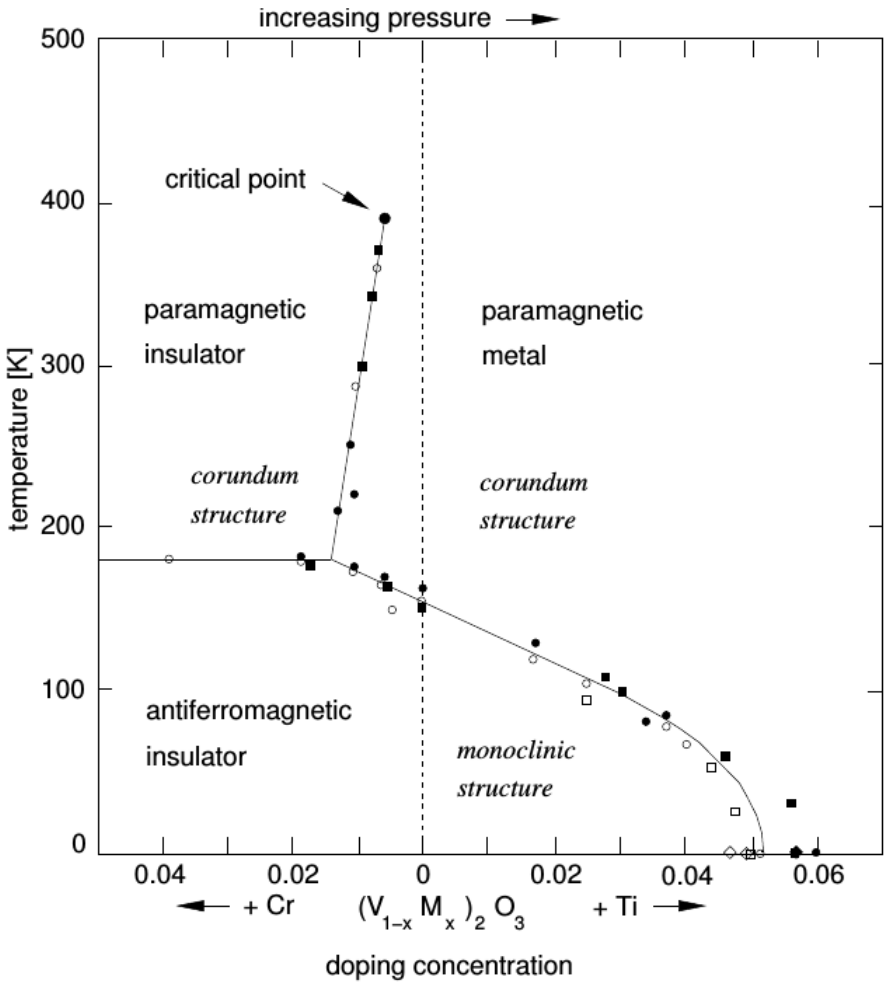

Figure 1.3: Phase diagram of V_2O_3 showing the MIT as a function of pressure and of doping with Cr and Ti[11].

bands. Transition metals such vanadium, iron and their oxides are some examples. Interaction among electrons is very strong in these materials as the conduction band is very narrow.

The simplest model to describe the band formation and localization in the second quantized language is the Hubbard model. Despite the fact that it is a very simplified model, it is very hard to solve. An exact solution of this model is known only for certain limiting cases. One of these is the large coordination limit where the dynamical mean-field theory (DMFT) becomes exact.

1.2.1 Metal-insulator transition and the Hubbard Model

Materials such as NiO, CrO_2 or V_2O_3 and the CuO_2 planes in the cuprates have been studied qualitatively using the Hubbard model. One of the common properties of these material is that the ground state is an antiferromagnetic insulator, and remains insulating even in the high temperature spin disordered paramagnetic phase. In addition to this, they may show a metal-insulator transition (MIT) as chemical composition, pressure or other control parameters changes[6]. In these materials, MIT is unexpected as in most of these the conduction band is partially filled and according to band theory they should be metallic. It is also found within density functional calculation that these materials are metallic. Figure [1.3] shows the phase diagram of V_2O_3 as a function of pressure and doping with Cr and Ti atoms. The antiferromagnetic phase at low temperature and the paramagnetic phase at temperature are seen in the phase diagram. All the transitions shown here are first order. The paramagnetic insulating phase is believed to be the Mott-Hubbard Insulator and this is a result of strong correlation. Therefore we need to describe the effect of Coulomb interactions more accurately.

Free electron theory predicts a material with odd number of electrons per unit cell will be a metallic system. As the lattice spacing decreases bands becomes narrower but it should remain as metal. During electrical conduction process electron will try to hop from one site to other site and more than one electron may occupy the same site. This will cost a Coulomb repulsion energy. In a typical narrow band system this Coulomb energy $(\sim 1-10eV)$ scale is much higher than the band width. Due to this large energy barrier charge fluctuations will be restricted (or almost completely forbidden) and it will be insulator as the band width decreases. This is a prototype Mott transition where a MIT occurs due to electron correlation effects. We will models such systems at the simplest level by adopting the Hubbard model where electron kinetic effects are considered within the tight binding approximation and Coulomb interaction

is considered to be local.

The single band Hubbard model is [12–14]

$$H = \sum_{\langle ij\rangle\sigma} t_{ij} c^{\dagger}_{i\sigma} c_{j\sigma} + U \sum_{i} n_{i\uparrow} n_{i\downarrow} - \mu \sum_{i\sigma} n_{i\sigma} \tag{1.24}$$

The first term describes the hopping of electrons from a lattice site i to a site j. The operators $c_{i\sigma}(c^{\dagger}_{i\sigma})$ are the standard fermionic annihilation (creation) operators of electrons at a site i with spin σ. The sum $\langle ij\rangle$ is restricted to nearest neighbors *i,e.,* t_{ij} takes a value $-t$ only when the sites i and j are nearest neighbors. Otherwise, it is equal to zero. $n_{i\sigma}$ is the number operator for an electron with spin σ at site i. As there is no orbital degeneracy, at most two electrons with opposite spin can occupy the same site. Second term of the above Hamiltonian says electrons have to pay an energy U if two of them with opposite spins inhabit the same site. We will consider this model on a two dimensional lattice and assume the lattice spacing to be unity.

Attractive *vs.* **repulsive Hubbard models**

If we perform a particle-hole transformation only for the spin down operator,

$$c_{i\downarrow} \rightarrow (-1)^{\mathbf{r}_i} c^{\dagger}_{i\downarrow}, \qquad c^{\dagger}_{i\downarrow} \rightarrow (-1)^{\mathbf{r}_i} c_{i\downarrow} \tag{1.25}$$

the Hamiltonian changes to

$$H(t,U,\mu) \rightarrow H(t,-U,-U/2) - (\mu - U/2) \sum_{i} (n_{i\uparrow} - n_{i\downarrow}) - \mu N \tag{1.26}$$

If the starting Hamiltonian is an attractive model ($U < 0$) then the transformed Hamiltonian is a repulsive model with a magnetic field $\mu + |U|/2$ along the $z-$axis. At half-filling, the chemical potential is $\mu = U/2$, so the magnetic field vanishes. Thus the attractive Hubbard Model is exactly mapped on to the repulsive one at half filling.

The local limit t = 0

In the absence of kinetic energy of the electron (when hopping $t \to 0$) the Hamiltonian reduces to

$$H_U = \sum_i \Big[U n_{i\uparrow} n_{i\downarrow} - \mu (n_{i\uparrow} + n_{i\downarrow}) \Big] \tag{1.27}$$

Every site is independent and decoupled from the rest of the lattice. The Hilbert space of the resulting single site problem contain four states: empty state $|0\rangle$ (energy $\varepsilon_0 = 0$), singly occupied states $|\sigma\rangle$ (energy $\varepsilon_\sigma = -\mu$) and doubly occupied state $|\uparrow\downarrow\rangle$ (energy $\varepsilon_{\uparrow\downarrow} = U - 2\mu$). The single particle Green's function which is defined as $G_\sigma(\tau) = -\langle T_\tau c_{i\sigma}(\tau) c^\dagger_{i\sigma}(0)\rangle$ is also a local quantity and it is given by

$$G_\sigma(i\omega_n) = \frac{1 - n_{\bar{\sigma}}}{i\omega_n + \mu} + \frac{n_{\bar{\sigma}}}{i\omega_n + \mu - U} \tag{1.28}$$

where

$$n_\sigma = \frac{1}{Z}(e^{\beta\mu} + e^{-\beta(U-2\mu)}) \tag{1.29}$$

Here, Z is the partition function of the system. The two pole structure of the single particle green function affords a simple physical interpretation. The pole at $\omega = U - \mu$ (with $i\omega_n \to \omega + i0^+$) corresponds to the excitation energy for the transition $|\sigma\rangle \Leftrightarrow |\uparrow\downarrow\rangle$ .The residue

$n_{\bar{\sigma}}$ give the probability either the site is occupied by a fermion with spin $\bar{\sigma}$ or double occupied. The other pole at $\omega = -\mu$ correspond to transition $|0\rangle \Leftrightarrow |\sigma\rangle$ and the residue $1 - n_{\bar{\sigma}}$ give the probability for either site is empty or occupied by the spin$-\sigma$ fermion.

The single particle Green's function $G_\sigma(i\omega_n)$ has a very nontrivial structure. It does not have any quasiparticle pole at $\omega = 0$ unless $\mu = 0$ or U. Perturbation theory in U is not a good starting point in the limit $t = 0$. For the half filling case $n_\sigma = 1/2$ and $\mu = U/2$, the Green's function can be written as $G_\sigma(i\omega_n) = [i\omega_n + \mu - \Sigma(i\omega_n)]^{-1}$ with a self energy

$$\Sigma(i\omega_n) = \frac{U}{2} + \frac{U^2}{4i\omega_n} \tag{1.30}$$

This self energy has a singular contribution in the low frequency region for finite U and it is hard to capture this kind of behavior within perturbation theory. The spectral function $A(\omega) = -\frac{1}{\pi} ImG(\omega)$ consists of two delta functions at $\omega = \pm U/2$ and these two peaks are well separated by a gap U. For finite t, $(t/U \ll 1)$ we expect that these two peak will broaden, but there will be a finite gap. The corresponding split bands are known as lower and upper Hubbard bands. For $U >> W$, these are well separated and at half filling the lower would be filled up completely, leaving an empty upper Hubbard band and, hence an insulator which band theory would not be able to capture.

1.2.2 Slater instability and antiferromagnetism

The antiferromagnetism on a bipartite lattice can arise quite naturally at certain fillings. The presence of an onsite Coulomb repulsion makes spin up and spin down electron interact repulsively. So the spins alternate themselves on the neighbouring sites at half filling. This gives rise to an ordering wave-vector $Q = (\pi, \pi)$. The amplitude of this spin density wave is very small in the weak coupling region $U \ll t$, *i.e.* $|\langle S_i \rangle| \ll 1$. This weak coupling antiferromagnetic state is

referred as Slater antiferromagnet.

We will try to capture the resulting physics this model using the Hartree-Fock (HF) theory. Within this approximation, the Hamiltonian can be written as

$$H_{HF} = -t \sum_{\langle ij \rangle \sigma} c^{\dagger}_{i\sigma} c_{j\sigma} + U \sum_{i} \Big(n_{i\uparrow} \langle n_{i\downarrow} \rangle + n_{i\downarrow} \langle n_{i\uparrow} \rangle - \langle n_{i\uparrow} \rangle \langle n_{i\downarrow} \rangle \Big) - \mu \sum_{i} (n_{i\uparrow} + n_{i\downarrow}) \tag{1.31}$$

For the half-filled case we will assume a variational solution for the $\langle n_{i\sigma} \rangle$ as

$$\langle n_{i\uparrow} \rangle = n + (-1)^{\mathbf{r}_i} m, \qquad \langle n_{i\downarrow} \rangle = n - (-1)^{\mathbf{r}_i} m \tag{1.32}$$

At zero temperature we get a self-consistent equation for m,

$$1 = \frac{U}{4\pi^2} \int d^2k \frac{1}{(\varepsilon_k^2 + \Delta^2)^{1/2}} \tag{1.33}$$

where $\Delta = Um$ and $\varepsilon_k = -2t(\cos k_x + \cos k_y) - \mu$. The above equation for m has a solution $m \neq 0$ for any finite value of U due to nesting of the Fermi surface. In terms of density of states $\rho(\varepsilon)$, the above equation can be written as

$$1 = U \int d\varepsilon \frac{\rho(\varepsilon)}{(\varepsilon^2 + \Delta^2)^{1/2}} \tag{1.34}$$

For two dimensional case the solution is given by

$$\Delta \approx t e^{-2\pi\sqrt{t/U}} \tag{1.35}$$

The spectrum of this system is given by

$$E_k = \sqrt{\varepsilon_k^2 + \Delta^2} \tag{1.36}$$

Electronic density of state has a gap $\Delta = min_k E_k$ and it is insulating. The origin of this insulating state is the spin density wave thus formed which leads to additional Bragg reflections resulting in the opening up of a gap. The Hartree-Fock antiferromagnetic transition temperature is given by

$$T_N^{HF} \approx te^{-2\pi\sqrt{t/U}} \tag{1.37}$$

As U increases, T_N^{HF} also increases very rapidly.

1.2.3 Strong coupling limit and the Heisenberg model

In the strong coupling limit (when $U >> W$), one could start from a single site problem and explore the physics perturbatively in t. At half filling and for large U, this is an insulator and double occupancy is strictly forbidden. Thus the charge degrees are frozen out. The remaining spins degrees develop a short ranged antiferromagnetic interaction. The higher energy excitations can be projected out by a canonical transformation[15, 16]. We will get an effective Hamiltonian using this transformation where the Hilbert space is restricted to only single occupied states. The effective Hamiltonian is called $t-J$ model which is given by

$$H_{eff} = -t \sum_{\langle ij\rangle\sigma} \tilde{c}_{i\sigma}^{\dagger}\tilde{c}_{j\sigma} + J\sum_{\langle ij\rangle}\left(\mathbf{S}_i.\mathbf{S}_j - \frac{1}{4}\tilde{n}_i\tilde{n}_j\right) \tag{1.38}$$

where the fermionic operator $\tilde{c}_{i\sigma}$ is defined as $\tilde{c}_{i\sigma} = (1-n_{i\bar{\sigma}})c_{i\sigma}$. The second term of this effective Hamiltonian acts only when double occupancy is completely forbidden.

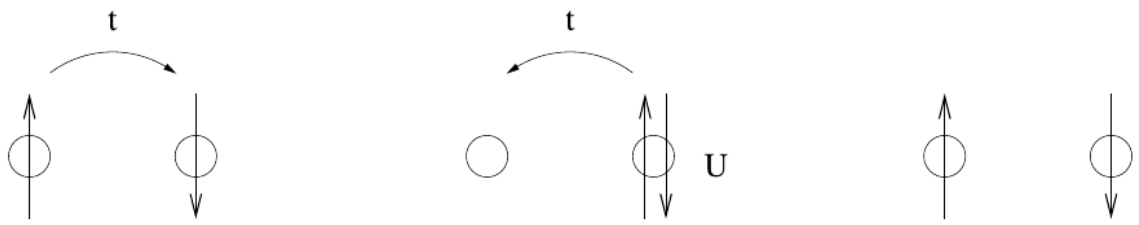

Figure 1.4: Antiferromagnetic exchange process in the t-J model.

The exchange processes are shown in the Figure[1.4]. Electrons can hop from one site to other if the spins are antiparallel to each other. This way antiferromagnetic correlations emerge. The aforementioned canonical transformation also produces higher order hopping terms which involve more than two sites. We have neglected those terms because it is very difficult to deal with them and these terms have contribution which are higher order of t/U. So in the large U limit higher order hopping processes have a negligible effect. Within second order perturbation theory, the exchange coupling becomes $J = 4t^2/U$.

First term of the effective Hamiltonian vanishes at half filling as it will involve double occupancy. The effective Hamiltonian is reduced to a Heisenberg model.

$$H = J \sum_{\langle ij \rangle} \mathbf{S}_i . \mathbf{S}_j \tag{1.39}$$

1.2.4 Metal Insulator transition and the Dynamical Mean Field Theory

Non-perturbative approaches are necessary for the understanding of the many-body physics of Hubbard Model. Exact solution of this model exists only in one dimension[17]. Dynamical Mean Field theory (DMFT) gave a full description of this model[18] within a controlled approximation. Before DMFT, perturbative approaches were tried in the weak and strong coupling region. Though these approaches were incomplete, they gave important physical insights and described how the transition is reached from the two sides.

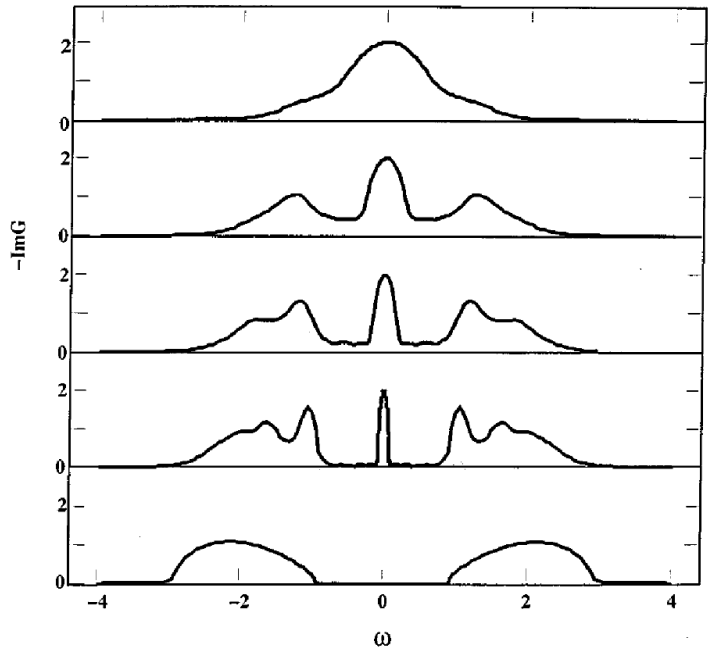

Figure 1.5: Density of states of the Hubbard model as computed in DMFT[18]. From top to bottom: evolution of the DOS for metallic solutions with increasing U , with the development of quasiparticle peak and high-energy incoherent bands, and characteristic DOS of the insulating phase (last panel).

Hubbard himself[19] first gave a physical explanation of the strong coupling physics. There will two bands in the very large U limit centered around $\pm U/2$ with a bandwidth W, as discussed in the previous subsection. The lower and upper bands are associated with holes and doubly-occupied sites respectively. These two bands have a gap $\approx U - W$ and as U decreases this gap also decreases and vanishes at $U \approx W$. Disappearance of the gap indicates an insulator to metal transition.

Brinkman and Rice[20] proposed a different theory for the Metal Insulator transition. They approached the MIT from the metallic side. They projected out the doubly occupied sites to

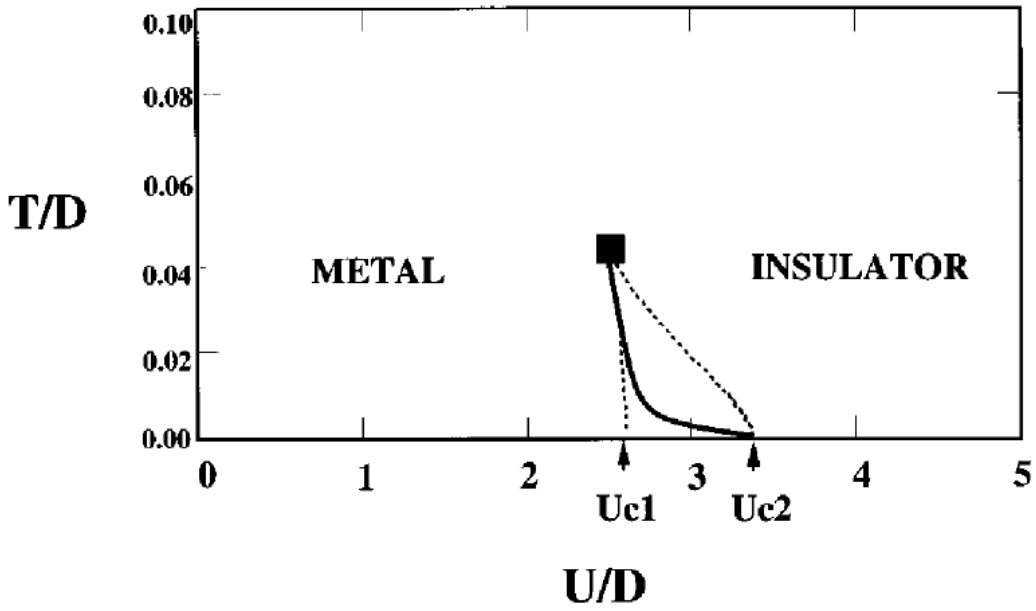

Figure 1.6: Phase diagram in the $U-T$ space for the single-band Hubbard model[[18]]. Dotted lines enclose a region in which metallic and insulating solutions coexist, solid line represents the first-order metal-insulator transition, which ends in two second-order critical points.

describe the metallic phase which is a renormalized Fermi liquid with a mean field double occurrence $d = \langle n_{i\uparrow} n_{i\downarrow} \rangle$. Double occupancy gives an energy cost of the order of U so as U increases d decreases and at some critical $U = U_{BR}$, d becomes zero. Effective mass of the quasiparticle diverges near the transition , $m^*/m \propto (U_{BR} - U)^{-1}$.

Dynamical mean field theory integrated these two limiting pictures. DMFT substitutes the original problem to a single site problem where that site is self-consistently coupled to an effective medium. This is in the same spirit as classical mean field theory (or, for that matter, Hartree-Fock theory) where one neglects spatial fluctuations. However, in DMFT the quantum fluctuations are kept in an exact way. Thus, DMFT gives a unique nonperturbative way of treating metallic and insulating phase. Fig.[1.5] shows Density of state(DOS) computed within Dynamical Mean Field Theory in the half-filled paramagnetic phase. As suggested by

Hubbard, there are two bands in the strong coupling region centered around $\pm U/2$ and they are called upper and lower Hubbard bands. The gap between these two bands decreases as U decreases and vanishes at $U = U_{c1}$. On the other hand starting from the metallic side, DOS develops a quasiparticle peak at low energy with a weight Z where Z is inverse of the effective mass. The metallic system also becomes strongly correlated and there is a Kondo peak appearing at the Fermi energy. Single particle density of states has zero weight below and above of this resonance peak. With increasing U this low energy weight gets transferred to the Hubbard bands and at a critical $U = U_{c2}$, Z goes to zero. The putative metal transforms to a strongly correlated metal with significant spectral changes before transforming to a Mott insulator. The region in between U_{c1} and U_{c2} shows a coexistence of metallic and insulating phases. In the $U - T$ (Fig.[1.6]) plane there is a critical temperature at which U_{c1} and U_{c2} meet at a point. At higher temperature there is a smooth crossover between metal and insulator.

1.2.5 Frustration

Most systems try to order at lower temperatures. These include solids, superconductors, ferromagnetic and anti-ferromagnetic materials. According to the second law of thermodynamics, most systems release entropy with decreasing temperature by selecting one particular configuration. Some system are not able to order at even the lowest temperatures. One way to realize such a spin system is by frustrating the local interactions amongst the spins.

Frustration is generally caused by either competing interactions or the geometric nature of the lattice (*e.g.*, in triangular lattice, face-centered cubic (fcc), and hexagonal closed-packed (hcp) lattices, with anti-ferromagnetic nearest neighbor interactions). The interaction energy for two spins S_i and S_j is $E = -JS_iS_j$. For $J < 0$, in a bipartite lattice such as square and cubic, an anti-parallel configuration of the nearest neighbor spins is the minimum energy configura-

tion. In a triangular lattice or other lattices which contain elements of triangles such as fcc or hcp, one cannot construct a ground state where all the bonds are satisfied. Its is impossible to achieve anti-parallel alignment of all three spins on a triangle. Ground state energy does not correspond to the sum of minimum energies for every pair of spins. In the literature this is called geometric frustration[21].

Non-collinear spin configuration.

For an antiferromagnetic systems of spins on a triangular lattice, the energy of a plaquette can be written as

$$\begin{aligned} E &= J(\mathbf{S}_1.\mathbf{S}_2 + \mathbf{S}_2.\mathbf{S}_3 + \mathbf{S}_3.\mathbf{S}_1) \\ &= JS^2[\cos(\theta_1-\theta_2)+\cos(\theta_2-\theta_3)+\cos(\theta_3-\theta_1)], \end{aligned} \tag{1.40}$$

where each spin $\mathbf{S}_i (i = 1,2,3)$ have an amplitude S and it makes an angle θ_i with the $x-$axis. To determine the ground state configuration we need to very the θ_i to minimize the energy *i.e.*, $\partial E/\partial\theta_i = 0$. This leads to the following set of equations.

$$\begin{aligned} \frac{\partial E}{\partial \theta_1} &= -JS^2[\sin(\theta_1-\theta_2)-\sin(\theta_3-\theta_1)] = 0, \\ \frac{\partial E}{\partial \theta_2} &= -JS^2[\sin(\theta_2-\theta_3)-\sin(\theta_1-\theta_2)] = 0, \\ \frac{\partial E}{\partial \theta_3} &= -JS^2[\sin(\theta_3-\theta_1)-\sin(\theta_2-\theta_3)] = 0. \end{aligned} \tag{1.41}$$

A solution of these equation is $\theta_1-\theta_2 = \theta_2-\theta_3 = \theta_3-\theta_1 = 2\pi/3$. The minimum energy configuration correspond to $\mathbf{S}_1+\mathbf{S}_2+\mathbf{S}_3 = 0$ and this configuration produce 120° spin structure.

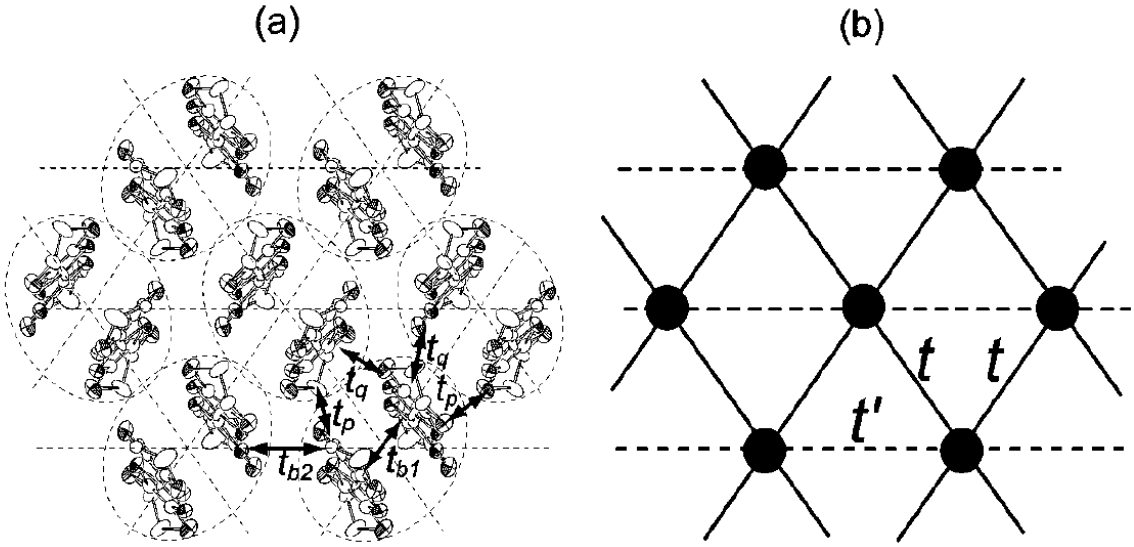

Figure 1.7: (a)Layer structure of organic $BEDT-TTF$ dimer. Two molecule enclosed in the dotted lines form a dimer. (b) Effective tight binding model of $BEDT-TTF$ layer where each dimer in replaced by the lattice point

The mean field transition temperature for a non-frustrated lattice is $\sim J$ and spin susceptibility (ξ) is $\propto (T-\theta_c)^{-1}$. θ_c is the negative of the transition temperature and by measuring susceptibility one can determine the transition temperature. However, in a frustrated system $1/\xi$ starts to deviate from linear behavior at much lower temperature (T_N) where system starts to order. The ratio $f = -\theta_c/T_N$ gives a measure of frustration present in the system and $f > 1$ indicate the presence of frustration.

Experimental Materials

Organic materials such as BEDT-TTF (Bis-ethylenedithio tetrathiafulvalene)(ET) are two dimensional material which show very interesting properties due to interplay of strong interaction and frustration. Electrons in these materials are subject strong correlations. At low temperature, these materials become anti-ferromagnetic and with high enough pressure some of them turn out to be superconducting. These also show strange metallic behavior as seen

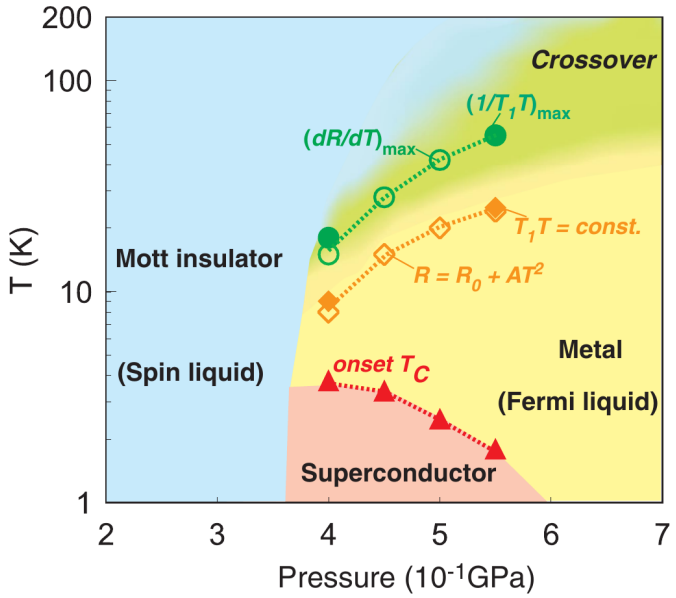

Figure 1.8: Phase diagram of organic Mott insulator $\kappa-(BDET-TTF)_2Cu_2(CN)_3$ [26]

in the cuprates. Like in the cuprates, we see an anti-ferromagnetic to superconductor transition with increasing pressure, as opposed to doping, in these materials. The general ingredients of these materials are $\kappa-(BEDT-TTF)_2X$, where X is a anion which can be $Cu(NCS)_2, Cu[N(CN)_2]Br, Cu_2(CN)_3, I_3$, etc[22, 23]. κ denotes the different arrangement of the molecule at each lattice point Fig[1.7].

The lattice structure of $\kappa-(BEDT-TTF)_2X$ consists of lattice of pairs (dimer) molecules. Dimers normally form a triangular lattice and electrons hop on this lattice between nearest and next nearest neighbors with hoping integrals t and t' as shown in the Fig[1.7]. The value of t and t' depends on the chemical composition and pressure. The relative strength of the t and t' also depends on the anion X. This also determines the degree of frustration on ground state properties. The ground state of $\kappa-(BEDT-TTF)_2Cu[N(CN)_2]Cl$[24] is a Nèel ordered state. Some of these compounds show an insulating behavior without exhibiting any signature of magnetic ordering due to presence of high level of geometric frustration.

The ratio of the transfer integrals t, t' of $\kappa-(BDET-TTF)_2Cu_2(CN)_3$ is almost unity, $t'/t = 1.06$. Nuclear magnetic resonance (NMR) measurements were done on this material to observe signatures of long range magnetic order. However, down to very low temperatures ($32mK$), no splitting of the NMR spectrum has been observed. $\kappa-(BDET-TTF)_2Cu_2(CN)_3$[25] is a spin liquid but with increasing pressure it becomes a superconductor at low temperature and a metal at high temperature Fig[1.8] . It is also observed that at high temperature there is a crossover from an insulator to a metal and the crossover region shows non-Fermi liquid behavior, *e.g.*, as seen in the temperature dependence of the resistivity.

Cs_2CuCl_4

Cs_2CuCl_4 is one of the first few materials which were believed to be Mott insulators with spin liquid behavior. Structure of this material is orthorhombic with very small inter-layer coupling. With this assumption, we can consider this material has a 2D lattice structure of an anisotropic triangular lattice. Electron-electron interaction in this material is very strong and it is enough to consider a Heisenberg Model. The spin-spin interaction is anisotropic with J (full-line bond in Fig[1.7]) and J' (dashed-line bond in Fig[1.7]). Neutron scattering measurements were done on this compound and a weak coupling between the layers stabilize the magnetic order below $T_N = 0.62K$. Neutron scattering measurements data is shown in the Fig[1.9] for two different values of temperature, one below the ordered temperature and other in the paramagnetic phase.

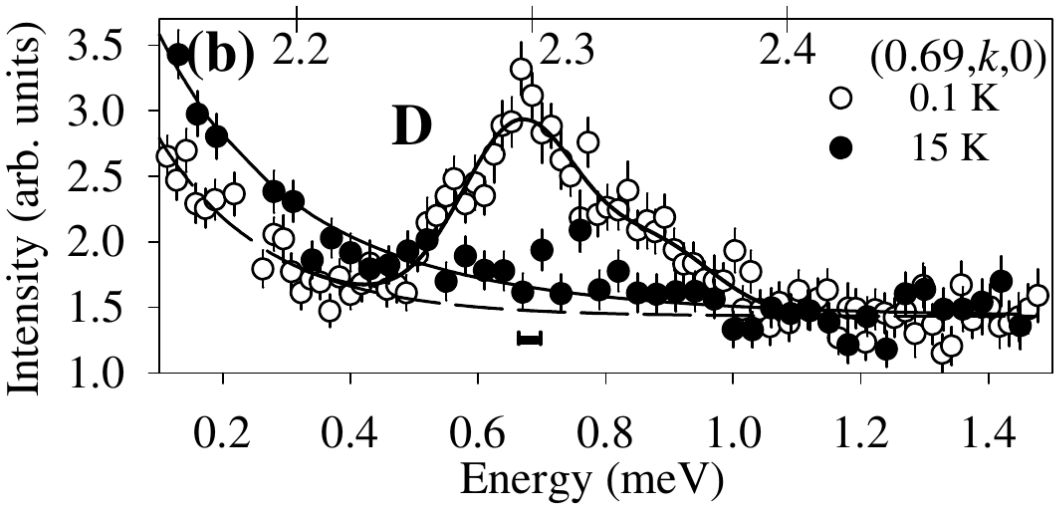

Figure 1.9: Neutron scattering intensity as a function of energy in the magnetically ordered phase at $0.1K$ (open circles) and in the para-magnetic phase at $15K$ (solid circles) [27].

Herbertsmithite

Herbertsmithite with chemical formula $ZnCu_3(OH)_6Cl_2$ is another material where strong correlation and frustration play a major role. In this material magnetic Cu atoms sit in a layer separated by nonmagnetic Zn layers. Cu atoms form an almost perfect Kagome lattice. The spin-spin coupling strength is estimated to be of the order of $170-190K$. This compound does not show any sign of long range magnetic order down to $50mK$ and is assumed to be in a spin liquid state[28].

1.3 Electron-phonon interaction

Conventional picture of a solid assumes, as was discussed earlier, that the lattice remains static or its effects are negligible on electron dynamics, except for providing a periodic potential. It is a good approximation for many covalently-bonded material such Group IV or III-V semiconductors where electrons and holes move through a crystal whose atoms have a fixed position.

Electron and holes can scatter from phonons but at low temperature when phonons are absent ionic displacements are ignored. This approximation fails for ionic or highly polar crystals (such as Group II-VI semiconductors, alkali halides, oxides and others). In these materials Coulomb interaction between the electrons and lattice ions - electrons coupling are very strong. Within the material positive ions attract electron towards it and negative ions repel electron from its neighbor. This means even when there is no real phonon present in the system electron always sees a cloud of virtual phonons. The electron and its virtual phonon cloud can be thought of as a composite particle known as polaron. The idea of polaron was introduced by Landau in 1963[29]. Polaron creates a potential in which electron sits and this potential is created by ionic displacements. This potential is confined to a length scale. A polaron is considered "large" polaron if the special extent of phonon cloud is much larger that the lattice spacing. On the other hand if lattice displacements is restricted to a single site then it is called small polaron.

In Fermi liquid picture electrons are described by quasiparticles which occupy single particle states. These states are described by $|k,\sigma\rangle$ where k is the wave-vector and σ is spin. Electrons move in an ideal periodic crystal without any scattering. However, in a material this periodicity is lost by the lattice vibration. Electrons gets scattered by these vibrations. This electron-phonon interaction induce creation or destruction of a phonon and a simultaneous excitation or de-excitation of electron from state $|k,\sigma\rangle$ to $|k\pm q,\sigma\rangle$. The general electron-phonon interaction can be written as :

$$H_{el-ph} = \sum_{k,q} g(k,q) c^{\dagger}_{k,\sigma} c_{k+q} Q_q \tag{1.42}$$

In our discussion we will consider the Holstein Model[30, 31] . In this model phonons are optical (rather Einstein-like with no dispersion) and couple only to the local electron. The model is defined as

$$\begin{aligned} H &= H_{tb} + H_{el-ph} + H_{ph} \\ H_{tb} &= -t \sum_{\langle ij \rangle, \sigma} (c^{\dagger}_{i\sigma} c_{j\sigma} + h.c.) - \mu \sum_i n_i \\ H_{ph} &= \sum_i \frac{\mathbf{p}^2}{2m} + \frac{K}{2} \sum_i \mathbf{Q}^2 \\ H_{el-ph} &= g \sum_i n_i \mathbf{Q}_i \end{aligned} \tag{1.43}$$

Here H_{tb} is the kinetic energy of the electronic system with t being the hopping parameter, c_i being an electron destruction operator at site i, and $\langle ij \rangle$ representing the nearest neighbors j of site i. H_{ph} is the Hamiltonian for the Einstein phonon with frequency $\omega = \sqrt{K/m}$. Since we are interested in half filling $\langle n_i \rangle = 1$. Since the classical single-site Holstein Hamiltonian has a polaronic minimum with a distortion $\rho = (g/K)$, and polaronic binding energy $E_{pol} = -\left(g^2/2K\right)$, we scale the phonon coordinate Q by ρ and phonon energies by $\left|E_{pol}\right|$. This results in a single dimensionless parameter (scaled in terms of energy unit t) for the phonon part of the Hamiltonian which we demote as V.

$$H_{eff} = -t \sum_{\langle ij \rangle, \sigma} c^{\dagger}_{i\sigma} c_{j\sigma} - \mu \sum_i n_i + \frac{V}{2} \sum_i n_i Q_i + V \sum_i Q_i^2 \tag{1.44}$$

In our work outlined in Chapters 3 and 4, we will further assume that the ionic masses are infinite, so that the kinetic part of the phonons can be dropped.

1.3.1 Peirels Instability and Charge Density Wave formation

Within the adiabatic approximation (large mass limit) the above Hamiltonian simplifies since $[H_{eff}, Q_i]_{=}0$ for all i. To determine the ground state of the above Hamiltonian we need to minimize the total energy $E = E_{el} + V/2 \sum_i Q_i^2$. To understand how charge density wave state

emerges from this simple model we will assume a variational solution of Q_i ,

$$Q_i = \langle Q \rangle + \Delta(-1)^{\mathbf{r}_i} \tag{1.45}$$

At zero temperature we get a self-consistent solution for Δ ,

$$1 = \frac{V}{4\pi^2} \int d^2k \frac{1}{\sqrt{\varepsilon_k^2 + (V\Delta)^2}} \tag{1.46}$$

We get a nonzero solution of Δ for finite V. The average value of number of particles at a site i is $\langle n_i \rangle = \langle n \rangle + \bar{n}(-1)^{\mathbf{r_i}}$. The phenomenon of inducing a charge modulation by electron-phonon coupling in known as Peierls instability. This way the system lowers the energy and is a charge analogue of the Slater instability discussed earlier. As charge modulation and phonon displacements doubles the unit cell system opens up a gap at the Fermi surface and it become a insulator. The dispersion of the fermions is $E_k = \pm\sqrt{\varepsilon_k^2 + (V\Delta)^2}$. The mean-field description gives a finite transition temperature below which charge density wave appears. However,t fluctuations strongly suppress the critical temperature and charge density wave appears only at $T = 0$. Notice that the nesting of the Fermi surface is crucial for obtaining both Slater and Peirels states and the instability is indeed driven by it.

Many lower dimensional such as materials (such as 1D or layered ones) readily show charge density wave transition. The halogen transition-metal tetrachalcogens MX_2 shows two-dimensional charge density wave transition. M is a transition metal which can be either Nb or Ta and $X = S$ or Se[32].

1.3.2 Strong Coupling Perturbation

Kinetic energy of the electron can be regarded as very small when electron-phonon coupling is large. Hopping term can be treated within perturbation theory. The local Hamiltonian in the absence of the hopping term can be solved by Lang-Firsov canonical transformation[33]. The unitary operator for this transformation is e^S where

$$S = -\frac{g}{\omega_0}\sum_i n_i(b_i^\dagger - b_i) \tag{1.47}$$

Any operator A transform as :

$$\tilde{A} = e^S A e^{-S} = A + [S,A] + \frac{1}{2}[S,[S,A]] + .. \tag{1.48}$$

Electron and phonon operators, under this transform ation, become

$$\tilde{b}_i = b_i + \frac{g}{\omega_0} n_i \tag{1.49}$$

$$\tilde{c}_i = c_i e^{\frac{g}{\omega_0}(b_i^\dagger - b_i)} \tag{1.50}$$

This transformation shifts the equilibrium position of the phonon displacement which minimizes the local part of the Hamiltonian.

$$\langle \tilde{x}_i \rangle = \langle \tilde{b}_i^\dagger + \tilde{b}_i \rangle = \langle x_i \rangle + \frac{2g}{\omega_0}\langle n_i \rangle \tag{1.51}$$

In terms of these transformed fermion and phonon operators the Hamiltonian becomes

$$H = H_t + H_0 \tag{1.52}$$

$$H_0 = \omega_0 \sum_i \tilde{b}_i^\dagger \tilde{b}_i - \frac{g^2}{\omega_0} \sum_i \tilde{n}_i \tag{1.53}$$

$$H_t = -t \sum_{\langle ij \rangle} (\tilde{c}_i^\dagger \tilde{c}_j X_i^\dagger X_j + h.c) \tag{1.54}$$

where

$$X_i = e^{-\frac{g}{\omega_0}(\tilde{b}_i^\dagger - \tilde{b}_i)} \tag{1.55}$$

As seen from the expression of H_0, the total energy is lowered due to lattice deformation in the presence an electron.

$$E_p = \frac{g^2}{\omega_0} \tag{1.56}$$

This approach relies on the fact that $t << \hbar\omega_0$, which is the anti-adiabatic limit.

Another dimensionless parameter in the problem is the ratio between this energy (E_p) and bare kinetic energy of the electron. The latter will be proportional to the t and coordination number of the lattice z. We define the dimensionless electron-phonon coupling strength (α) as

,

$$\alpha = \frac{g^2}{z\omega_0 t} \tag{1.57}$$

The ground state of the Hamiltonian H_0 has N degeneracy where N being the lattice size and the electron become site localized. First order correction due to H_t lifts this degeneracy with a reduced effective hoping integral ,

$$t_{eff} = t\langle i|\tilde{c}_i^\dagger \tilde{c}_j X_i^\dagger X_j\rangle = te^{-\frac{g^2}{\omega_0}} = te^{-\frac{\alpha z t}{\omega_0}} \tag{1.58}$$

Second order perturbation has dramatic effect on the electrons. It gives a mechanism to de-

localize the electron. Two intermediate states for the perturbation are states with lattice deformation without having electron on that site and a site with electron without lattice deformation. The second order correction is

$$E^{(2)} = -2z\frac{t^2}{2E_p} = -\frac{t}{\alpha} \tag{1.59}$$

The detailed calculation of this perturbation is done in [34]. Polaron dispersion within the second order perturbation theory reads :

$$E(k) = -\alpha zt - \frac{t}{\alpha} - 2t_{eff}\sum_{i=1}^{2}\cos(k_i) \tag{1.60}$$

Re-normalization of the hoping integral exponentially enhances the effective mass of the electron

$$m^* = me^{\frac{\alpha zt}{\omega_0}} \tag{1.61}$$

Total number of phonon (N_{ph}) can also be calculated in zeroth order

$$N_{ph} = \langle b_i^\dagger b_i\rangle = \langle(\tilde{b}_i^\dagger - \frac{g}{\omega_0})(\tilde{b}_i - \frac{g}{\omega_0})\rangle = \frac{g^2}{\omega_0^2} = \frac{\alpha zt}{\omega_0} \tag{1.62}$$

Both the agove approaches suggest that the electron-phon system has an instability as the dimensionless parameters such as anti-adiabaticity or Migdal parameters are varied.

1.4 Superconducting systems and the Role of Disorder

Superconductivity was first discovered by H. Kamerlingh Onnes in 1911. He observed that dc resistivity of mercury vanishes to zero when it is cooled below the critical temperature $T_c = 4.15K$ [35]. This zero resistivity or infinite conductivity means if a current flows through superconductor it will continue to flow forever without any loss of energy. Another property

of superconductor is the perfect diamagnetism. Meissner and Ochsenfeld [36] observed that magnetic field penetrates only a finite length in the material and goes to zero inside a bulk superconductor. Superconductivity also gets destroyed with increasing magnetic field. This effect is known as Meissner effect. Experimentally it was observed that with increasing isotope mass transition temperature decreases. From this it was anticipated that the electron-phonon coupling is responsible for the superconductivity. A phonon with characteristics frequency ω_q with momentum q generate, due to electron-phonon coupling, a effective electron-electron interaction which is $\propto(\omega^2-\omega_q^2)^{-1}$. Hence, for $\omega<\omega_q$ phonons can mediate na attractive interaction between a pair of electrons..

Copper pair

Cooper in 1956[37] showed that in the presence of an attractive interaction electron-electron pair states near the Fermi energy have lower energy than their combined Fermi energy. He argued that in the low temperature limit when thermal energy is irrelevant, electron can form pairs. Let us assume a singlet paired state as

$$|\psi(r_1,r_2)\rangle=\sum_k g_k e^{k.(r_1-r_2)}(|\uparrow\downarrow\rangle-|\downarrow\uparrow\rangle) \tag{1.63}$$

This results in a self-consistent equation

$$(E-2\varepsilon_k)g_k=\sum_{k'>k_F} g_{k'}V_{kk'} \tag{1.64}$$

where V is the attractive interaction and for simplicity we will assume $V_{kk'}=-V$ for $\varepsilon_{k_F}<\varepsilon_k<\varepsilon_{k_F}+\hbar\omega_c$ and $V_{kk'}=0$ otherwise. ω_c is the cutoff frequency above which attractive interaction

vanishes. This can be identified with the Debye frequency of the lattice.

With these assumptions one can simplify the eigenvalue equation and energy of the paired state will be

$$E = 2\varepsilon_F - 2\hbar\omega_c e^{-1/N_0 V} \tag{1.65}$$

This energy indeed is lower than the Fermi energy of two electron ($2\varepsilon_F$).

1.4.1 The BCS Theory

J. Bardeen, L. Cooper and J. R. Schrieffer first proposed the microscopic theory of superconductivity. In the superconducting state a finite fraction of total electrons form Copper pairs with opposite spin and momenta. These pair of electrons "Bose condens" to a superfluid state at low enough temperatures. The effective microscopic Hamiltonian proposed by them (capturing the essential physics) in the second quantised form is

$$H = \sum_{\vec{k},\sigma} \varepsilon_k c^\dagger_{k,\sigma} c_{k,\sigma} + \sum_{k,k',\sigma} V_{k,k'} c^\dagger_{k,\sigma} c^\dagger_{-k,-\sigma} c_{-k,-\sigma} c_{k,\sigma} \tag{1.66}$$

$V_{k,k'}$ is the effective interaction between the electrons , ε_k is the kinetic energy of the electron and $c^\dagger_{k,\sigma}(c_{k,\sigma})$ is the creation (annihilation) operator for the electron with momentum k and spin σ. Now we will decompose the four fermion term of the Hamiltonian by using mean field theory.

$$\Delta_k = \langle c_{k\uparrow} c_{-k,\downarrow} \rangle \tag{1.67}$$

$$\Delta^*_k = \langle c^\dagger_{k\uparrow} c^\dagger_{-k,\downarrow} \rangle \tag{1.68}$$

Neglecting the higher order fluctuation of Δ_k, we will get

$$H = \sum_{\vec{k},\sigma} \varepsilon_k c^\dagger_{k,\sigma} c_{k,\sigma} + \sum_k \left[V_{kk'} \left(\Delta_{k'} c^\dagger_{k\uparrow} c^\dagger_{-k,\downarrow} + \Delta^*_{k'} c_{k\uparrow} c_{-k,\downarrow} \right) - \frac{|\Delta_{k'}|^2}{V_{kk'}} \right] \tag{1.69}$$

The above Hamiltonian can be diagonalized by defining new fermionic operators η_k and γ_k

.

$$c_{k,\uparrow} = \cos\theta \eta_k - \sin\theta \gamma^\dagger_k \tag{1.70}$$

$$c^\dagger_{-k,\downarrow} = \sin\theta \eta_k + \cos\theta \gamma^\dagger_k \tag{1.71}$$

where $\tan(2\theta) = -\frac{\Delta_k}{\varepsilon_k}$. The mean field Hamiltonian can be rewritten as :

$$H = \sum_{k,\sigma} \left[\varepsilon_k + \frac{|\Delta_k|^2}{V} \right] + \sum_k E_k (\eta^\dagger_k \eta_k - \gamma^\dagger_k \gamma_k) \tag{1.72}$$

The quasi-particle energy eigenvalues are s $E_k = \sqrt{\varepsilon_k^2 + |\Delta_k|^2}$. Δ_k is the gap in the spectrum and regarded as the order parameter of the superconducting state . We will assume $V_{k,k'} = -V$. Minimising the free energy corresponding to this Hamiltonian, we obtain the self-consistent solution for the gap Δ_k

$$\Delta_k = -\sum_{k'} V_{kk'} \Delta_{k'} \frac{\tanh(\beta E_{k'}/2)}{2E_{k'}} \Rightarrow 1 = V \sum_{k'} \frac{\tanh(\beta E_{k'}/2)}{2E_{k'}} \tag{1.73}$$

Near the transition temperature $\Delta_k \to 0$ and $E_k \simeq \varepsilon_k$ and replacing the density of states by its value near the Fermi energy $D(0)$, we get the transition temperature (T_c) as :

$$K_B T_c = \frac{2e^\gamma}{\pi} \omega_D e^{-1/\lambda} \tag{1.74}$$

where $\gamma \simeq 0.5772$ is the Euler number. The value of the gap at zero temperature $\Delta(T = 0) =$

$2\omega_D e^{-1/\lambda}$. Ratio of the zero temperature gap and the critical temperature is universal.

$$\frac{\Delta(T=0)}{K_B T_c} \approx 1.76 \tag{1.75}$$

Bogoliubov-de Gennes Mean-Field Theory

The above mean field formalism can also be extended to the realspace when spacial fluctuations are important. The attractive Hubbard model has a local onsite interaction which can be decomposed within mean field theory as [38].

$$-U c^\dagger_{i\uparrow} c^\dagger_{i\downarrow} c_{i\downarrow} c_{i\uparrow} \Rightarrow \Delta_i c^\dagger_{i\uparrow} c^\dagger_{i\downarrow} + \Delta^*_i c_{i\downarrow} c_{i\uparrow} + (U/2)\langle n_i \rangle n_i \tag{1.76}$$

The Hamiltonian becomes quadratic in term of fermionic operator and can be solved by the Bogoliubov transformation.

$$c_{i\uparrow} = \sum_n u_n(r_i)\gamma_{n\uparrow} - v^*_n(r_i)\gamma^\dagger_{n\downarrow}, \qquad c_{i\downarrow} = \sum_n u_n(r_i)\gamma_{n\downarrow} + v^*_n(r_i)\gamma^\dagger_{n\uparrow} \tag{1.77}$$

With this transformation we can write down the Hamiltonial in a matrix form :

$$\begin{pmatrix} \hat{K} & \hat{\Delta} \\ \hat{\Delta}^* & -\hat{K}^* \end{pmatrix} \begin{pmatrix} u_n(r_i) \\ v_n(r_i) \end{pmatrix} = E_n \begin{pmatrix} u_n(r_i) \\ v_n(r_i) \end{pmatrix} \tag{1.78}$$

where $\hat{K}$ contains the kinetic part of the Hamiltonian (with the chemical potential incorporated to fix the particle density) and $\hat{\Delta}$ is a diagonal matrix with $\{\Delta(r_i)\}$ as entries. The self-consistent solution are

$$\begin{aligned} \Delta(r_i) &= U \sum_n u_n(r_i) v^*_n(r_i) \\ \langle n_i \rangle &= 2 \sum_n |v_n(r_i)|^2 \end{aligned} \tag{1.79}$$

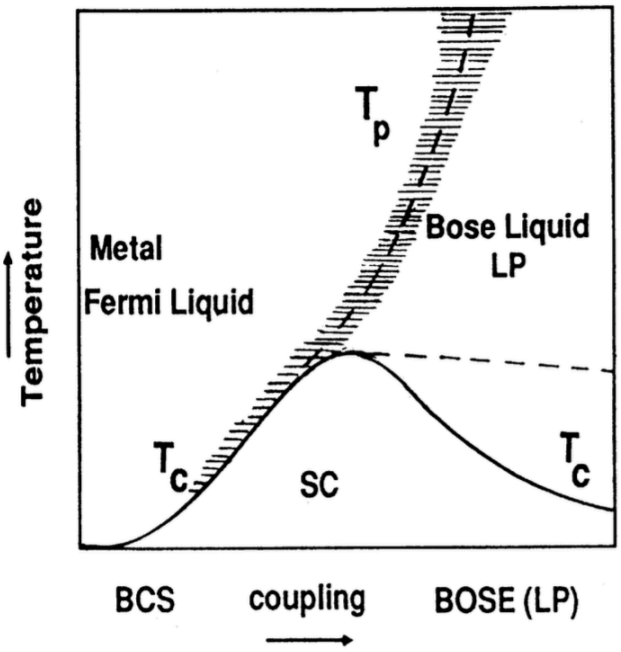

Figure 1.10: Schematic phase diagram for systems in which the BCS-BEC crossover takes place. The continuation of T_c, determined within continuum model, is denoted by the dashed line in the phase diagram. [39].

1.4.2 BCS-BEC Crossover

The properties of electrons in the presence of attractive interaction shows very different behavior in the weak and strong coupling region. The superconductivity of these two limits are explained by BCS and BEC theory respectively. In the BCS limit pair formation and condensation happen simultaneously at the transition temperature (T_C). Below this critical temperature pairing take place in the vicinity of the Fermi surface. Pair size is large compared to inter atomic distances so there is large overlap between pairs. As the attractive interactions among the electron are very weak the superconducting gap is small compared to the bandwidth. As the temperature increases this gap in the spectrum decreases monotonically and vanishes at the transition temperature (T_c). The normal state above the critical temperature is described by Fermi liquid theory.

Electronic properties are very different in the BEC limit when attractive interaction become large compared to the kinetic energy scale. Cooper pairs are formed at a higher temperature (T_p) and superconducting transition happen at very lower temperature ($T_c \ll T_p$). Though Cooper pairs are formed at T_p, phases of these electron pairs are uncorrelated and global phase coherence develops only below T_c. Pairing of the electrons happen in real space and all the electron participate. Size of individual pairs is small compared to the average distance between electrons. The normal state above T_c and below T_p is described by a strongly bound phase incoherent electron pairs. Fig[1.10] show a schematic phase diagram of the attractive Hubbard model. $T_c \propto \exp(-1/N(0)U)$ in the weak coupling region and $T_c \propto 1/U$ in the strong coupling region. T_c as a function of interaction strength shows a smooth crossover between these two limit. In the intermediate and strong coupling region a "pseudogap" phase appears in single particle spectrum (dashed in the fig[1.10]). The pair formation temperature (T_p) scales with interaction strength (U). We will discuss the physics of this transition in detail in subsequent chapters.

1.4.3 Disordered Superconductors

Although BCS theory had tremendous success describing clean superconductors, it lacks a general framework for the disordered superconductors. One of the main reasons is that BCS theory is a mean field theory whereas in a disordered system, fluctuation effects have a strong impact, especially leading to breaking of phase coherence.

The effect of disorder on a superconductor was first studied by Anderson[48] and Gor'kov [49]. They observed that nonmagnetic impurities have very little effect on the superconductor. Especially gap in the spectrum and transition temperature remain unaffected for a weakly dis-

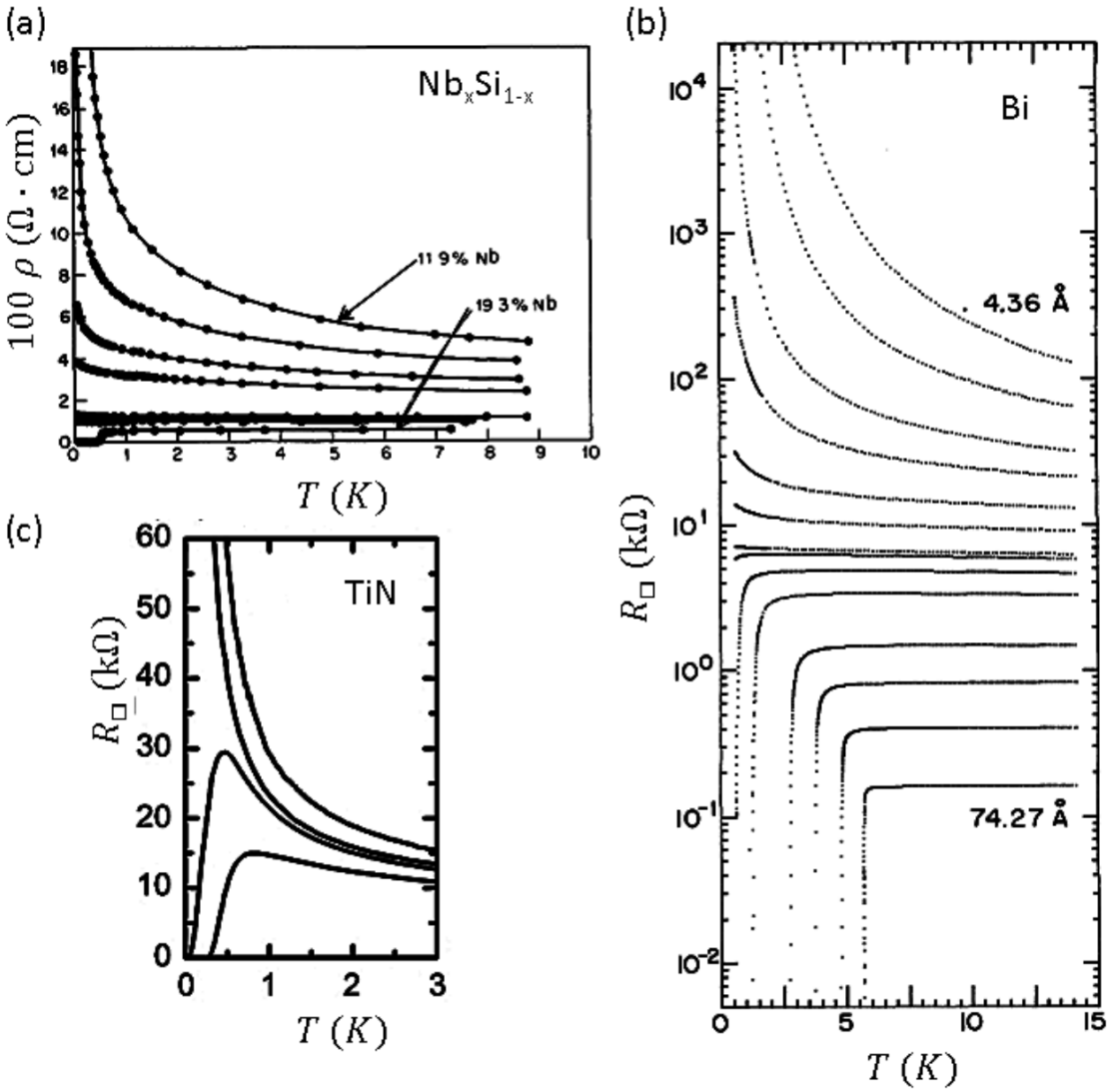

Figure 1.11: Three examples of the film resistance as a function of temperature for a family of curves for various materials displaying the superconductor-to-insulator transition (SIT). (a) SIT observed for a series of amorphous Nb_xSi_{1x} films with increasing concentrations of Nb from the upper part of figure downwards. Figure from Ref. [50]. (b) SIT in a family of amorphous Bi films with the film thickness increasing from the upper part of the figure downwards. Figure from Ref.[51] . (c) SIT for a series of TiN films being thinned by soft plasma etching in order to control the normal state sheet resistance. Figure from Ref. [52].

ordered system. Within BCS theory, an electron of momentum and spin of $k, \uparrow$ is paired with another electron of $-k, \downarrow$ labels. In a disordered system, momentum (k) is not a good quantum number. However, in the presence of nonmagnetic impurities time reversal symmetry is preserved and the ground state can be constructed from time reversed states. In this situation, Cooper pairs can be composed of time reversed partner states.

The competition between superconductivity and localization is one of the fundamental problem over decades. These two phenomena show distinct behavior in the electrical transport measurements. Localized states in the presence of disorder have wave-functions with limited spatial extent and decay exponentially. This makes the electrons unable to conduct in the material and lead to vanishing conductivity and infinite resistivity. Superconductivity, on the other hand, arises due to long-range phase coherent Cooper pairs and a superconductor has zero d.c. resistivity. In two dimensions, the interplay between these two phases become much more complex. The proper superconducting long range order happens at $T = 0$ with a BKT transition at finite temperature. Scaling theory of localization [4] predicts that in the presence of arbitrarily weak disorder, all electronic states will be localized in two dimensions.

Thin film metals are good systems to study this interplay. These samples are made by evaporating a metal and depositing on a substrate held at very low temperature. Due to the rapid cooling of the material there will be some inherent disorder in the film. This disorder will affect the conductivity of the film. We can quantify the disorder by the sheet resistance. Film thickness controls the degree of disorder and disorderness increases with decreases in sample thickness. For thin disordered films, wave-functions will be localized, making them insulators at $T = 0$. For very thick films disorder is reduced and superconductivity wins over the localization.

As disorder strength is varied there will be a superconductor to insulator transition (SIT). This transition has been observed in different materials with various controlling parameters. These materials are amorphous niobium silicon ($NbSi$) [50], amorphous bismuth (Bi) films [51], and polycrystalline titanium nitride (TiN) films [52]. In $NbSi$, Nb concentration controls the SIT. Film thickness is the controlling parameter of Bi and TiN films. In all the cases critical temperature monotonically decreases with increasing disorder strength and resistivity shows an upturn at low temperature. Most prominent competition between the superconductivity and localization is seen in the TiN thin films. Even for a superconducting sample at low temperature, the resistivity shows a negative temperature dependence.

1.5 Outline of the thesis

In this thesis we investigate two dimensional models of strongly correlated electrons by taking into account both electron-electron and electron-phonon interaction. The two dimensional Holstein-Hubbard model is a promising effective model for electronic and phonon degree of freedom. Though this is an oversimplified description of both electron-electron and electron-phonon interactions, it retains all the relevant degrees of freedom of a solid state system when both short range Coulomb repulsion and phonon mediated interactions are present.This model shows many different phases. We have also studied the effect of geometric frustration on these ordered phases. The second part of this thesis focuses on the effect of site dilution in attractive Hubbard Model which has superconducting ground state. The effect of spacial and thermal fluctuations become very important in an inhomogeneous background. We have studied this model in two different situation in which the system is either metal or insulator in the absence of interaction. We also touch upon the effect of site dilution in an otherwise, parent FFLO state. Before presenting the main results we will also discuss various benchmarking efforts to test the

reliability of the methodology. The remaining chapters of the thesis are organized as follows.

Chapter 2. We describe the models we used in this thesis and the computational method that we have implemented to solve those models. In the Holstein-Hubbard part we have assumed the phonon are adiabatic or they have very large mass ($m \to \infty$). To deal with the quartic onsite Coulomb interaction term we have introduced two Hubbard-Stratonivich fields, one couples to charge and the other couples to spin of the itinerant electrons. Though this transformation is exact to proceed with, we have dropped the time dependence of these fields to simplify the numerics. We need to calculate the most probable distribution of these fields. We have used Monte Carlo sampling procedure to sample the configurations of phonon and HS fields. During each Monte Carlo update procedure we need to integrate the fermion degree of freedom to calculate the change in free energy. Once the equilibrium is reached we have done configuration average to calculate different physical properties like spectrum, resistivity *etc*.

Chapter 3. We discuss the Holstein-Hubbard model at half filling to explore the ordered phases such as the charge density wave and antiferromagnet. The Coulomb interaction is rewritten in terms of auxiliary fields. By treating the auxiliary fields and phonons as classical, we obtain real space features of the system and transition between the phases from weak to strong coupling. When both interactions are weak, mutual competition between them leads to a metallic phase in an otherwise insulator dominated phase diagram. Spatial correlations induced by thermal fluctuations lead to pseudogap features at intermediate range of coupling.

Chapter 4. We investigate the Holstein-Hubbard Model on an isotropic triangular lattice to study the effect of geometric frustration. We have obtained the zero temperature phase diagram along with finite temperature properties. System shows transition from a weak coupling metal to a strong coupling Mott insulator. In the insulating region we have found two long range ordered states of charge and spin degree of freedom as frustration is tuned. Both magnetic and charge structure factors take a maximum at $q = (2\pi/3, 2\pi/3)$ in the fully frustrated case.

Chapter 5. We study the effect of randomly placed attractive centres in a host metal and look at the percolative superconducting transition as the density of attractive centres grow. A real space picture is employed using the Hubbard - Stratanovich transformation of the attractive interaction that is capable of capturing weak-to-strong coupling scenario. The method allows us to extract spectral and transport properties in detail. BCS-BEC crossover is discussed in the context of site dilution scenario.

Chapter 6. We present the results of site dilution in an attractive Hubbard model with an insulating host. This brings out the competition among various energy scales such as the local attraction, disorder, and the insulating gap. We choose a system which has a charge density wave phase as ground state at half filling. Towards the end, we also explore the role of site dilution in FFLO systems.

We conclude by pointing out the salient results obtained and comment upon the methodology employed. Possible extensions of the present study are mentioned. Drawbacks of the methodology are highlighted and put in a physical perspective.

Chapter 2

Models and Methods

In this chapter, we give a brief introduction to the models that are used in the present study and the methods adopted to explore these problems. The models fall into two classes. The first one explores the interplay between electron-electron interactions and electron-lattice coupling. At the simplest level, this is captured by the Holstein-Hubbard model. The second class of problem deals with the effect of site dilution in superconductors. We use an attractive Hubbard model to capture the physics of such systems. In both the cases, we reduce the quartic fermion problem into a quadratic one by introducing an auxiliary field. By assuming these fields to be static, we are able to elucidate the finite temperature properties of the systems of interest.

2.1 The Holstein-Hubbard model

The quanta of collective vibrations of atoms arranged on a regular lattice are called phonons. Energy or frequency of these collective modes depend on the wave vector (k). Accordingly there are two kind of phonons, acoustic and optical. Optical phonon frequency does not depend appreciably on the wave-vector $(\omega(k) = \omega_0)$ and acoustic phonon depend linearly on the wave-vector $(\omega(k) = ck)$ where c is the sound velocity. We will consider only optical phonons in our study. The simplest model to treat electron-phonon coupling is the Holstein Model. In

this model a band of electrons is coupled to dispersionless phonons and the coupling is through the local charge density[30]. Due to strong screening of electric field in most metals, electron-phonon interaction can be assumed to be local. Non-local aspects of the electron-phonon interaction is discussed in different works[53–57]. The electrons also interact among themselves *via* on-site Coulomb repulsion. This interaction is captured using the Hubbard model introduced in the previous chapter. Although this is a simplified model there are various parameter which control the phases of it. The bare band-width of the electron, electron-phonon and electron-electron interactions, and the number of particles determine the multidimensional phase diagram.

The model reads

$$\begin{aligned} H &= -t\sum_{\langle ij\rangle}\left(c^{\dagger}_{i\sigma}c_{j\sigma}+h.c.\right)-\mu\sum_{i}n_i+U\sum_{i}n_{i\uparrow}n_{i\downarrow} \\ &\quad +\sum_{i}\left(\frac{1}{2M}P_i^2+\frac{K}{2}Q_i^2\right)-g\sum_{i}Q_in_i \end{aligned} \tag{2.1}$$

$\langle..\rangle$ sum runs over the nearest neighbor sites on a square or triangular lattice. $c_{i\sigma}$ ($c^{\dagger}_{i\sigma}$) is the annihilation (creation) operator for the fermions at a site i with spin σ. μ is the chemical potential which fixes the average number of particle. For example, half filling corresponds to ($\langle n\rangle = 1$. U is the repulsion energy between two electron on the same site with opposite spins. P_i, Q_i are the ionic/atomic momentum and displacement operator at site i.

2.1.1 Analytical approaches

One of the earliest analysis of the electron-phonon problem was done by Migdal and Eliashberg [58, 59]. Migdal demonstrated that the vertex corrections and momentum dependence of self-energy will be insignificant when the phonon frequency is very small compared to the Fermi energy [58]. Later Eliashberg extended Migdal's method to study superconductivity [59]. Migdal assumed that most of the emitted phonon are the one which are absorbed first. This is consistent as long as the phonon frequency and electron-phonon coupling strength are small compared to

the electron bandwidth. In earlier days most of the studied material were in the weak coupling region where Migdal-Eliashberg theory was successful. However, Migdal-Eliashberg theory does not work accurately for large phonon frequency and strong electron-phonon coupling.

Integrating out the phonon degrees of freedom we get a local on-site interaction among electrons[60]. The effective interaction is

$$U(i\omega_n) = \frac{V\omega_0^2}{\omega_0^2 + \omega_n^2} \tag{2.2}$$

where $\omega_n = 2\pi nT$ is the Matsubara frequency for bosons with n being an integer. $V = -g^2/M\omega^2$ determine the strength of the effective electron-electron interaction. This interaction has two important limits

- In the $\omega_0 \to 0$ limit effective interaction become a Kronecker delta function. Holstein model in this limit was investigated within the dynamical mean field theory (DMFT) [61, 62]. If the phonon frequency and the coupling strength are small then vertex corrections will be negligible and self-energy will be nearly momentum independent. Dynamical Mean Field Approximation being a local theory becomes exact in this region.

- The effective interaction $U(i\omega_n)$ becomes independent of ω_n when $\omega_0 \to \infty$ and it reduced to an attractive Hubbard model. Vertex corrections become large and Migdal's approach does not hold properly in this limit.

2.2 Auxiliary field method for the Hubbard interaction

In the presence of Hubbard interaction it is very difficult to solve this model. With the help of an exact Hubbard-Stratonovich transformation, we will decompose the four fermion term into

a quadratic form. Hubbard interaction can be written at the expense of charge (ϕ_i) and spin ($\mathbf{m}_i$) auxiliary fields as

$$\exp\Big[U\sum_i n_{i\uparrow}n_{i\downarrow}\Big] = \int\prod_i \frac{d\phi d\mathbf{m}_i}{4\pi^2 U}\exp\Big[\frac{\phi_i^2}{U} + i\phi_i n_i + \frac{\mathbf{m}_i^2}{U} - 2\mathbf{m}_i.\mathbf{s_i}\Big] \tag{2.3}$$

where charge (n_i) and spin ($\mathbf{s_i}$) operators are defined as

$$n_i = \sum_\sigma c^\dagger_{i\sigma}c_{i\sigma}, \mathbf{s_i} = \frac{1}{2}\sum_{a,b} = c^\dagger_{ia}\vec{\sigma}_{ab}c_{ib} \tag{2.4}$$

The Partition function can be written as

$$Z = \int\prod_i \frac{\mathcal{D}[c_{i\sigma}, c^\dagger_{i\sigma}]d\phi_i d\mathbf{m}_i}{4\pi^2 U}\exp\Big[-\int_0^\beta \mathcal{L}(\tau)\Big] \tag{2.5}$$

The Lagrangian $\mathcal{L}(\tau)$ is

$$\mathcal{L}(\tau) = \sum_{i\sigma} c^\dagger_{i\sigma}\partial_\tau c_{i\sigma} + H_0(\tau) + \sum_i\Big[\frac{\phi_i^2}{U} + +(i\phi_i - \mu)n_i + \frac{\mathbf{m}_i^2}{U} - 2\mathbf{m}_i.\mathbf{s_i}\Big] \tag{2.6}$$

All the fermionic operators ($c^\dagger_{i\sigma}, c_{i\sigma}$) explicitly depend on time (τ). H_0 contains all the other terms of the Hubbard Hamiltonian except the on-site repulsion term. We consider this model at half filling *i.e.*, $\langle n_i\rangle = 1$

Below we will make some approximations to make progress

- We will replace ϕ_i by its saddle point solution. At half filling saddle point solution is $i\phi_i = \frac{U}{2}\langle n_i\rangle = \frac{U}{2}$. At half-filling charge fluctuation is believed to be less important, especially in the strong coupling regime. Away from half-filling charge fluctuations become relevant. Also movement of the electron become very restricted at large U.

- We will also drop the time dependence of the $\mathbf{m}_i$ fields. This gives us a quadratic fermion problem in the background of classical vector field $\mathbf{m}_i$. At $T = 0$ this will reduce to unrestricted Hartree-Fock approximation; however, we will take into account all the thermal and spacial fluctuations.

We will rescale $\mathbf{m}_i$ field to $\frac{U}{2}\mathbf{m}_i$. With these approximation the semiclassical effective Hamiltonian becomes,

$$H = H_0 + \sum_{i\sigma}(\frac{U}{2} - \mu)n_{i\sigma} - \frac{U}{2}\sum_i \mathbf{m}_i.\vec{\sigma}_i + \frac{U}{4}\mathbf{m}_i^2 \tag{2.7}$$

Certainly by making these assumptions we have made some sacrifices. However, this has some added advantages over other methods.

- We can access complicated magnetic structures for different lattices. We can correctly predict the magnetic transition temperatures in the weak and strong coupling region.

- Spectral and transport properties can be calculated without analytic continuation which is needed in QMC and DMFT based calculations.

- This method can also study magnetically disordered systems apart from long range magnetic orders systems.

Though this method is superior for calculating many physically measurable quantities and accessing finite temperature physics, it lacks the quantum dynamics of the $\mathbf{m}_i$ and ϕ_i fields. Due to this correlation effects will be less prominent and it will underestimate the critical U/t for metal-insulator transition. More exotic states like quantum spin liquids[63, 64] will not appear within this method.

2.2.1 Classical phonons

The free Hamiltonian for the Holstein phonon is

$$H_{ph} = \sum_i \frac{\mathbf{P}_i^2}{2m} + \frac{K}{2}\sum_i \mathbf{Q}_i^2 \tag{2.8}$$

In this model phonon are dispersionless and the frequency of this Einstein phonon is $\omega_0 = \sqrt{\frac{K}{m}}$. In our study we will take the limit of $m \to \infty$. Kinetic energy associated with lattice displacements, thus, become negligible and we will drop this term. Q_i are now classical variables, but thermally and spatially fluctuating. The electron-phonon interaction reduces to

$$H_{el-ph} = g\sum_{i\sigma} \mathbf{Q}_i n_{i\sigma} \tag{2.9}$$

When each site has an electron, the ground state energy is minimised when

$$\mathbf{Q}_i = -\frac{g}{K} = \mathbf{Q}_0 \tag{2.10}$$

The minimum energy is

$$E_0 = -\frac{g^2}{2K} \tag{2.11}$$

To make $\mathbf{Q}_i$ dimensionless we will rescale it with $\mathbf{Q}_0$.

$$H_{el-ph} = \frac{g^2}{k}\sum_{i\sigma} \mathbf{Q}_i n_{i\sigma} \qquad \text{and,} \qquad H_{ph} = \frac{g^2}{2K}\sum_i \mathbf{Q}_i^2 \tag{2.12}$$

Now we introduce a new parameter $V = \frac{g^2}{K}$ which proportional to polaron binding energy. The effective Hamiltonian incorporating all these assumptions become

$$H_{eff} = H_{el} + H_{cl}$$

$$H_{el} = -t\sum_{\langle ij\langle}(c^{\dagger}_{i\sigma}c_{j\sigma}+h.c)-\mu\sum_{i\sigma}n_{i\sigma}-\frac{U}{2}\sum_{i}\mathbf{m}_i.\vec{\sigma}_i+V\sum_{i}Q_in_i$$
$$H_{cl} = \frac{U}{4}\sum_{i}\mathbf{m}_i^2+V\sum_{i}Q_i^2 \tag{2.13}$$

2.3 Numerical methods

The effective Hamiltonian (equation 2.13) describes the properties of electron which are interacting with classical vector field $\mathbf{m}_i$ and phonon displacement Q_i. We will solve this problem in the entire range of coupling from weak to strong. Obviously this goes far beyond conventional perturbative approaches. The partition function of this Hamiltonian (equation 2.13) is

$$Z = \int \mathcal{D}(\mathbf{m}_i)\mathcal{D}(Q_i)Tr_{c,c^{\dagger}}e^{-\beta H_{eff}} \tag{2.14}$$

The Hartree-Fock results with mean field solution of Q_i become exact at $T = 0$. However, at finite temperature this reduces to solving a quadratic fermionic problem in the background of fluctuating classical fields $\{\mathbf{m}_i, Q_i\}$. The probability of a $\{\mathbf{m}_i, Q_i\}$ configuration at any finite temperature is

$$P\{\mathbf{m}_i, Q_i\} = Tr_{c,c^{\dagger}}e^{-\beta H_{eff}} \tag{2.15}$$

The electron free energy for a give configuration of $\{\mathbf{m}_i, Q_i\}$ is defined as

$$e^{-\beta F} = P\{\mathbf{m}_i, Q_i\} \tag{2.16}$$

The trace over the Grassmann variables ($\{c, c^{\dagger}\}$) cannot be done analytically for any given of $\{\mathbf{m}_i, Q_i\}$. However, numerically this can be done by diagonalizing the H_{eff} as this Hamiltonian only involves quadratic fermionic terms. In this way one can calculate the free energy F. We sample the $\{\mathbf{m}_i, Q_i\}$ configuration using real space Monte Carlo method starting from high temperature to low temperature.

Electronic part of the free energy in term of the eigenvalues (ε_n) of H_{el} can be written as

$$F_{el} = -\frac{1}{\beta}\sum_n \ln(1+\exp(-\beta\varepsilon_n)) \tag{2.17}$$

2.3.1 Monte Carlo Method

To access the thermal properties of the system we simulate it using Monte Carlo methods. The Boltzmann weight for a particular configuration is give by

$$P\{\mathbf{m}_i, Q_i\} = e^{-\beta F} \tag{2.18}$$

We sample the configuration of the classical fields to achieve thermal equilibrium at a finite temperature. One of the standard method to do this sampling is via Metropolis algorithm [65]. We start with a random configuration of $\{\mathbf{m}_i, Q_i\}$ at high temperature. Then we select a site i randomly from the lattice and change the classical fields $(\mathbf{m}_i, Q_i)$ at that site. We calculate the free energy before (F_{initial}) and after (F_{final}) the change. We accept the new configuration if the change in the free energy $\Delta E (= F_{\text{final}} - F_{\text{initial}}) < 0$. This implies that this kind of move will decrease the system energy. If the charge in free energy $\Delta E > 0$, we accept the move with a probability $\exp(-\beta\Delta E)$. This is done by generating a random number (x) using a Pseudo Random Number generator (PRNG) in the range $[0,1]$. We accept the proposed configuration if $x < \exp(-\beta\Delta E)$ and reject it otherwise. Depending on whether a move is accepted or rejected, the new configuration (for the next update procedure) is proposed as the initial configuration.

Metropolis algorithm is a guided random walk in the configuration space of the classical fields. The probability distribution of the states visited during the random walk are consistent

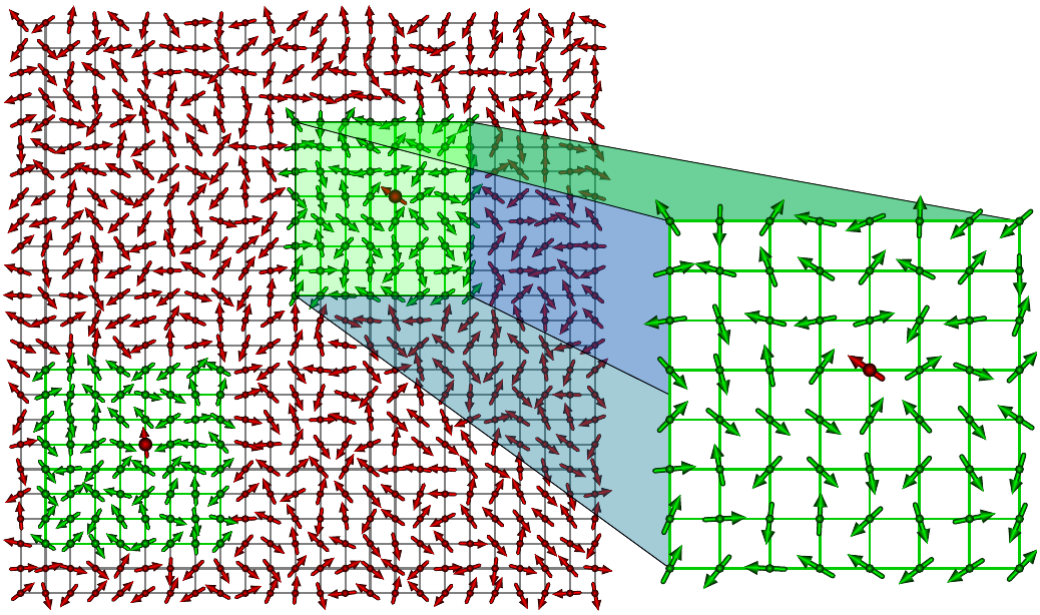

Figure 2.1: Visualization of the our cluster based update scheme.[67]

with the canonical ensemble. Once a single site updates is carried out, we repeat the process for all the sites on the lattice. This is called a single MC sweep. At each temperature we have done 2000 sweeps to equilibrate the system and use the next 2000 sweeps to evaluate transport and spectral properties. After the equilibrium sweeps are done some configuration are saved to take thermal averages of different quantities. This process is repeated while lowering the temperature.

2.3.2 Traveling cluster

As we have discussed in the previous section Monte Carlo can been done on any system size. However, the most computationally expensive part is the diagonalization of a lattice Hamiltonian. The matrix size is $N \times N$ for a two dimensional $L \times L$ lattice where $N \sim L^2$. During each single site update a diagonalization of H_{eff} costs $\sim \mathcal{O}(N^3)$. One single sweep costs $\sim \mathcal{O}(N^4)$. With the currently available resources we can simulate a maximum lattice size of 12×12. The scaling of computational cost with system size limits the maximum lattice size we can access. To circumvent this higher cost we have adopted a traveling cluster algorithm (TCA) [66]. This

method replaces the full lattice Hamiltonian diagonalization by a small cluster lattice Hamiltonian diagonalization. The size of the cluster is small ($L_c \times L_c$) and it is centered around the site at which Monte Carlo update needs to be done (Fig. 2.1). The matrix size of the cluster Hamiltonian is $N_c = L_c^2$. The diagonalization of this matrix will cost $\sim \mathcal{O}(N_c^3)$ and a single sweep will cost $\sim N \times \mathcal{O}(N_c^3)$. This greatly lowers the computational cost and increase the accessible lattice size. Maximum lattice size we have studied is 32×32.

2.3.3 Thermal average

The electronic properties can be calculated with equilibrated configurations of classical fields. There are two kind of physical quantities that can be evaluated, one of them involves various combination of classical fields $\mathbf{m}_i$ and Q_i and the other measures physical quantities which are functions of c_i and $c_i^\dagger$. We can trivially take the thermal average of the $\mathbf{m}_i$ and Q_i, but for the quantities that depend on fermionic variables, we need to take the averages over the quantum variables first and then thermally average them over the different configuration of the background fields.

Any fermionic quantity $f(c_i, c_i^\dagger)$ can be written as

$$\langle f(c_i, c_i^\dagger) \rangle = \mathcal{Z}^{-1} \int \mathcal{D}(\mathbf{m}_i) \mathcal{D}(Q_i) Tr_{c,c^\dagger} f(c_i, c_i^\dagger) e^{-\beta H_{eff}} \tag{2.19}$$

Trace over the fermionic degree of freedom is done by diagonalizing H_{eff} in a specific, equilibrium background of the classical fields. They are then averaged over different equilibrium configurations at a particular temperature.

2.3.4 Auxiliary field properties

Spatial correlations of the auxiliary field $\mathbf{m}_i$ can be studied by analysing the structure factor.

$$S(\mathbf{q}) = \frac{1}{N^2}\sum_{ij}\langle \mathbf{m_i}.\mathbf{m_j}\rangle e^{i\mathbf{q}.(\mathbf{r_i}-\mathbf{r_j})} \tag{2.20}$$

The sum runs over all the lattice sites . $\langle..\rangle$ stands for averaging over many sampled configurations. $S(\mathbf{q})$ gives an indication of any magnetic ordering in the system. When there is long ranged magnetic order $\langle \mathbf{m_i}.\mathbf{m_j}\rangle$ will be non-zero even when $|i-j$ becomes large. If the system has a magnetically ordered structure for some wave vector $\mathbf{Q}$ at low temperatures, $S(\mathbf{q}=\mathbf{Q})$ increases rapidly below the critical temperature T_c.

We have also calculated phonon displacement distribution.

$$P(Q) = \frac{1}{N}\sum_{i}\langle \delta(Q-Q_i)\rangle \tag{2.21}$$

In the polaronic region $P(Q)$ will be a single peaked function whereas in the bipolaronic region it will have a two peak structure.

2.3.5 Electronic properties

Density of states:

Single particle density of state $N(\omega)$ is obtained by thermal averaging different equilibrium configuration.

$$N(\omega) = \frac{1}{N}\sum_{n}\langle \delta(\omega-\varepsilon_n)\rangle \tag{2.22}$$

Here, ε_n is the eigenvalue of a single configuration.

Optical conductivity $\sigma(\omega)$:

Optical conductivity is a material property that relates an applied electric files $\vec{E}(q,\omega)$ and the electric current $\vec{J}(q,\omega)$ for a general wave vector q and frequency ω.

$$\vec{J}(q,\omega) = \sigma_{xx}(q,\omega)\vec{E}(q,\omega) \tag{2.23}$$

We are mostly interested in the long wavelength limit of the optical conductivity, which is the $\sigma_{xx}(q \to 0,\omega) = \sigma_{xx}(\omega)$. Within the linear response theory optical conductivity can be calculated using the Kubo formula.

$$\sigma_x(\omega) = \frac{\sigma_0}{N}\sum_{\alpha\beta}\frac{n_\alpha - n_\beta}{\varepsilon_\beta - \varepsilon_\alpha}|\langle\alpha|\mathbf{J}_x|\beta\rangle|^2\delta(\omega - (\varepsilon_\beta - \varepsilon_\alpha)) \tag{2.24}$$

where the current operator is

$$\vec{J} = -i\sum_{i\sigma\vec{\delta}}\left[\vec{\delta}t_{\vec{\delta}}c^\dagger_{i,\sigma}c_{i+\vec{\delta},\sigma} - h.c.\right] \tag{2.25}$$

$\varepsilon_\alpha, |\alpha\rangle$ are the eigenvalues and eigenstates of the Hamiltonian H_{eff} for a specific configuration of classical fields. σ_0 in two dimension is $\frac{\pi e^2}{\hbar}$ and $n_\alpha = f(\varepsilon_\alpha)$ is the Fermi function.

DC resistivity (ρ):

DC resistivity is obtained by taking the zero frequency limit of the optical conductivity. For a finite system the delta function in the equation (2.24) cannot be satisfied exactly for any frequency. We regularize the delta function by an average over a small frequency window. The averaged value of optical conductivity is defined as

$$\sigma_{av}(\Delta\omega) = \frac{1}{\Delta\omega}\int_0^{\Delta\omega}\sigma(\omega)d\omega \tag{2.26}$$

For a system of size N, typical level spacing is $\sim w/N$ where w is the bandwidth of the tight binding model. We have taken the value of $\Delta\omega$ of the order of the label spacing. Finite temperature resistivity is defined as :

$$\rho(T) = 1/\sigma_{av} \tag{2.27}$$

We have used $d\rho/dT > 0$ to define metallic behavior and $d\rho/dT < 0$ for an insulating one.

2.4 The attractive Hubbard model

As a lattice model for superconductivity we consider a attractive Hubbard model.

$$H = -t \sum_{\langle ij\rangle,\sigma} c^{\dagger}_{i\sigma} c_{j\sigma} - U \sum_{i} n_{i\uparrow} n_{i\downarrow} - \mu \sum_{i} n_i. \tag{2.28}$$

Here t is the nearest neighbor hopping integral (which we take to be unity to set the energy scales), U is the strength of the attractive interaction, μ is the chemical potential which fixes the total electron density. Here we fix the total electron density to be $n = 0.875$. However, we have checked that the physics remains the same if we relax this condition.

2.4.1 Auxiliary fields

We employ a Hubbard-Stratanovich transformation of this interacting, quartic Hamiltonian to reduce it to a quadratic fermionic Hamiltonian coupled to a pairing field $\Delta_i(\tau)$, which is a complex number and a charge field $\phi_i(\tau)$. The action becomes

$$S = \int_0^{\beta} \sum_{i\sigma} \left(c^{\dagger}_{i\sigma} \partial_{\tau} c_{i\sigma} + H_{kin} + H_{cl} + H_{int} \right) \tag{2.29}$$

H_{kin} is the kinetic energy of the electron and other terms are ,

$$H_{int} = \sum_{i} \left(\Delta_i c^{\dagger}_{i\uparrow} c^{\dagger}_{i\downarrow} + h.c \right) + \sum_{i} n_i \phi_i \tag{2.30}$$

$$H_{cl} = \frac{1}{U_i}\sum_i \left(|\Delta_i|^2 + \phi_i^2\right) \tag{2.31}$$

While at this level, the action is exact, to make progress, we assume that the pairing and charge fields are static (with no intrinsic quantum fluctuations), but their amplitudes and phases are site dependent. Hence, the resulting action becomes that of a quadratic fermionic problem in which fermions interact with classical fields. This will lead to an effective Hamiltonian that reads

$$\begin{aligned} H_{eff} &= -t\sum_{\langle ij\rangle\sigma} c^\dagger_{i\sigma}c_{j\sigma} - \mu\sum_i n_i + \sum_i \left(\Delta_i c^\dagger_{i\uparrow}c^\dagger_{i\downarrow} + h.c.\right) \\ &+ \sum_i \frac{|\Delta_i|^2}{U_i} - \sum_i \phi_i n_i + \sum_i \frac{\phi_i^2}{U_i} \end{aligned} \tag{2.32}$$

The partition function is:

$$Z = \int \mathcal{D}\Delta\mathcal{D}\Delta^*\mathcal{D}\phi \mathrm{Tr}_{c,c^\dagger} e^{-\beta H_{eff}} \tag{2.33}$$

The saddle point solutions of the action corresponding to this Hamiltonian gives Bogoliubov-de Gennes equation for the pairing field Δ_i and the charge field ϕ_i.

2.4.2 Bogoliubov-de Gennes transformation

We need to diagonalize the Hamiltonian H_{eff} at each Monte Carlo update. This involves the Bogoliubov-de Gennes transformation of the original fermion operator $c_{i\sigma}$ to a new fermion operator γ_n.

$$\begin{aligned} c_{i\uparrow} &= \sum_n \left(u^i_{n\uparrow} \gamma_n - v^*_{n\uparrow} \gamma^\dagger_n \right) \\ c_{i\downarrow} &= \sum_n \left(u^i_{n\downarrow} \gamma_n - v^*_{n\downarrow} \gamma^\dagger_n \right) \end{aligned} \tag{2.34}$$

$u_{i\sigma}$ and $v_{i\sigma}$ are the complete set of N eigenvectors which will diagonalize the Hamiltonian H_{eff}. These eigenvectors are such that H_{eff} can be written as :

$$H_{eff} = E_0 + \sum_n \varepsilon_n \gamma^\dagger_n \gamma_n \tag{2.35}$$

Here E_0 is a constant term and ε_n are the eigen energies of the system for a given background configuration of $\{\Delta_i, \phi_i\}$ fields. Using the above equation one can write

$$\begin{aligned} \left[H_{eff}, \gamma_n \right] &= -\varepsilon_n \gamma_n \\ \left[H_{eff}, \gamma^\dagger_n \right] &= \varepsilon_n \gamma^\dagger_n \end{aligned} \tag{2.36}$$

Above equations define an eigenvalue problem for the $u_{n\sigma}$ and $v_{n\sigma}$ and the matrix is

$$A = \begin{pmatrix} \hat{K} & \hat{\Delta} & 0 & 0 \\ \hat{\Delta}^* & -\hat{K} & 0 & 0 \\ 0 & 0 & \hat{K} & \hat{\Delta} \\ 0 & 0 & \hat{\Delta}^* & -\hat{K} \end{pmatrix} \tag{2.37}$$

where $\hat{K}$ is the modified kinetic energy part of the Hamiltonian. $\hat{K} = -t\delta_{i+\vec{\delta},j} - (\mu + \phi_i)\delta_{ij}$. $\delta_{i+\vec{\delta},j}$ is nonzero only when the sites i and j are nearest neighbors in the direction $\vec{\delta}$ and $\hat{\Delta}_{ij} = \Delta_i \delta_{ij}$.

The Eigenvalue problem is given by

$$A\Psi = \varepsilon_n \Psi \tag{2.38}$$

where Ψ is a column vector

$$\Psi = \begin{pmatrix} \{u_{n\uparrow}\} \\ \{v_{n\downarrow}\} \\ \{u_{n\downarrow}\} \\ \{v_{n\uparrow}\} \end{pmatrix} \tag{2.39}$$

The dimension of the matrix $\hat{K}$ and $\hat{\Delta}$ is $N \times N$ where $N = L^2$ for a lattice size of L. So the matrix size of A becomes $4N \times 4N$. Due to the block diagonal structure of the matrix A, one needs to diagonalize either the upper part or lower part of the matrix A. Thus the eigenvalue problem reduces to $B\Psi = \varepsilon_n \Psi$ where B and ψ are

$$B = \begin{pmatrix} \hat{K} & \hat{\Delta} \\ \hat{\Delta}^* & -\hat{K} \end{pmatrix} \tag{2.40}$$

and

$$\Psi = \begin{pmatrix} \{u_{n\uparrow}\} \\ \{v_{n\downarrow}\} \end{pmatrix} \qquad \text{or} \qquad \Psi = \begin{pmatrix} \{u_{n\downarrow}\} \\ \{v_{n\uparrow}\} \end{pmatrix} \tag{2.41}$$

With this new definition of eigenvectors we also redefine the quasiparticle creation and annihilation operators. In our previous definition creation operator was γ_n where n runs from 1 to $4N$. We rename them as $\gamma_{n\uparrow}$ and $\gamma_{n\downarrow}$ where n runs from 1 to $2N$. We can rewrite the original fermion operators as

$$c_{i\uparrow} = \sum_n (u_n^i \gamma_{n\uparrow} - v_n^{i*} \gamma_{n\downarrow}^\dagger)$$

$$c_{i\uparrow} = \sum_n (u_n^i \gamma_{n\downarrow} - v_n^{i*} \gamma_{n\uparrow}^\dagger) \tag{2.42}$$

where the eigenvectors $\{u_{n\uparrow}, v_{n\downarrow}\}$ are represented as $\{u_n, v_n\}$. Due to the structure of the matrix B eigenvalues are symmetric about $\varepsilon_n = 0$. We can calculate all average values just using the eigenvectors whose eigenvalues are positive ($\varepsilon_n > 0$).

In terms of the quasiparticle operators we can write the effective Hamiltonian as

$$H_{eff} = E_0 + \sum_{n\sigma, \varepsilon_n > 0} \varepsilon_n \gamma_{n\sigma}^\dagger \gamma_{n\sigma} \tag{2.43}$$

E_0 is the ground state energy.

$$E_0 = - \sum_{in, \varepsilon_n > 0} 2\varepsilon_n |v_n^i|^2 \tag{2.44}$$

The free energy $F(\{\Delta_i, \phi_i\})$ for a given configuration of $\{\Delta_i, \phi_i\}$ can be calculated after integrating the quasiparticle degrees of freedom.

$$F(\{\Delta_i, \phi_i\}) = - \sum_{in, \varepsilon_n > 0} 2\varepsilon_n |v_n^i|^2 - \frac{2}{\beta} \sum_{n, \varepsilon_n > 0} \ln(1 + \exp(-\beta \varepsilon_n)) \tag{2.45}$$

2.4.3 Monte Carlo procedure

We have employed Monte Carlo method to sample the $\{\Delta_i, \phi_i\}$ fields with Boltzmann weight $P(\{\Delta_i, \phi_i\}) = \exp(-\beta F)$ for any configuration. At finite temperatures, this still leaves us with the problem of thermally averaging over their most probable configurations, which we do using a Monte Carlo estimation of their weights. We start with a random configuration of the auxiliary fields and diagonalise the Hamiltonian and use the Monte Carlo algorithm discusses in the previous section for updating. The equilibrium configurations are averaged over to calculate thermodynamic properties, as well as the spectral properties of the electrons and the transport. This method severely restricts the system size to give any meaning full results. This is circumvented using a traveling cluster algorithmic which the fermion problem is diagonalised for

a smaller cluster around the chosen MC update site, embedded in a much larger lattice. The cluster moves during every MC update restoring the ergodicity.

2.4.4 Auxiliary Field properties

Below the superconducting critical temperature (T_c), we expect the coherence of Cooper pairs through out the system. We can infer this long range order from the correlation function $M_{ij} = \langle (c_{i\downarrow} c_{i\uparrow})(c^{\dagger}_{j\uparrow} c^{\dagger}_{j\downarrow}) \rangle$. At the mean field level Δ_i is the average value of the $(c_{i\downarrow} c_{i\uparrow})$. So at low temperature there will be a long range order of the Δ_i fields and Δ_i correlation function $\langle \Delta_i \Delta_j \rangle$ should behave as M_{ij}.

The structure factor of the Δ_i fields is defined as,

$$S(\mathbf{q}) = \frac{1}{N^2} \sum_{ij} \Delta_i \Delta_j^* e^{i(\mathbf{r}_i - \mathbf{r}_j).\mathbf{q}} \tag{2.46}$$

For our problem we expect the superconducting ground state to be one with a $s-$wave symmetry. Phase coherence of a $s-$wave superconductor implies a large of $S(\mathbf{q})$ for $\mathbf{q} \to 0$. So $S(\mathbf{q} = 0)$ measures the global phase coherence of the system. At high temperatures the phase of the Δ_i fields is random so on the average $S(0)$ will be vanishingly small. However, as we lower the temperature, below a certain temperature, phase coherence starts to establish and $S(0)$ increases and saturates to $\mathcal{O}(1)$ as $T \to 0$. The temperature at which $S(0)$ increases is identified as the critical temperature of the superconducting transition.

2.4.5 Electronic Properties

- **Density of states**

Single particle electronic density of states can be written as

$$N(\omega) = \sum_{n,i} \left(|u_i^n| \delta(\omega - \varepsilon_n) + |v_n^i|^2 \delta(\omega + \varepsilon_n) \right) \tag{2.47}$$

For a finite system, there are finite number of quasiparticle energy states. We need to regularize the δ function. We choose a box function which is defined as

$$\delta(x) = \begin{cases} \frac{1}{2a} & \text{if } |x| < a \\ 0 & \text{if } |x| > a \end{cases} \tag{2.48}$$

We have taken a to be of the order of the average label spacing w/N where w is the bandwidth of the tight binding model. We calculate $N(\omega)$ for a give configuration of $\{\Delta_i, \phi_i\}$ and average over many configuration.

2.5 Benchmarking

In this section we apply the static auxiliary field method to three models for benchmarking. The results obtained establishes the utility of the present approach.

2.5.1 The Hubbard model at half filling

This model does not have a metallic ground state[68–70] for any nonzero value of U and has long range AF order in the ground state. For small U, a Slater instability results due to nesting of the Fermi surface and the system is a spin density wave with a gap in the spectrum. For large U, the physics of super exchange takes over, due to the "no double occupancy constraint" and the resulting kinetic energy reduction due to virtual hopping. The system is a Mott-Hubbard insulator with local moments present whose low energy properties are governed by the anti-ferromagnetic Heisenberg model. The magnetic transitions resulting from these two behaviors

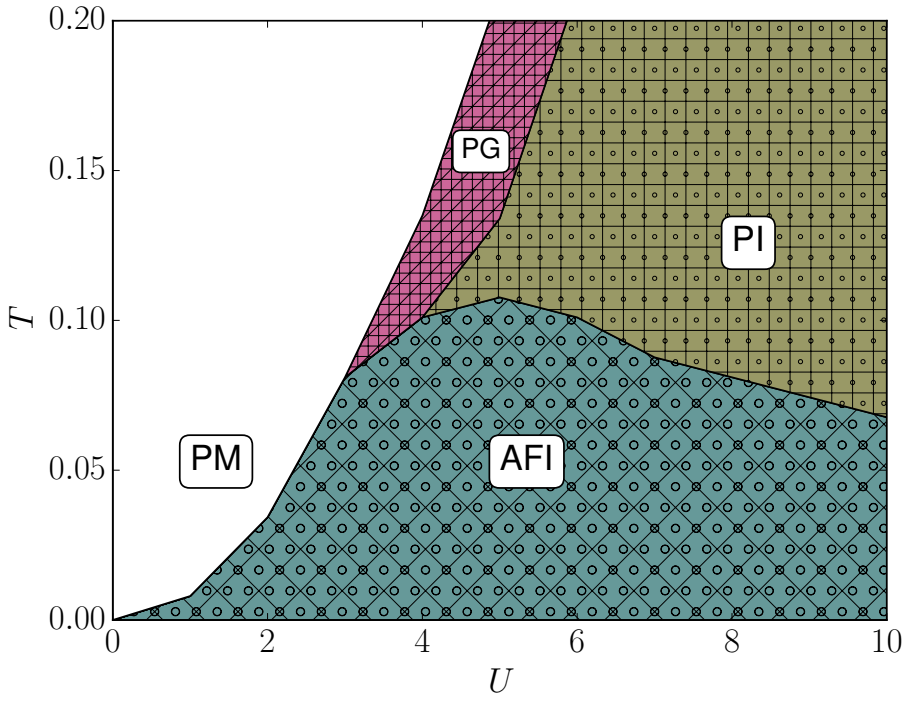

Figure 2.2: The phase diagram of the Hubbard model on a two dimensional square lattice at half filling. AFI, PM, PI, PG represent antiferromagnetic insulator, paramagnetic metal, paramagnetic insulator and pseudogap phases.

have very different U dependence. At small U , T_N scales with U as expected in an unrestricted HF treatment. However, at large U, $T_N \sim (1/U)$ due to Mott physics. The present method captures both these behaviors very well. The finite temperature phase diagram also looks qualitatively different from the HF phenomenology. While for small U, the Slater gap closes at T_N leading to a metallic paramagnetic state, there is a pseudogap state that appears at intermediate values which crosses over to a paramagnetic Mott-Hubbard insulating state at large U. The paramagnetic state has strong AF fluctuations, especially in the intermediate range of the coupling constant which results in pseudogap features in the spectral function. We give the phase diagrams in $U-T$ planes in Fig. (2.2).

Single particle spectrum

As we said earlier this model does not have metallic ground state. Fig. (2.3) shows single particle density of state for two values of U. In the weak coupling region ($U = 2.0$) system shows

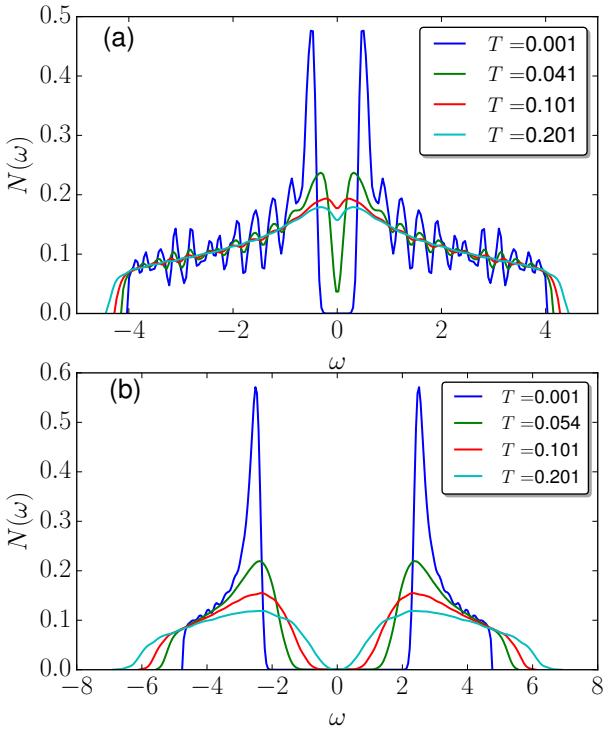

Figure 2.3: Temperature dependence of single density of state for Hubbard model for different values of U. Upper panel shows for $U = 2.0(a)$ and lower panel for $U = 6.0$. The lower temperature oscillation of density of state is a artifact of finite system size.

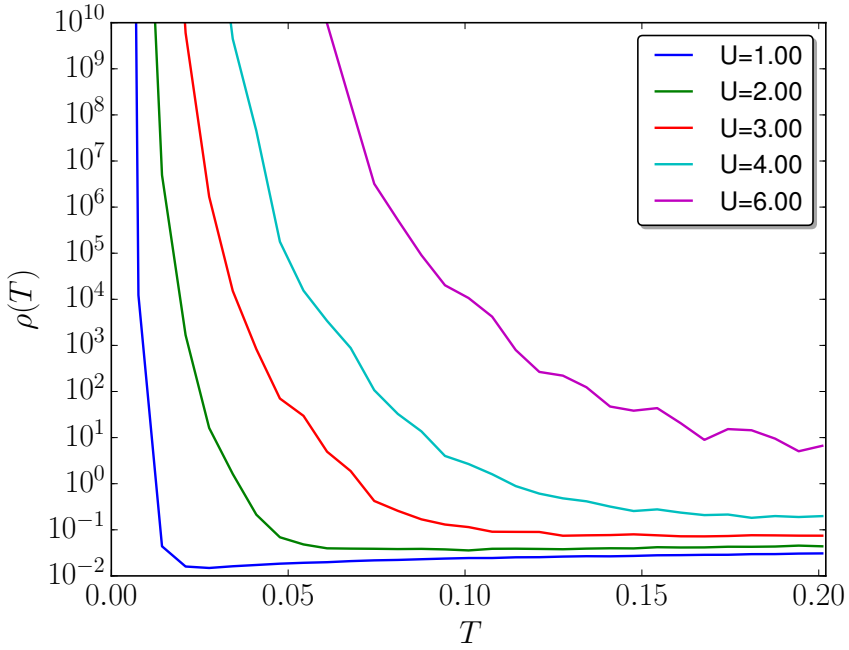

Figure 2.4: The resistivity, $\rho(T)$, in the unit of $h/(\pi e^2)$ shows metal insulator transition (MIT) for different U.

antiferromagnetic long range order and density of state becomes gapped at low temperatures. Gap decreases with increasing temperature and vanishes at the antiferromagnetic transition temperature, T_N.

Density of states displays very different characteristics at strong coupling region for $U = 6$. At low temperature it has a very large gap. This gap decrease with increasing temperature similar to the weak coupling behavior but it does not vanish at the critical temperature. The gap in the density of states disappears only at very high temperatures (of the order of U).

Resistivity

We can clearly see an insulator-metal transition for lower values of U as a function of temperature . At high temperature it has a metallic behavior and in the low temperature region it become a insulator. In the insulating side temperature dependence of resistivity can be written as $\rho(T) \propto \exp(E_g/T)$ where E_g is the order of the gap in density of state. Fig. (2.4) also shows that metal-insulator transition temperature also increases with U.

2.5.2 The Holstein model at half-filling

This model again does not have a metallic ground state for any nonzero V. For small V, there is a Peierls instability leading to a charge density wave due to nesting, with a gap in the spectrum. At finite temperatures, the gap shrinks and vanishes at T_{CDW} above which the system is metallic. As V increases, the ground state of the system evolves through this charge ordered state resulting in a bipolaronic insulator at large V. This can be understood due to a mechanism similar to super-exchange for the spins. Since U is absent, there is no energy cost for double occupancy and a bipolaronic state lowers the energy through virtual fluctuations of charge. In this limit the physics can be described using a nearest neighbor interaction model, *i.e.*, $H = \alpha \sum_{\langle ij \rangle} n_i n_j$

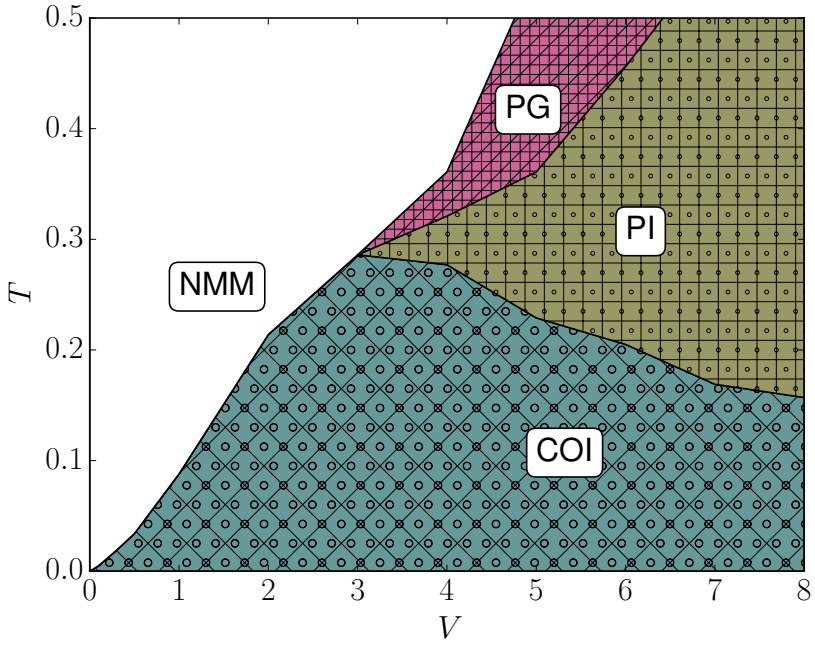

Figure 2.5: The phase diagram of the Holstein model on a two dimensional square lattice at half filling. CO, NMM, PI, PG represent charge ordered insulator, nonmagnetic metal, bipolaronic insulator and pseudogap phases.

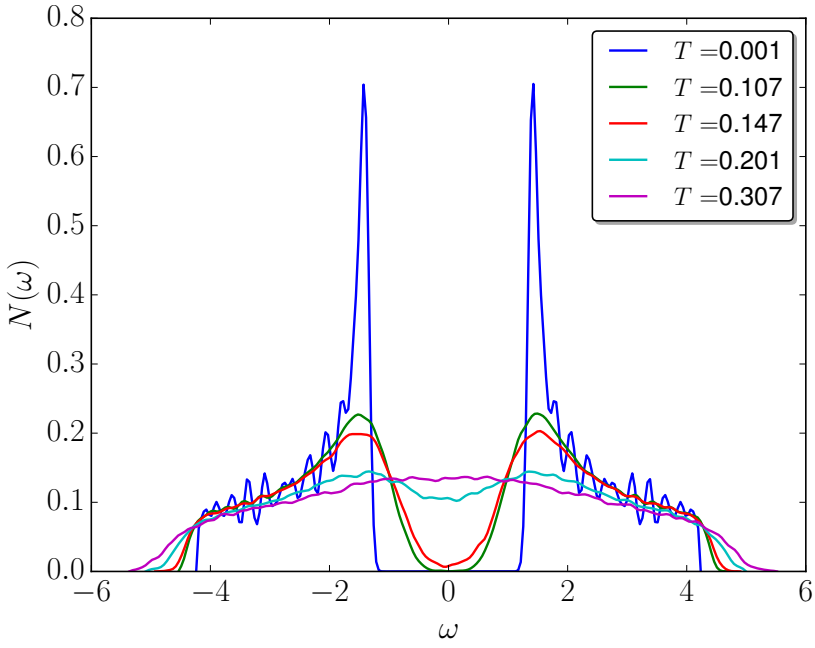

Figure 2.6: Density of state for Holstein Model for different temperature at $V = 2.0$.

where $\alpha \sim (1/V)$ and hence the charge ordering temperature goes as $(1/V)$. At intermediate values of V, a pseudogap phase intervenes which has spectral and transport features similar to the one previously mentioned. The finite temperature, large V phase is insulating with charges remaining as bipolarons, but losing their long range order. The spin degrees of freedom are passive in the entire phase diagram and the magnetization vanishes. We give the phase diagrams in $V-T$ planes in Fig. (2.5). CDW transition temperature increase with V. With increasing temperature system goes from an insulating state to a metallic state near the CDW transition temperature. However, in the strong coupling limit new energy scale emerges and $T_{CDW} \propto 1/V$. T_{CDW} decreases with V for large values V and there is a temperature window in between $1/V$ and V where spectrum is gapped even in the absence of any CDW order.

Density of state

We have shown the temperature evolution of density of states in the Fig. (2.6) for $V = 2$. Density of states shows a gap in the spectrum at lowest temperature due to the onset of charge density wave. The gap in the density of state decreases with increasing temperature.

2.5.3 The attractive Hubbard model and BCS-BEC crossover

We will now discuss the attractive Hubbard model on a two dimensional square lattice

$$H = \sum_{\langle ij \rangle \sigma} t_{ij} c^{\dagger}_{i\sigma} c_{j\sigma} - |U| \sum_{i} n_{i\uparrow} n_{i\downarrow} \tag{2.49}$$

This model has a superconducting ground state at all values of U. In the weak coupling limit ($U \ll t_{ij}$) it shows a standard BCS superconducting state whereas in the strong coupling limit ($U \gg t_{ij}$) it has a Bose-Einstein condensation (BEC) of local pairs. Due to the small value of binding energy in the weak coupling limit, Cooper pairs have very large size and have strong overlap amongst them. In the opposite limit of strong interactions, size of the Cooper pairs becomes very small and they can be thought of as charged Bosons. In this limit global super-

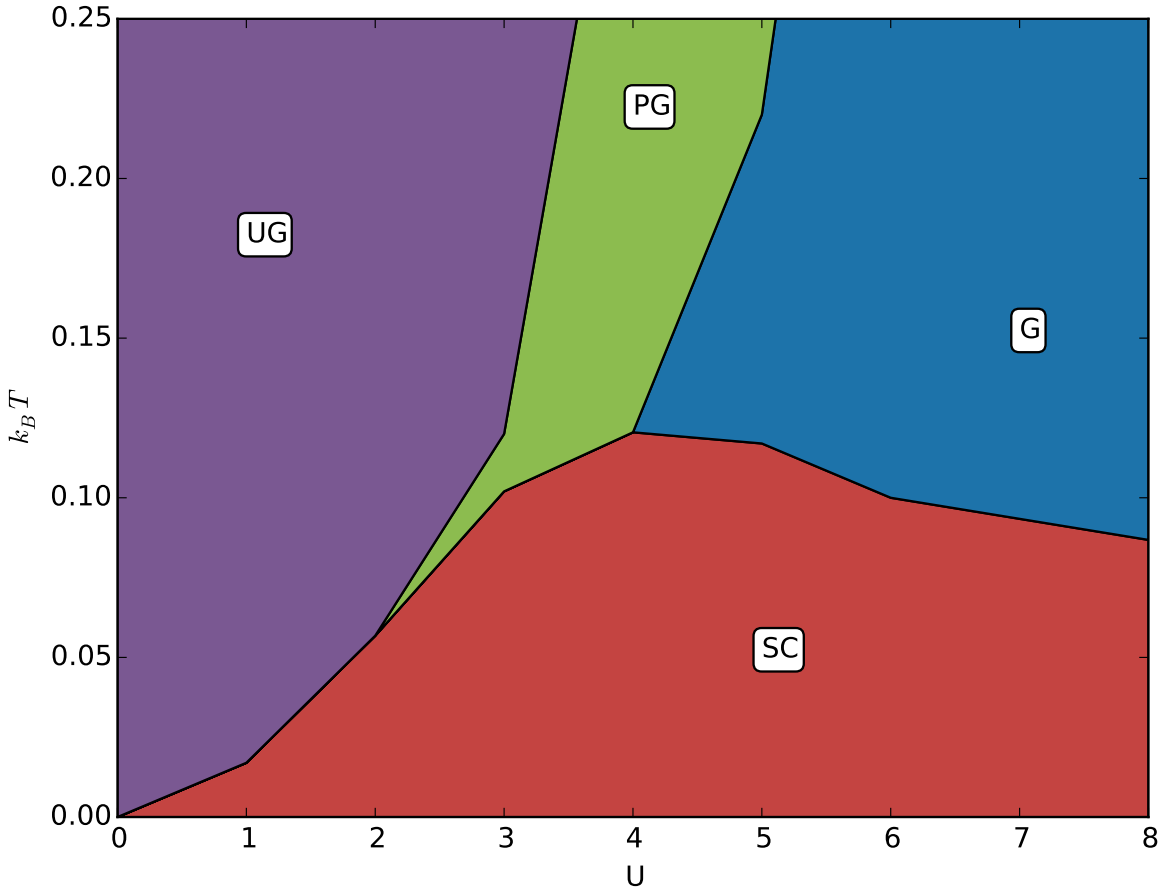

Figure 2.7: Phase diagram of attractive Hubbard Model in the $U - T$ plane.

conductivity arises not because of formation of Cooper pairs as it happens in the weak coupling limit. Superconducting transition temperature (T_c) is determined by the superfluid transition which is related to the Bose condensation of the electron pairs. In this region T_c is not determined by the breaking of the Cooper pairs which is of the order of gap in the spectrum. Global superconductivity sets in when the phase coherence appears in the condensate and the T_c scale is determined by the superfluid stiffness.

Fig. (2.7) shows the different phases of the attractive Hubbard Model. In the weak coupling region there is a transition from the ungapped (UG) state to superconducting (SC) state at low temperatures. Pseudogap(PG) features appear in the intermediate coupling due thermal

fluctuations of the order parameter. In the strong coupling region the system goes to a non-superconducting, gaped(G) state above the superconducting transition temperature.

Chapter 3

Hubbard-Holstein Model on a square lattice

3.1 Introduction

Several materials, notably transition metal oxides[6], exhibit strong Coulomb interactions among their constituent electrons[71] as well as strong coupling between electrons with the underlying lattice[30]. Interplay of such competing many body interactions often leads to emergence of effective energy scales and various broken symmetry phases and transitions among them, giving rise to significant changes in their low energy behavior[72, 73]. Understanding the combined effect of these two is a challenging problem and there has been some remarkable progress in the last couple of decades. Some of the systems that are known to have both these interactions playing a role include high T_c superconducting cuprates[74–78], alkali doped fullerides[79–81], bismuthates[82, 83], and most notably doped manganites[84, 85]. The electron-phonon interaction can give rise to instabalities of the metallic state *e.g.,* to charge density wave and conventional superconductivity. Effective mass of the electrons in a metallic system can increase in many fold in the presence of $e-ph$ interaction due to strong polaronic effects. Electrical resistivity have contribution from the electron-phonon interaction in metal and semiconductor. They also contribute to the optical absorption in indirect-gap semiconductor. $e-ph$ interaction helps to thermalize hot electrons and distort the band structure. This leads to characteristic kinks and

Kohn anomalies in photoemission and Raman and neutron spectra . In cuprates strong $e-e$ interaction is responsible for the Mott insulating state in the undoped region and also related to the linear temperature dependence of the resisitivity in doped samples. Phonon was not visible in early experimental setups and believed that phonon does not play any role in Cuprates. However various experiments such as isotopic effects , polaronic spectroscopic features in underdoped cuprates confirms the presence of $e-ph$ interaction.

In cuprates[74, 86], kinks observed in ARPES are believed to be features arising from strong electron-phonon coupling which also give rise to prominent features in inelastic neutron scattering and tunneling. The system also has strong electron-electron interactions as evidenced by the Mott insulating state of the parent compound. In fullerides, an antiferromagnetic phase stabilized by Coulomb interactions, evolves to an *s*-wave superconducting state and it is believed that phonon effects are likely to be present. In doped bismuthates, a charge density wave[87] transforms to a *s*-wave superconducting state upon doping; valence skipping arising due to Coulomb interactions and coupling of charge carriers to breathing mode phonons are believed to be responsible for the behavior. Manganites[88–90] present the most compelling case where orbitally degenerate electrons experience strong Mott-Hubbard interactions and are also coupled to octahedral symmetry lifting Jahn-Teller phonon modes. It is being realised that conventional way of treating only one of the interactions is inadequate for a proper understanding of these materials.

The Holstein-Hubbard Model [61, 91–104] is the simplest starting point to theoretically explore the combined effect of these two interactions. It describes a single-band electron coupled to an Einstein phonon mode. The Coulomb interaction is modeled by an on-site Hubbard term capturing the energy cost when two electrons of opposite spins are present at a given site. In real systems, this model could be an oversimplification. There could be multiple orbitals relevant[105] as in manganites, leading to inter- and intra- Coulomb matrix elements.

There could also be multiple phonon modes involved as happens in Jahn-Teller systems[14]. However, general features, leaving out specifics such as orbital ordering, would be very well captured by the simplest model itself. For example, on a two dimensional square lattice at half filling, the Hubbard interaction is expected to give rise to a weak coupling spin density wave transforming to a local moment antiferromagnetic Mott-Hubbard insulator at strong coupling accompanied by a metal-insulator transition at finite temperatures[68, 106]. On the contrary, the Holstein interaction promotes coexisting charge density wave and superconducting ground states, if phonon dynamics is retained. However, for static phonons, it is expected that a weak coupling charge density wave state would crossover to a bipolaronic insulator at strong coupling. Obviously, these phases will compete strongly when both interactions are present. Motivated by this, there has been several studies in recent years. These include analysis of various aspects of the problem using Migdal-Eliashberg theory[94], quantum Monte Carlo[94, 107], Exact diagonalisation[108, 109], variational treatments[110] such as Gutzwiller approximation for correlation, and dynamic mean field [92, 111–114] theory. In particular, Bauer and Hewson[113] studied the ground state of the model at half filling using DMFT[98, 115–118] in conjunction with numerical re-normalization group[119, 120]. A recent study[92] using dynamical mean field theory with continuous time quantum Monte Carlo as an impurity solver has brought out several interesting features . These include strong re-normalization of superconducting T_c and the emergence of a paramagnetic metallic phase in the weak coupling limit. While DMFT is by far one of the most reliable tools to study strongly correlated systems, it has certain limitations. It is exact in infinite dimensions or when coordination number is large; however the theory being a local one does not capture the full real space features. If the system has geometrical constraints or frustration, a local theory will not be able to shed light on features intrinsic to them. It is also not possible to include disorder in any meaningful way since crucial features of interference cannot be captured in a single site theory. Some new techniques are needed to overcome these problems and complement DMFT in cases mentioned above. While

such methods too will have their own limitations, range of applicability, they may be able to explore systems that DMFT cannot handle, especially when they are bench-marked in known cases. We use such a method to explore the problem at hand.

The method[12, 68, 69, 106, 121–124] includes rewriting the quartic fermion interaction in terms of auxiliary fields corresponding to charge and spin degrees of freedom. However, the resulting problem is still a many body one, albeit with new fields. To simplify matters, we concentrate on the static part of these fields[123, 124] and also assume that the phonons are static. This results in a problem of a single band electron moving in the background of three classical fields : the charge and magnetisation auxiliary fields and lattice displacements. At any temperature, the statistically significant configurations of classical fields can be sampled employing a Monte Carlo (MC) procedure[66, 75]. The electron problem can be solved by exact diagonalisation. The method captures both weak and strong coupling regimes as described in Section III.

We find that when only the Hubbard interaction is present, the system evolves from a Slater[125] to a Mott insulator[6] with non monotonic variation of the Neel temperature. When only the lattice coupling is present, it transforms from a weak coupling charge density wave[87] to a bipolaronic insulator at strong coupling. When both are present, a critical line separates the two phases. At finite temperatures, the disordered phase appears to be metallic at weak coupling, but insulating at strong coupling. However, at intermediate coupling significant pseudogap features appear[70] in the spectral function that modifies response of the electronic system such as optical transport in a significant way

In Section II, we describe the model in detail and the method employed. Section III is devoted to bench-marking with previous studies when only one of the interactions is present. In the next section, we give the ground state (low temperature) phase diagram of the model result-

ing from the present study, followed by a detailed finite temperature analysis of the electronic properties. Finally we conclude, describing the limitations of the method, advantages it has, and spell out future plans.

3.2 Model and the static auxiliary field method

As mentioned earlier, we look at the simplest model of a one-band electronic model coupled to a single mode Einstein phonon with the Coulomb interaction assumed to be local. The Hamiltonian is given by

$$\begin{aligned} H &= H_{tb} + H_{Hubbard} + H_{el-ph} + H_{ph} \\ H_{tb} &= -t \sum_{\langle ij \rangle, \sigma} c^{\dagger}_{i\sigma} c_{j\sigma} + h.c. \\ H_{Hubbard} &= U \sum_{i} n_{i\uparrow} n_{i\downarrow} \\ H_{ph} &= \sum_{i} \frac{\mathbf{p}^2}{2m} + \frac{K}{2} \sum_{i} \mathbf{Q}^2 \\ H_{el-ph} &= g \sum_{i} (n_i - \langle n_i \rangle) \mathbf{Q}_i \end{aligned} \tag{3.1}$$

Here H_{tb} is the kinetic energy of the electronic system with t being the hopping parameter, c_i being an electron destruction operator at site i, and $\langle ij \rangle$ representing the nearest neighbors j of site i. U is the on-site Hubbard interaction and g is Holstein electron-phonon coupling. H_{ph} is the Hamiltonian for the Einstein phonon with frequency $\omega = \sqrt{K/m}$. Since we are interested in half filling $\langle n_i \rangle = 1$. Since the classical single-site Holstein Hamiltonian has a polaronic minimum with a distortion $\rho = (g/K)$, and polaronic binding energy $E_{pol} = -\left(g^2/2K\right)$, we scale the phonon coordinate Q by ρ and phonon energies by $\left|E_{pol}\right|$. This results in a single dimensionless parameter (scaled in terms of energy unit t) for the phonon part of the Hamiltonian which we demote as V. From now on, we denote the dimensionless Hubbard interaction (in units of t) as U. We shall explore the physics of this model as functions of these two dimensionless parame-

ters.

To simplify this many body problem, we perform a Hubbard-Stratanovich (HS)[12, 121] transformation of the quartic interaction term by introducing two auxiliary fields, one each for the charge and magnetization sectors,. The scalar valued charge auxiliary field at each site is $\phi_i(\tau)$ and the vector-valued magnetization auxiliary field is $\mathbf{m}_i(\tau)$. This results in a quadratic fermion problem in which fermions move around in a (quantum mechanical, time-dependent) background of the two auxiliary fields and the phonon field which is computationally, still, a challenging problem. We make the following approximations. We assume that all the three background fields are classical and hence neglect their time-dependence. We retain their spatial dependence and do a numerically exact thermal average of their configurations at every temperature.

The partitions function is given by

$$\begin{aligned}
\mathcal{Z} &= \int \Pi_i \frac{dc_i^\dagger dc_i d\phi_i d\mathbf{m}_i}{4\pi^2 U} dQ_i \exp\left(-\int_0^\beta d\tau \mathcal{L}(\tau)\right), \\
\mathcal{L}(\tau) &= \sum_{i,\sigma} c_{i\sigma}^\dagger(\tau)\,\partial_\tau c_{i\sigma}(\tau) - t \sum_{\langle ij\rangle,\sigma} c_{i\sigma}^\dagger c_{j\sigma} \\
&+ \mathcal{L}_{cl}(\phi_i(\tau), \mathbf{m}_i(\tau)) + \mathcal{L}_{ph}, \\
\mathcal{L}_{cl} &= \sum_i \left[\frac{\phi_i^2}{U} + i\phi_i n_i + \frac{\mathbf{m}_i^2}{U} - 2\mathbf{m}_i \cdot \mathbf{s}_i\right],
\end{aligned} \tag{3.2}$$

where $\mathcal{L}_{ph}$ is the phonon Lagrangian.

We limit ourselves to half-filling, *i.e.*, one electron per site, in this paper. In spirit of it, we make a saddle point approximation for the static charge field, *i.e.*, $\phi_i \to \langle\phi\rangle = (U/2)\langle n_i\rangle = U/2$, and this is taken to be site independent.

Upon rescaling $\mathbf{m}_i \rightarrow (U/2)\,\mathbf{m}_i$, the resulting Hamiltonian reads :[106, 124]

$$\begin{aligned} H_{eff} &= -t \sum_{\langle ij\rangle,\sigma} c^{\dagger}_{i\sigma} c_{j\sigma} - \mu_{eff} N - \frac{U}{2}\sum_i \mathbf{m}_i \cdot \vec{\sigma}_i + \frac{U}{4}\sum_i \mathbf{m}_i^2 \\ &+ V\sum_i (n_i - \langle n_i\rangle)\, Q_i + V\sum_i Q_i^2 \end{aligned} \tag{3.3}$$

where $\mu_{eff} = \mu - U/2$ with the partition function being given by

$$\mathcal{Z} = \int \mathcal{D}\mathbf{m}\mathcal{D}Q\mathcal{D}\left[c^{\dagger}, c\right] \exp\left(-\beta H_{eff}\right). \tag{3.4}$$

For a given configuration of Q_i and $\mathbf{m}_i$, the Hamiltonian (quadratic in fermions) need to be diagonalised just once. However, one needs to sample most probable configurations of both Q_i and $\mathbf{m}_i$ at every temperature and they have to be determined from corresponding distributions :

$$P(Q_i) = \frac{\int \mathcal{D}\mathbf{m} Tr_{c,c^{\dagger}} e^{-\beta H_{eff}}}{\int \mathcal{D}\mathbf{m}\mathcal{D}Q Tr_{c,c^{\dagger}} e^{-\beta H_{eff}}} \tag{3.5}$$

$$P(\mathbf{m}_i) = \frac{\int \mathcal{D}Q Tr_{c,c^{\dagger}} e^{-\beta H_{eff}}}{\int \mathcal{D}\mathbf{m}\mathcal{D}Q Tr_{c,c^{\dagger}} e^{-\beta H_{eff}}} \tag{3.6}$$

While it appears that the neglect of time dependent effects reduces this method to unrestricted Hartree-Fock for the ground state, it retains the full classical thermal fluctuations in an unbiased way which leads to significant changes from HF results at finite temperature and smoothly interpolates between known limits at weak and strong coupling.

The probability distribution functions appearing above are not exactly calculable since they involve tracing over fermions and integrating over all static configurations of the classical fields. We generate the equilibrium configurations for the classical field self-consistently using a Monte Carlo method[88]. This is achieved by starting with a given set of configurations, and attempting an update which requires diagonalising the fermion Hamiltonian and generating most probable configurations using the standard MC method. However, this severely restricts the system size

of the problem, even though the fermionic part is quadratic. To explore higher system sizes, we use a traveling cluster algorithm[66], in which a small cluster around the reference site is diagonlized and energy cost evaluated for MC update. During the MC procedure, as the reference site keeps moving on the lattice, so does the cluster. The results presented in this paper employ a cluster size of 8×8 and the largest system size used is 32×32. Once the system reaches equilibrium, we evaluate thermal averages of structure factor for charge density and magnetization.

$$N(\mathbf{q}) = \frac{1}{N^2}\sum_{ij}\left\langle n_i n_j \right\rangle e^{i\mathbf{q}\cdot\left(\mathbf{R}_i-\mathbf{R}_j\right)} \tag{3.7}$$

$$S(\mathbf{q}) = \frac{1}{N^2}\sum_{ij}\left\langle \mathbf{m}_i \cdot \mathbf{m}_j \right\rangle e^{i\mathbf{q}\cdot\left(\mathbf{R}_i-\mathbf{R}_j\right)} \tag{3.8}$$

Spectral and transport properties for the fermion system have also been evaluated in thermal equilibrium which is described in Section V.

3.3 Exploring the Hubbard and Holstein Physics

In this section, we present the phase diagram of the model for the individual cases when either the Holstein term is absent (the Hubbard model), and when the Hubbard term is absent (the Holstein model). Both these problems have been studied extensively in the past and it will help us benchmark our results.

When the Holstein term is absent, the model reduces to a single band Hubbard model on a two dimensional square lattice at half filling. This does not have a metallic ground state[68–70] for any nonzero value of U and has long range AF order in the ground state. For small U, a Slater instability results due to nesting of the Fermi surface and the system is spin density wave with a gap in the spectrum. For large U, the physics of super exchange takes over, due to the ”no dou-

ble occupancy constraint" and the resulting kinetic energy reduction due to virtual hopping. The system is a Mott-Hubbard insulator with local moments present whose low energy properties are governed by the anti-ferromagnetic Heisenberg model. The magnetic transitions resulting from these two behaviors have very different U dependence. At small U the T_N scales with U as expected in an unrestricted HF treatment. However, at large U, $T_N \sim (1/U)$ due to Mott physics. The present method captures both these behaviors very well. The finite temperature phase diagram also looks qualitatively different from the HF phenomenology. While for small U, the Slater gap closes at T_N leading to a metallic paramagnetic state, there is a pseudogap state that appears at intermediate values which crosses over to a paramagnetic Mott-Hubbard insulating state at large U. The paramagnetic state has strong AF fluctuations, especially in the intermediate range of the coupling constant which results in pseudogap features in the spectral function.

We now consider the case when the Hubbard term is absent, resulting in the half filled Holstein model on a two dimensional square lattice. This model again does not have a metallic ground state for any nonzero V. For small V, there is a Peierls instability leading to a charge density wave due to nesting, with a gap in the spectrum. At finite temperatures, the gap shrinks and vanishes at T_{CDW} above which the system is metallic. As V increases, the ground state of the system evolves through this charge ordered state resulting in a bipolaronic insulator at large V. This can be understood due to a mechanism similar to super-exchange for the spins. Since U is absent, there is no energy cost for double occupancy and a bipolaronic state lowers the energy through virtual fluctuations of charge. In this limit the physics can be described using a nearest neighbor interaction model, *i.e.*, $H = \alpha \sum_{\langle ij \rangle} n_i n_j$ where $\alpha \sim (1/V)$ and hence the charge ordering temperature goes as $(1/V)$. At intermediate values of V, a pseudogap phase intervenes which has spectral and transport features similar to the one previously mentioned. The finite temperature, large V phase is insulating with charges remaining as bipolarons, but losing their long range order.The spin degrees of freedom are passive in the entire phase diagram and the

magnetization vanishes. We give the two phase diagrams in $U-T$ and $V-T$ planes in Fig. (3.1).

In passing, we wish to point out that the above results are indeed not exactly what is expected in two dimensions since there cannot be any finite-temperature transitions. These results should be taken as suggestive of what would happen in higher dimensions or as crossover scales where correlation lengths increase rapidly. (See the concluding section.) Further, we characterize the pseudogap phase as one in which the density of states does not have any perceptible hard gap, but has a dip at the chemical potential, suggesting a dramatic decrease of the low-energy spectral weight. There is no real phase transition occurring here. It should be thought of as a crossover to a region where the density of state appears quite different from that of an insulator with a hard gap.

3.4 Ground state properties and Phase Transitions

Having clarified the trends that one obtains for the Hubbard and Holstein interactions separately, we now proceed to discuss the results for the full problem. However, in this section, we will concentrate on the ground state properties and the nature of the phase transitions at finite temperatures. This includes the $U-V$ phase diagram at $T=0$, spectral functions of the fermions, probability density functions for the lattice variables, and charge and magnetisation field configurations in real space. The above information would help us correlate various trends and elucidate the physics that emerges. As the phases change while changing parameters, we will see that correlated changes occur in properties of the fermionic, phononic, and auxiliary field variables.

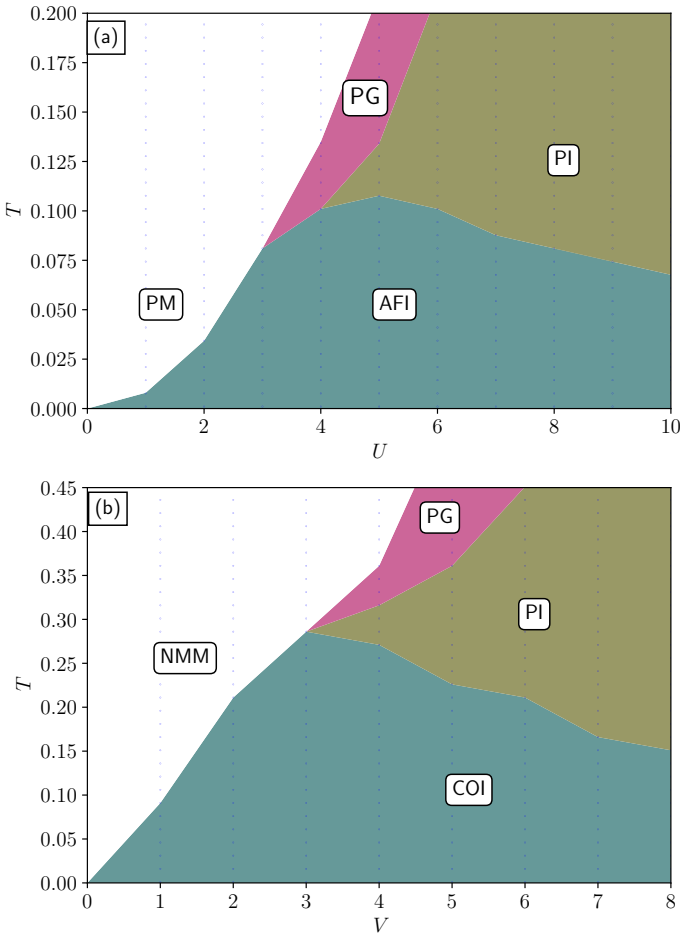

Figure 3.1: (a) The phase diagram of the Hubbard model on a two dimensional square lattice at half filling. AFI, PM, PI, PG represent antiferromagnetic insulator, paramagnetic metal, paramagnetic insulator and pseudogap phases. (b) The phase diagram of the Holstein model on a two dimensional square lattice at half filling. CO, NMM, BPI, PG represent charge ordered insulator, nonmagnetic metal, bipolaronic insulator and pseudogap phases.

In Fig. (3.2) we present the ground state phase diagram of the Holstein-Hubbard model as a function of U and V. As expected the results along the horizontal and vertical axes (corresponding to cases when one of the parameters is absent) confirm to the discussion in the previous section. The phase diagram is almost entirely dominated by insulating regions. This is not surprising since individually, each interaction tries to localize electrons giving rise to a band/Mott/bipolaronic insulator. In the intermediate[92, 95] to large values of the scaled parameters, there is a transition between a charge disordered magnetic insulator to a charge ordered nonmagnetic insulator. For example, at large values of U, an otherwise MI in absence of Holstein interaction, transforms to a BPI as V increases. This is a result of the two competing interactions. While a large U tries to localize individual electrons at every lattice site at half filling, the Holstein interaction develops bipolaronic instability as discussed in the last section. When the energy scales become comparable, the system develops an instability and moves from one to the other..Notice that the spin structure factor at (π,π) is nonzero in AF phase, $S(\mathbf{q}) = 0$ in BPI phase signaling a nonmagnetic state. Similarly, the charge structure factor has a peak at $\mathbf{q} = (0,0)$ in AF phase, the modulation vector changes to (π,π) in BPI phase. At intermediate values of U and V this behavior persists for both the structure factors but is much less pronounced compared to the strong coupling limit. This is the crossover regime between the Slater-MHI due to Hubbard correlations and Peierls-BPI crossover due to Holstein interaction. Fig. (3.3) depicts trends of both the structure factors as a function of U and V and confirms our conclusion about the transitions. However, there exists a thin sliver of window in the $U-V$ plane at low interaction strengths where the system is metallic. This is in contrast to the case where the system is insulating when only one of the interactions is present This behavior is exemplified in Fig. (3.3) where structure factor at these values are plotted. A metallic phase appears in the weak coupling region where the effect of the competition becomes stronger. This metalic phase has a finite DoS at the Fermi energy. Optical conductivity shows Drude like be-

havior (shown in Fig (3.7)) . This metallic state is susceptible to charge or spin ordered state at low enough temperature. Close to zero temperature our method becomes equivalent to the mean-field theory. At zero temperature within mean-field theory system develop a gap in the DoS due to magnetic or charge ordering. This metallic behavior has been observed in previous studies of this model employing DMFT[92, 95] using continuous time QMC and NRG as impurity solvers. This unexpected metallic phase results from the fact that while the nesting[87, 125] at half filling in the two dimensional tight binding model supports magnetic or charge ordering instabilities separately, the competing interactions have a destructive effect on the transition since it frustrates different degrees of freedom, *viz.*, charge and spin in our case. The energy gained by a small mean field gap opening up in either channel is not sufficient to lower the absolute ground state energy when the other channel is included. This phase, in fact, brings out the true competition between the two interactions, where one acts predominantly over the spin sector while the other over the charge sector. Further, notice that the phase boundaries merge to zero values of both parameters in our case in contrast to DMFT results. This is easily understood since, our exact numerical method preserves the nesting instability of the two dimensional non-interacting electron system whereas methods such as DMFT ignore them.

The structure of Fermi surface of the free electron can give rise to magnetic instability in the system. Tight binding square lattice has a nested Fermi-surface namely $\varepsilon_{k+Q} = \varepsilon_k$ for $Q = (\pi, \pi)$. The non-interacting susceptibility diverges at this momentum(Q) and a small finite repulsive interaction give rise a magnetic ordered ground state. Introduction of the t' destroys this nesting properties and introduces frustration in the system. local interaction such Hubbard U can give rise to magnetic ground state at a critical U_c. There other way one can introduce frustration in the system. Strong long range interaction can also give rise competing magnetic interaction. Tendency towards a magnetic ordered state becomes weaker away from the commensurate filling factor.

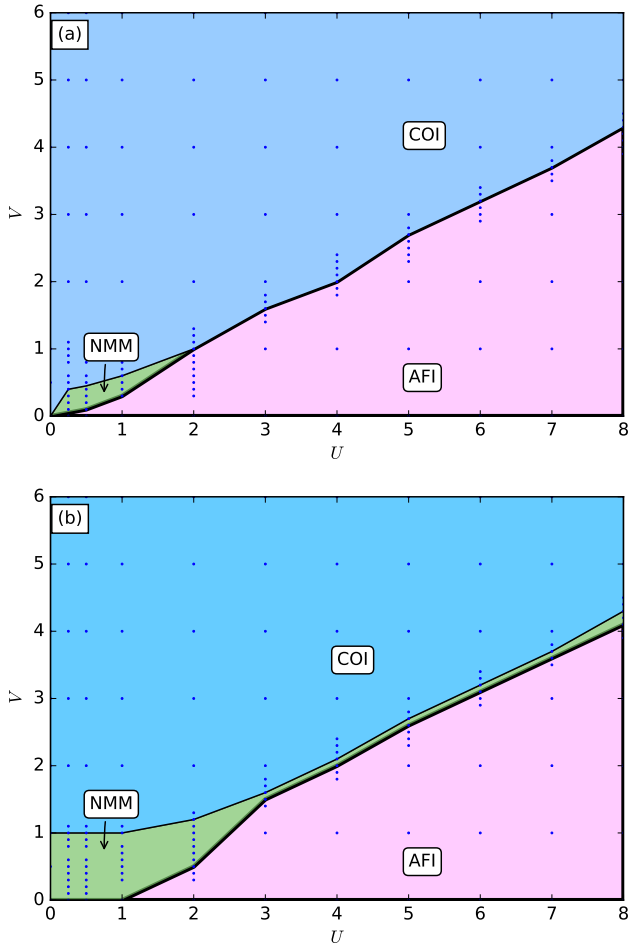

Figure 3.2: The ground state and finite temperature phase diagram of the Holstein-Hubbard model as a function of scaled parameters U and V. AFI, COI, NMM represent antiferromagnetic insulating, charge ordered insulating and nonmagnetic metal phases. The transition between AFI and COI is a weak first order one. The temperatures are (a) $T = 0.001$ and (b) $T = 0.050$

The MC procedure allows us to track the PDF of the phonon displacement variables across the transitions/crossover which is plotted in Fig. (3.4). In the AF phases we see that $P(Q)$ is a unimodal function peaked at $Q = 0$, which implies that while every lattice site is distorted, it accommodates at most one electron per site. The distribution grows sharper as we grow from Slater to Mott limit, but the unimodal nature does not change. In this limit, Hubbard correla-

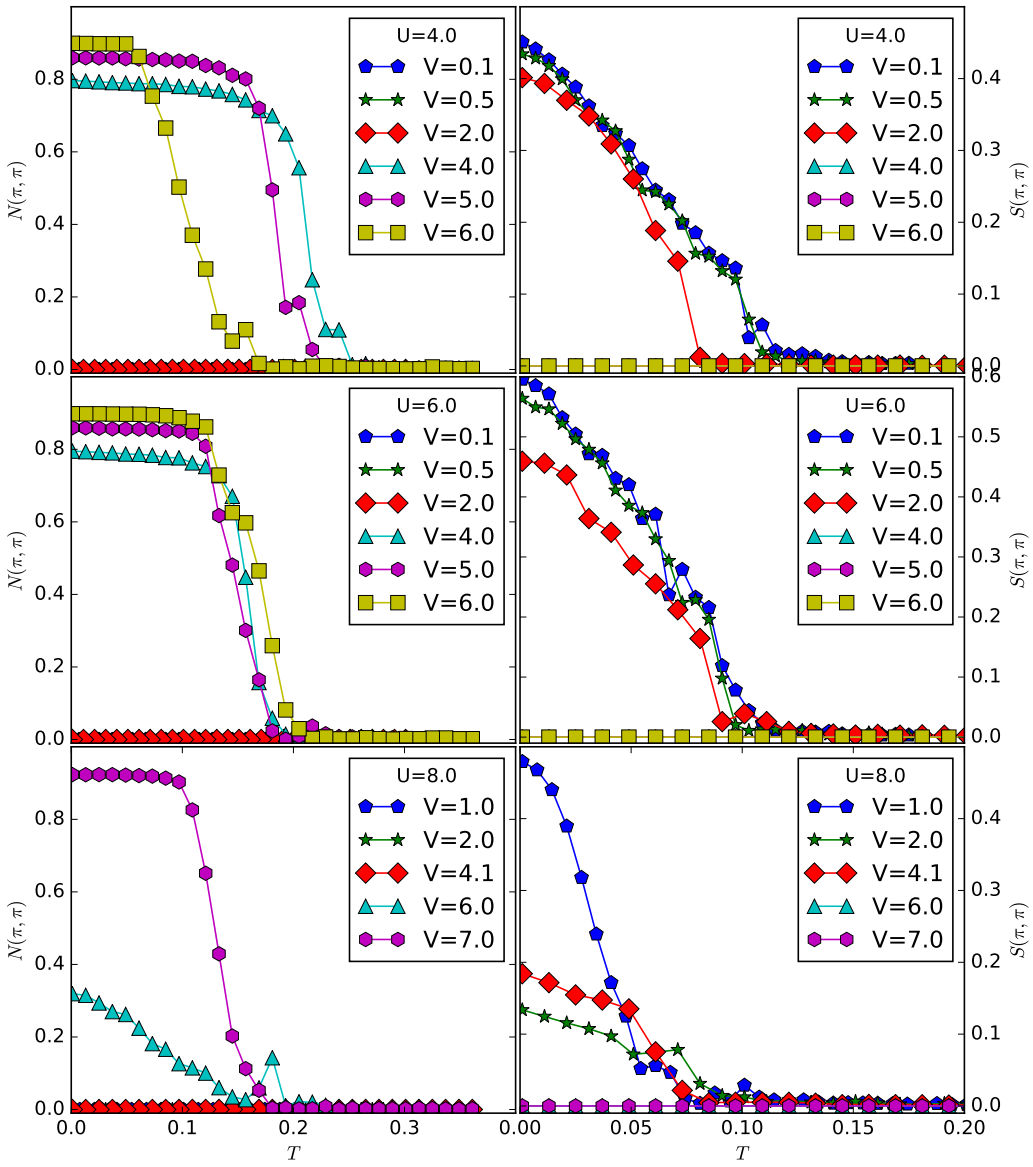

Figure 3.3: Temperature versus structure factor corresponding to charge density wave $N(\pi,\pi)$(left) and anti-ferromagnetic $S(\pi,\pi)$(right) structure factor.

tions play a larger role and the system tries to reduce the maximum number of electrons to one per site. At intermediate and strong coupling, at fixed U as we increase V, we find that this unimodal distribution slowly crosses over to a bimodal one. This occurs because of the weakening of the Hubbard correlation and increasing role of the polaronic distortion energies. Two electrons of opposite spin occupying the same site lowers the electron phone energy more and the system develops a bipolaronic instability. In the nontrivial metallic phase, while every site

is still distorted, the amplitude is very small. These results, indeed, correlate with the charge structure factor and phonon probability distribution function.

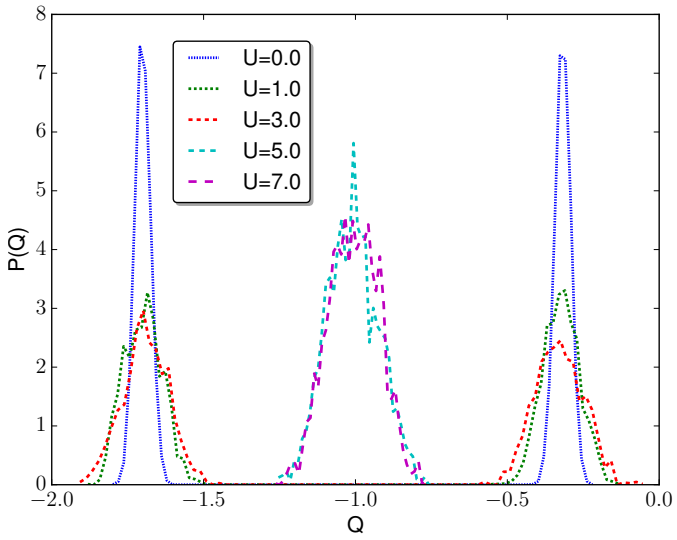

Figure 3.4: Phonon probability distribution for different values of U at $V = 2.0, T = 0.001$.

Our method allows us to provide a direct picture of the real space correlations between the static magnetic auxiliary field, charge density, and the phonon variables at a given site. This will elucidate the character of the transition and especially the metallic phase that arises. In Fig. (3.5) we present snapshots of spin and charge over the lattice for a given set of parameters at a given instant of MC simulation after the system has equilibrated. As expected, for lower values of V, spin correlations develop as U increases moving to a local moment value in the MI phase. Such spin correlations are absent in the COI phase. On the contrary, charge densities modulate as V is changed for a given U resulting in a bipolaronic state. In the corresponding phases spin modulation is negligible. In the metallic phase, both densities remain negligible on an average, but there are fluctuations. The snapshots show a given configuration with some variation in the densities. However, an average over such configurations results in uniform charge density and negligible magnetization confirming that it is indeed a metallic phase.

The various physical quantities that we have used to characterize the ground state properties confirm to the expected behavior and is reflected in such diverse variables as charge, magnetization, distribution of lattice displacements, and fermion spectral functions. The real space picture gives a handle on how to correlate them. As will be discussed in the final section, this gives added advantage of visualizing such changes in non-trivial geometries and especially on frustrated lattices, which is intractable or computationally expensive using other methods such as DMFT or its cluster variants.

To conclude this section, within the static auxiliary field approximation of the decoupled HS fields that we have resorted to, we find a phase diagram that at low values of electron-phonon coupling crosses over from a Slater to MH insulator as U is increased, and a Peierls to BPI as V is increases for low values of Hubbard interaction. At intermediate to large values of coupling, there is a transition from anti-ferromagnetic MHI to a nonmagnetic charge ordered or bipolaronic insulator. However, there is a sliver of metallic phase at low coupling that results from frustrating effects of two interactions in different (charge and spin) channels. The behavior of different degrees of freedom correlate with these changes providing us with an efficient way to extract physics from weak to strong coupling.

3.5 Spectral and Transport Properties

Significant changes are expected in the phase diagram at finite temperatures due to the inclusion of ”full” thermal fluctuations of the static field through configuration sampling. This was already noted in Section III where the effect of each interaction was looked at separately. In this section we present the results for various physical properties at finite temperatures and converge on the finite temperature phase diagram.

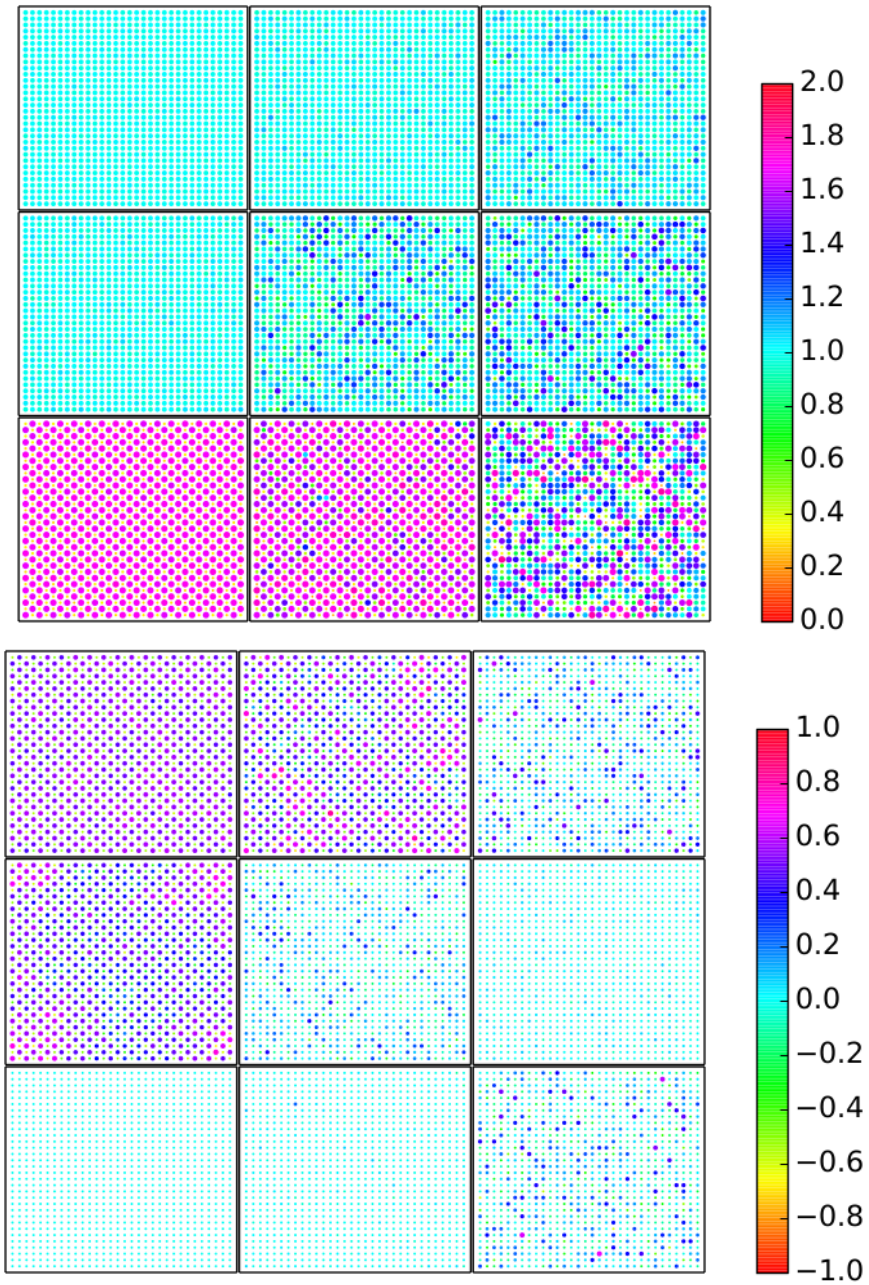

Figure 3.5: (upper)Charge(n_i) and (lower)spin configuration ($\mathbf{S_i}.\mathbf{S_0}$) for $U = 2.0$. Temperature increases from left to right. Centre column shows the configuration near the T_c. Three rows for $V = 0.50$(top), 1.0(middle), 2.0(bottom) and the system size is 32×32.

Fig. (3.6) shows the thermal averaged single electron spectral function $A(\omega)$ for different parameters at different temperatures. Deep in the insulating phase and at low temperatures they show a very clear gap and there are no states available at the Fermi energy as expected. In the region where metallic ground state appears, on the contrary, there is nonzero spectral weight at the Fermi energy even at the lowest temperatures. As temperature increases, we notice three regimes signifying different spectral features. For large values of U and/or V, we find that the gap persists even for large temperature. This is due to the Mott-Hubbard or bipolaronic nature of the phases. The fact that this feature survives at these values of parameters shows that the present method is capable of capturing the strong coupling physics of this problem in both channels. At weak couplings, where a Slater or Peierls insulating phase is expected or the metallic phase emerges, the spectral features are very different at high temperatures. The gap vanishes entirely in the former cases and there is sufficient weight at the Fermi energy in all the three regimes. This clearly shows that the gap arises solely due to the nesting instability of the underlying Fermi system and the resulting order in either spin or charge channels. Once the order is destroyed, so does the gap. The most interesting features arise at intermediate values. Here a hard gap is not seen though there is significant reduction of spectral weight near the Fermi energy. There is spectral weight transfer from the coherence peaks to energies within the gap. This pseudogap feature arises due to persistence of local correlations in static fields even after the long range order is destroyed.

The MC snapshots throw more light on the existence of short range order in either spin or charge degrees of freedom at temperatures near or above the ordering temperatures. This is shown in Fig. (3.5). In each case, the states evolve from the ground states shown in Fig. (3.5). However, unlike the low coupling counterparts, the local order persists even above transition

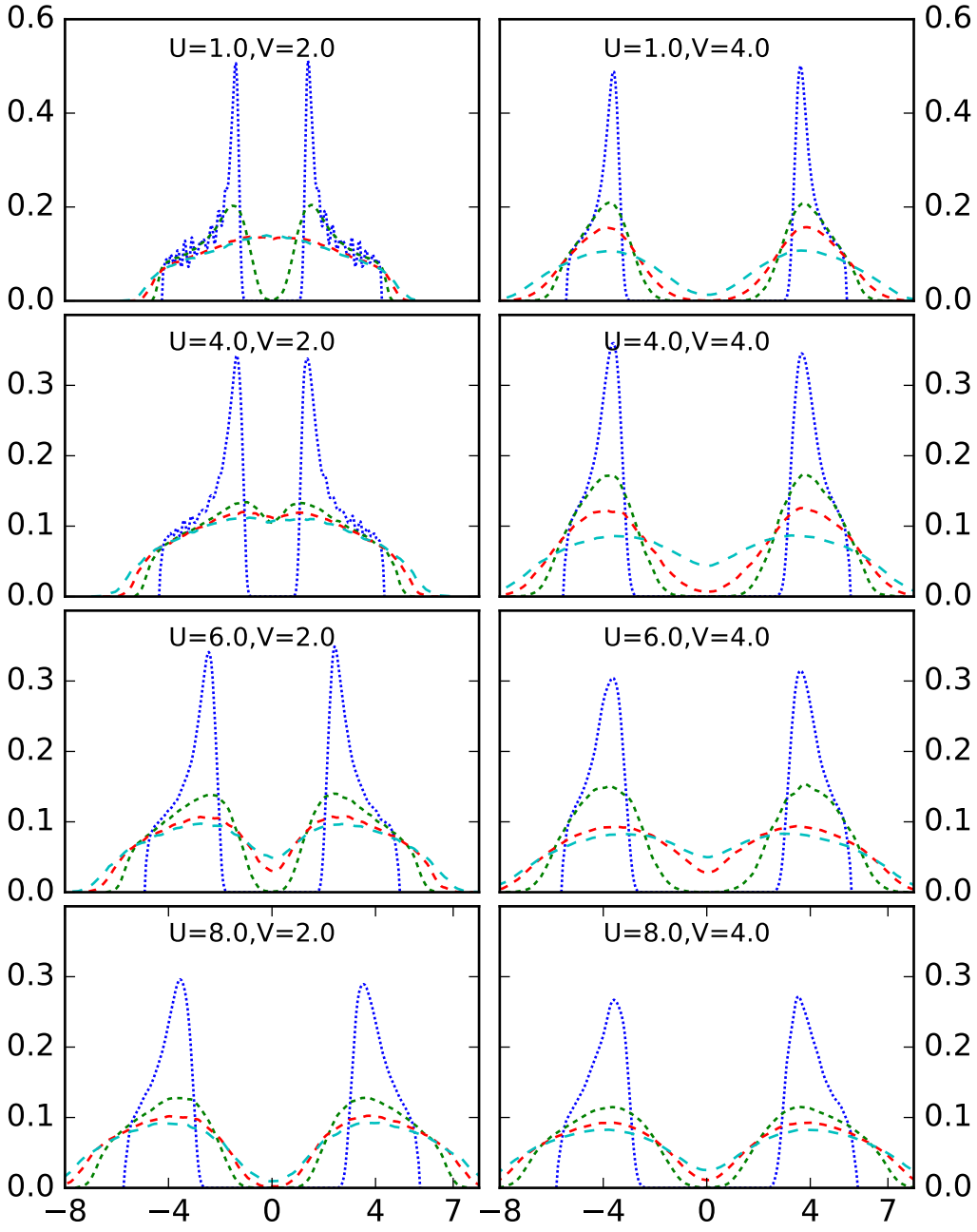

Figure 3.6: Density of state for different values temperature at constant V=2.00 and U varying across the charge density wave - anti-ferromagnetic transition. Temperature points are $0.001, 0.10, 0.20, 0.30$ with increasing dash length.

temperatures. This local order, we believe, is the reason for appearance of pseudogap like features in spectral functions. However, unlike the strong coupling cases, where a local moment or a bipolaron formation is favored and the spectrum shows a hard gap, the intermediate range does allow fluctuations in charge and spin variables at very site, leading to spectral weight appearing in the otherwise gapped region. We have verified that the phonon PDFs also exhibit persistence of bimodality in this region.

The transport can be captured in an exact way without resorting to approximations as in cluster-DMFT. To this end, we use Kubo formula[124] for the in-plane resistivity which involves the exact eigenvalues and wave functions of fermions obtained from diagonalisation at several equilibrium configurations. Fig. (3.7) shows the evolution of optical conductivity for a fixed value of V, but for varying U at different temperatures. A notable feature is the non-Drude behavior of $\sigma(\omega)$. Further, the pronounced low frequency hump in the optical conductivity for small frequencies evolves into an inter band Hubbard peak as U increases. A similar feature has been observed as we vary V where the Hubbard peak gets replaced by the higher energy bipolaronic peak. The non-Drude behavior emanates from the pseudogap nature of the electronic spectral function that originates from strong local charge/spin fluctuations as discussed earlier. The dc resistivity is plotted in Fig. (3.8) for a fixed value of V, but varying values of U at different temperatures. A Metal to Insulator (MIT) is clearly visible for weak coupling regime ($U = 1$) in the inset.

Finally, we present the finite temperature phase diagram of the model in Fig. (3.9). The phases include AF or CO insulating phases at low temperatures except for the sliver of metallic phase discussed earlier, metallic nonmagnetic phases at weak couplings, Mott-Hubbard and

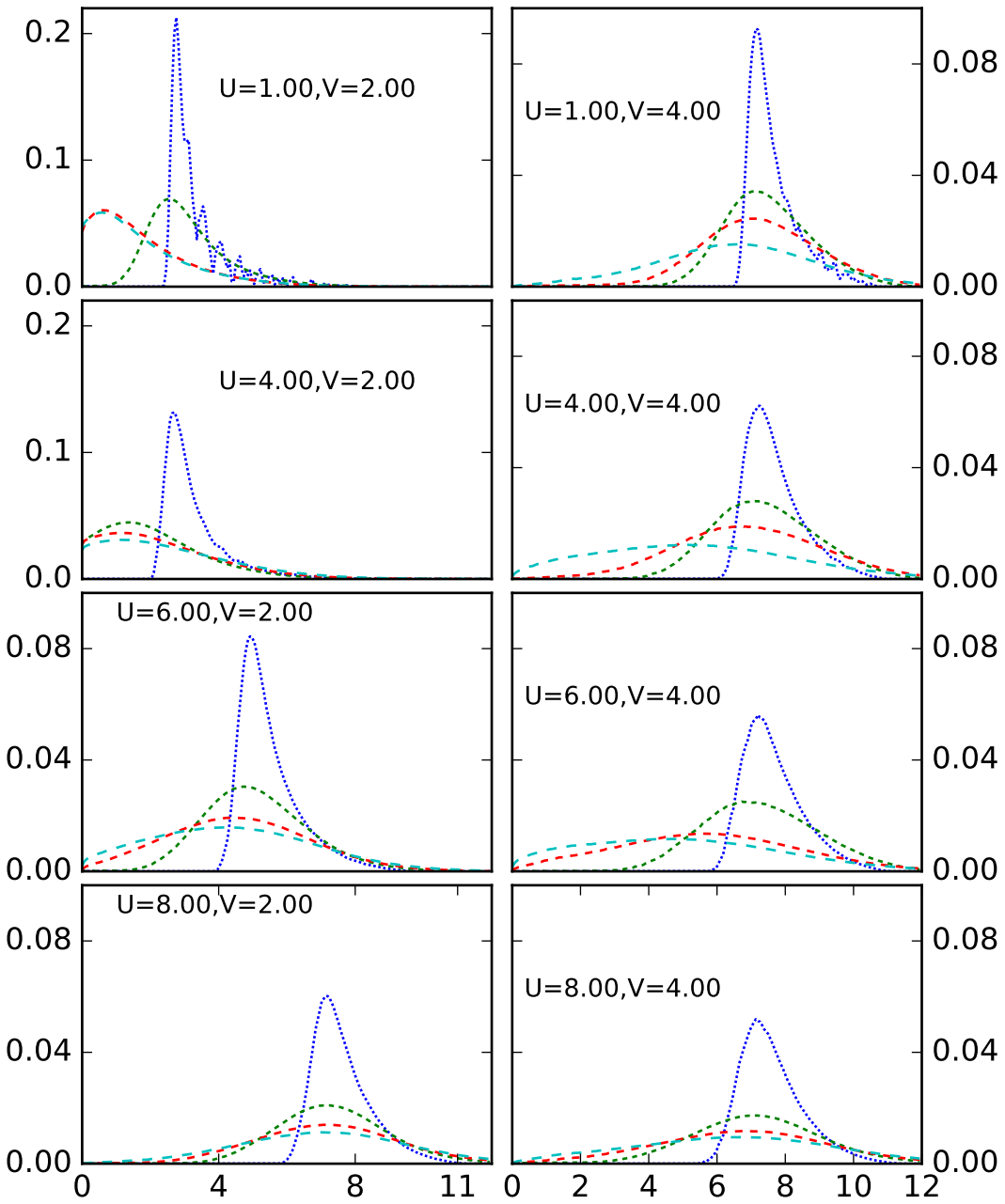

Figure 3.7: Temperature dependence of the Optical conductivity for different values of U and V. Temperature points are $0.001, 0.10, 0.20, 0.30$ with increasing dash length.

bipolaronic insulating phases at large couplings, and the pseudogap phase at intermediate coupling. The high temperature behavior from metallic to insulating one is a crossover. Note that we characterize the finite temperature metallic phase by sign of the temperature variation of the resistivity, $d\rho/dT$. It remains open as to how these instabilities would be affected due to

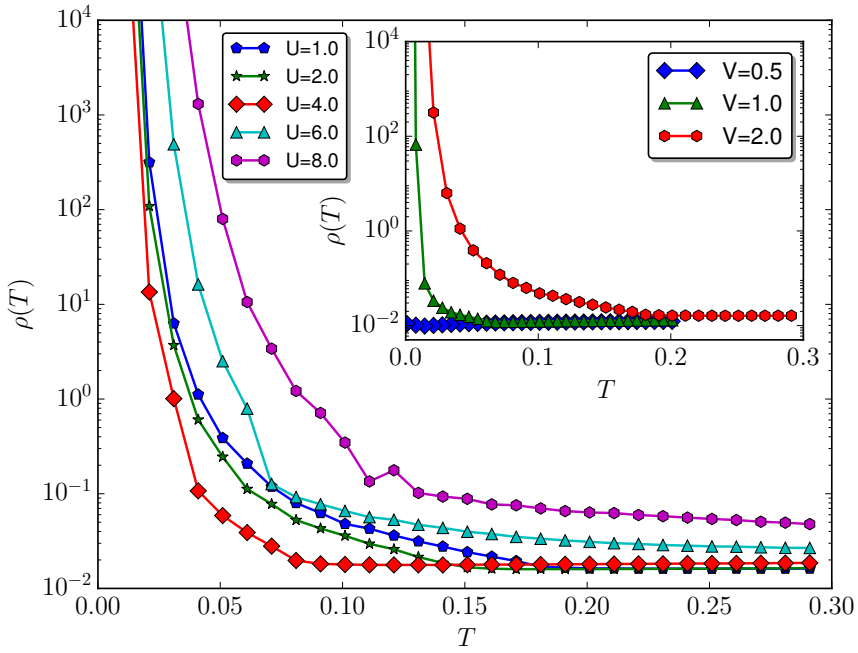

Figure 3.8: Temperature dependence of resistivity, $\rho(T)$ for various values of U at $V = 2.0$. Metal- Insulator transition in the weak coupling region for $U = 1.0$(inset).

quantum dynamics of the auxiliary field or phonons. However, remarkable qualitative agreement with previous DMFT studies suggests that the quantum dynamics of these fields may not be relevant for the regime we have concentrated on. Further, it appears that the current method may be used for geometry and systems where DMFT treatment may not be applicable as we discuss below.

3.6 Conclusions

We presented above a numerical study of the static Holstein-Hubbard model by employing Hubbard-Stratanovich auxiliary fields for the charge and spin sectors. It captures many of the features obtained in previous DMF studies. More importantly, it sheds light into new physics at finite temperatures and intermediate couplings due to the inclusion of spatial dependence (unlike DMFT) and classical thermal fluctuations through configuration sampling. The method works very well at all strengths of coupling. Being a real space method it allows one to visu-

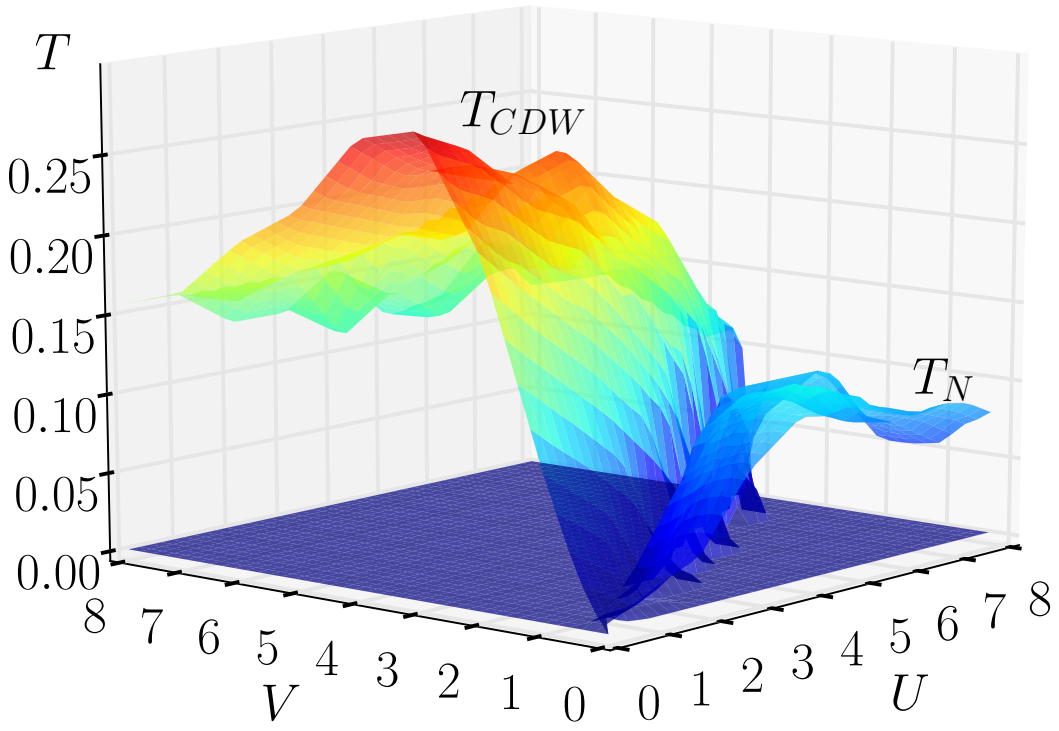

Figure 3.9: Transition temperature for the charge density wave and antiferromagnetic phase for different values of U and V.

alise the phases at various temperatures and how different orders develop and transform into others. It is numerically more efficient and large system sizes can be accessed. Various physical properties, such as single particle spectral functions, phonon distributions, and transport can be readily evaluated.

The salient results include the appearance of a nonmagnetic metallic phase at low values of coupling parameters, which was also seen in previous DMFT study, in addition to the ordered phases, including antiferromagnetic and charge modulated ones. However, the finite temperature phase diagram shows rich features and includes a pseudogap phase at intermediate coupling. This arises due to the persistence of local order in charge and spin degrees. Inclusion of spatial correlations is essential to capture this region. However, a couple of remarks are in order. Firstly, the ground state transition from AF to CO is expected to be a first order one. However, we find that this is a very weak transition and we are not able to resolve it accurately within

the numerical error bars. The weak nature of this transition was also noted in previous DMFT studies. The low temperature insulating states at small couplings could be a result of the fact that we used a two dimensional square lattice. This necessarily gives a nesting instability at half filling and results in Slater or Peirels transition at low temperatures. Inclusion of quantum fluctuations or use of different lattice geometries may obscure these phases. Indeed, DMFT study shows that the metallic phase exists at low strengths even when one of them is zero. Thirdly, one could wonder whether these transitions are numerical artifacts since we have used a two dimensional system. Since thermal fluctuations destroy any order at nonzero temperatures, we expect $T_N = 0$ and $T_{CDW} = 0$. However, it is expected that there would be a coherence temperature roughly mimicking the above transition temperatures even in two dimensions below which the correlation lengths increase rapidly. In other-wards, the system enters the renormalized classical regime[106]. If so, even a weak coupling to a third dimension will stabilize the ordered phases. There could be some qualitative changes such as disappearance of insulating phases at weak couplings since nesting is no longer possible, but we expect gross features to remain the same.

The method presented neglects time dependence in auxiliary fields and phonons. Comparison of our results with previous DMFT studies suggests that quantum dynamical effects may not be highly relevant for these phases especially since the system orders at low temperatures. However, this is indeed a handicap and does not allow us to explore other instabilities such as superconductivity. The present method may be thought of in the same spirit as spin wave theory applied to correlated electrons. Essentially, one is looking at how fermion dynamics changes when coupled to thermally fluctuating background classical fields. A natural way of capturing corrections would be to allow small amplitude fluctuation of the classical variables around their equilibrium value at a Gaussian level and look at the stability of phases. That necessitates a new line of study and we postpone it for future.

The method can be expanded to study many problems of current interest. We mention a couple of them. In the present study we have limited ourselves to a single band Hubbard model coupled to a single phonon mode. Many interesting realistic systems, such as manganites[84, 85] and iridates[126], involve multi orbitals and multi phonon modes. However, the present method can be generalised naturally to include them. The computational complexity increases marginally, but the problem is tractable within the approximations used. Most theoretical studies discusses the properties of the Holstein model with single phonon mode. But in real material there are many optical and acoustic phonon modes. It is assumed that coupling of one mode is large compared to others and perturbatively the effect of other modes are small. Also Numerical methods such as exact diagonalization, diagramatic Monte Carlo and variational methods becomes very expensive once one include more phonon mode. But Within our methods we can include more with less numerical cost. The generalized Holstein Hamiltonian is [30]

$$H = \sum_{k\sigma} \varepsilon_k c^\dagger_{k\sigma} c_{k\sigma} + \sum_{q\alpha} \Omega^q_\alpha b^{\alpha\dagger}_q b^\alpha_q + \sum_{\alpha,k,q} \frac{g\alpha}{\sqrt{N}} c^\dagger_{k-q\sigma} c_{k\sigma} (b^{\alpha\dagger}_q + b^\alpha_{-q}) \tag{3.9}$$

Second term describe phonon modes (acoustic or optical) and third describes electron-phonon coupling. Phonon needs to interact non-locally describe the Debye phonons . In real space Debye phonon can be described as

$$H_{ph} = \sum_i \frac{1}{2m} P_i^2 + \frac{K}{2} \sum_{\langle i,j \rangle} (x_i - x_j)^2 \tag{3.10}$$

with $\Omega_q = 2\sqrt{\frac{K}{m}} |\sin(qa/2)|$. In the low energy region ($k \to 0$) phonon dispersion become $\Omega_q = v|q|$ and $v = a\sqrt{\frac{K}{m}}$ is the sound velocity . We can drop the kinetic part of phonons assuming phonon mass is very large and do Monte Carlo sampleing of the phonon displacement as we did for the single mode Holstein model.

The method could also be extended to study interfaces[127] and/or heterostructures[128] of

correlated, electron-phonon problems which are difficult to handle in conventional methods that are being currently used.

A central feature of the method lies in capturing spatial correlations. This is essential for capturing features arising due to local order. More importantly, methods such as DMFT that neglect spatial dependence are not suited to study geometries[126, 129, 130] where spatial features are important. A case in relevance is the Holstein-Hubbard physics in frustrated geometries. We explore this problem in the next chapter.

Chapter 4

The Holstein-Hubbard model on a triangular lattice

Geometric frustration in an interacting electron system is an outstanding problem which has started receiving attention only in the last couple of decades. Quite generally, it generates non-trivial magnetic fluctuations, disfavouring long ranged magnetic order, and promotes a complex electronic state with short range correlations. The nature and impact of such incommensurate magnetic fluctuations on the metal-insulator transition is much less understood. In several quasi two dimensional systems (for example, organic salts), frustrations gives rise to a spin liquid ground state with significant quantum correlations. In three dimensions, such structures may lead to spin ice behavior and exotic excitations such as magnetic monopoles are expected. Most of the current studies have revolved around the theme of magnetism in insulating antiferromagnets with geometrically frustrating structural motifs. Much less is understood on states close to Mott transition, or rather the nature of transition itself. The addition of electron-phonon coupling brings in new difficulties since polaronic charge ordering also suffers due to geometrical constraints. There is only a limited effort in understanding the nature of spatial fluctuations that could be significant. With this in mind, we explore the Holstein-Hubbard model at half filling on a geometrically frustrating lattice, namely the triangular one. It is not a bipartite

lattice and the noninteracting electron dispersion does not have a nested Fermi surface unlike inn a square lattice. Both these are expected to affect the nature of electronic states significantly.

After a brief introduction to the model that we have used, we first discuss the phase diagram when either of the two interactions are absent. The results differ qualitatively from the well studied square lattice geometry. In particular, at weak coupling, there is no charge or magnetic order even in the ground state, and a critical interaction in either channels is needed to get an ordered ground state. We explore the evolution of these states as a function of temperature and study the transport and spectral features.

4.1 Model and Methods

We consider Holstein-Hubbard Model on a square lattice[132–136].

$$\begin{aligned} H &= -\sum_{\langle ij\rangle} t_{ij}\left(c^{\dagger}_{i\sigma}c_{j\sigma}+h.c.\right)-\mu\sum_i n_i+U\sum_i n_{i\uparrow}n_{i\downarrow} \\ &\quad +\sum_i\left(\frac{1}{2M}P_i^2+\frac{K}{2}Q_i^2\right)-g\sum_i Q_i n_i \end{aligned} \tag{4.1}$$

Here, $c_{i\sigma}$ ($c^{\dagger}_{i\sigma}$) is the annihilation (creation) operator for the fermions on a site i with spin σ. μ is the chemical potential which fixes the average number of particle $\langle n\rangle = 1$. U is the repulsion energy between two electron on same site with opposite spin. P_i, Q_i are the atomic momentum and displacement operator of the phonon at site i.

The hopping t_{ij} is chosen to be anisotropic. $t_{ij} = t$ when $\mathbf{R}_i - \mathbf{R}_j = \pm a_0\mathbf{x}$ or $\pm a_0\mathbf{y}$ where a_0 is the lattice spacing and $t_{ij} = t'$ when $\mathbf{R}_i - \mathbf{R}_j = \pm a_0(\mathbf{x}+\mathbf{y})$. This effectively reduces the square

lattice to a triangular lattice with anisotropic hopping. $t' = t$ reduces to a square geometry and $t' = 0$ gives an isotropic triangular lattice. We set $t = 1$. We focus on the isotropic triangular case for the most of the rest of the chapter, except when it is mentioned otherwise. Introducing auxiliary fields and treating them and phonons to be classical, we get the effective Hamiltonian to be

$$\begin{aligned} H_{eff} &= -t\sum_{\langle ij\rangle}\left(c^{\dagger}_{i\sigma}c_{j\sigma}+h.c.\right)-\mu\sum_i n_i-\sum_i \mathbf{m}_i.\overrightarrow{s}_i \\ &\quad +\sum_i\frac{\mathbf{m}_i^2}{U}+\frac{V}{2}\sum_i Q_i^2-V\sum_i Q_i n_i \end{aligned} \tag{4.2}$$

Since we are focusing on the triangular case, for brevity, we have only used the nearest neighbor hopping $t' = t$ here. We extract the physics of this model using the Monte Carlo procedure described earlier, employing a traveling cluster algorithm.

4.2 Results

Fig[4.1] summarizes the main results when either electron-electron of electron-phonon interaction is present. We have obtained the phase diagram Fig[4.1(a)] when electron-electron repulsive interaction is absent. In the weak electron-phonon regime the system become metallic without any ordered phase. This is because, in contrast to the square lattice where due to nesting at the wave-vector$q = \pi, \pi$ an arbitrarily small enough V would lead to an ordered charge density wave phase at low temperatures due to Peirels instability, the triangular lattice does not have the any such nesting wave-vector. A critical V is required to get charge ordering. Critical temperature below which the ordered phase appears shows a non-monotonic behavior as a function of V. It increases with V, reaching to a maximum, and then decreases in the strong coupling region. The strong coupling behavior can be understood by using a second order perturbation theory assuming that the electron kinetic energy is small compared to V. One will get a term

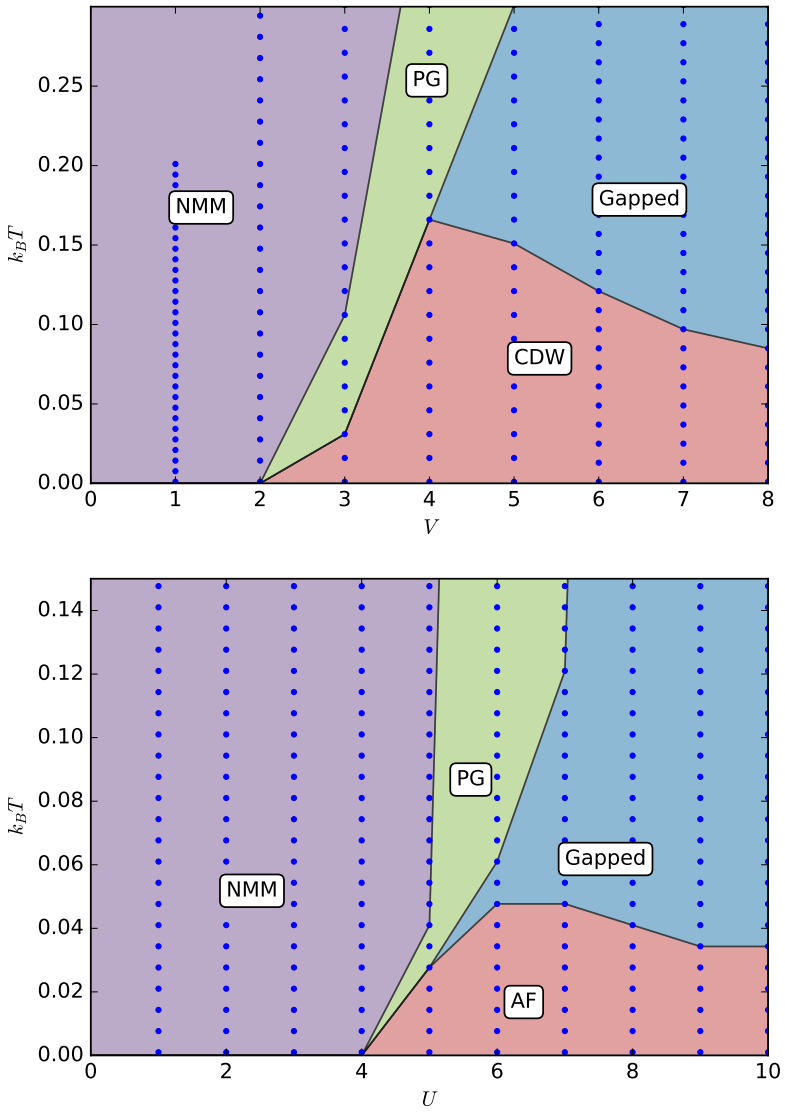

Figure 4.1: Finite temperature phase diagram obtained within Monte Carlo calculation on a 32×32 system for $U = 0$(a) and $V = 0$(b). Different phases are non-magnetic metal(NMM), antiferromagnetic (AF) insulator, pseudo-gapped(PG) , gapped and charge density wave (CDW) insulator.

$n_i n_j$ where ij restricted over the nearest neighbors of the triangular lattice and strength of this term is proportional to $1/V$. Due to this order a gap opens up in the single particle spectrum at moderate coupling and at low temperatures. This hard gap vanishes at the critical temperature with a residual pseudogap remaining in the intermediate regime. This picture changes in the strong coupling regime. Spectrum continues to have a gap above the critical temperature .

Fig[4.1(b)] presents the phase diagram when electron-phonon interaction is absent. The nesting argument giving a metallic phase applies to the Hubbard Model also on a triangular lattice. We need a critical U to have a magnetically ordered state. Critical temperature also shows a non-monotonic behavior as a function of U. It increases in the weak to moderate coupling regime. However, in the strong coupling region critical temperature decreases with U since the order is driven by a super exchange process. In the strong coupling region, we see a gap in density of state even above the critical the temperature for the magnetic ordered state. There is also some pseudo-gap region at intermediate temperatures.

Fig[4.2] show the phase diagram at lowest temperature ($T = 0.001$) in the $\{U,V\}$ plane. When both U and V are weak there is metallic region without any charge and spin order. As U or V increases we find spin or charge ordered state. A line $U = 2V$ separates the charge and spin ordered phases for large values of U and V.

Fig[4.3] shows the charge and spin structure factors for different values of U,V. In the low temperature region charge structure factor shows a peak at $2\pi/3, 2\pi/3$ and $4\pi/3, 4\pi/3$. These are the characteristic ordering wave vectors for the triangular geometry. This two peak structure vanishes above the critical temperature. In the Fig[4.3] we have chosen two set of values of U,V for which system has charge or spin ordered state at low temperatures.

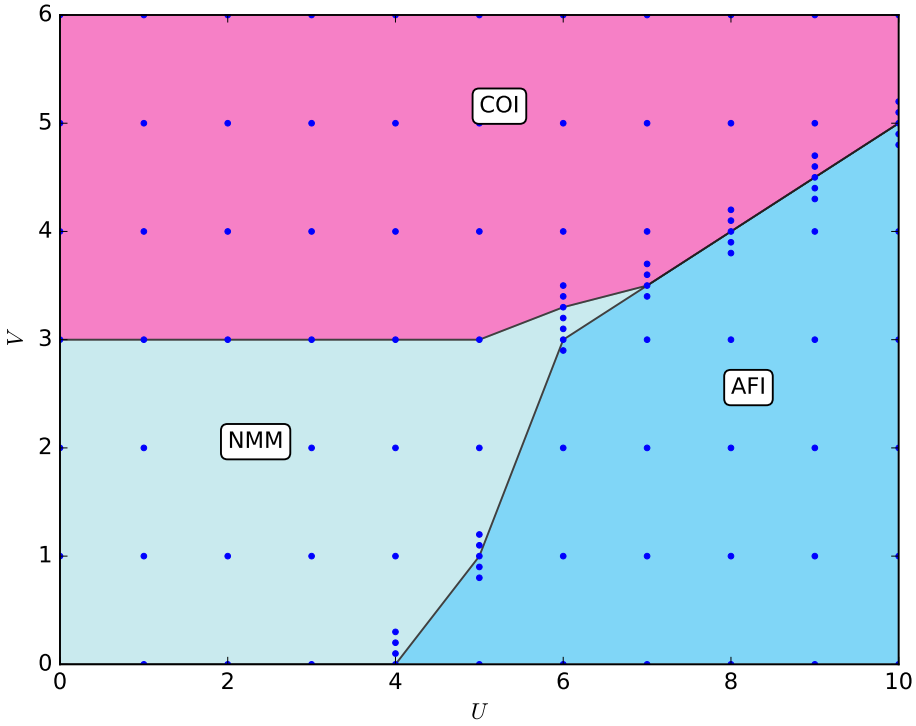

Figure 4.2: Lowest temperature ($k_BT = 0.001$) phase diagram as a function of U and V. Different phases are non-magnetic metal(NMM) , charge ordered insulator (COI) and antiferromagnetic insulator (AFI)

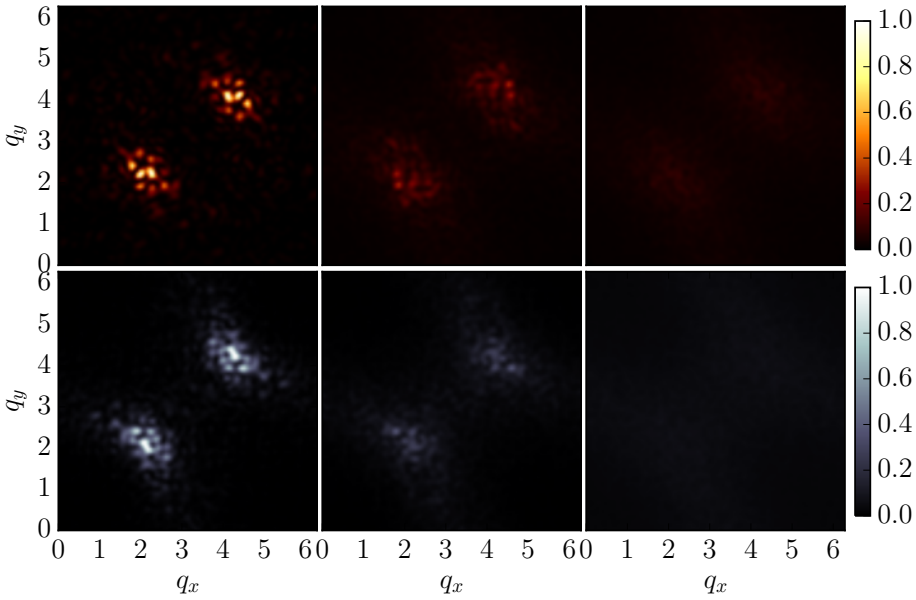

Figure 4.3: (top row) Charge structure factor for $U = 2.0$ and $V = 4.0$ with increasing temperature from left to right. Spin structure factor for $U = 8.0$ and $V = 2.0$ with increasing temperature from left to right (bottom row).

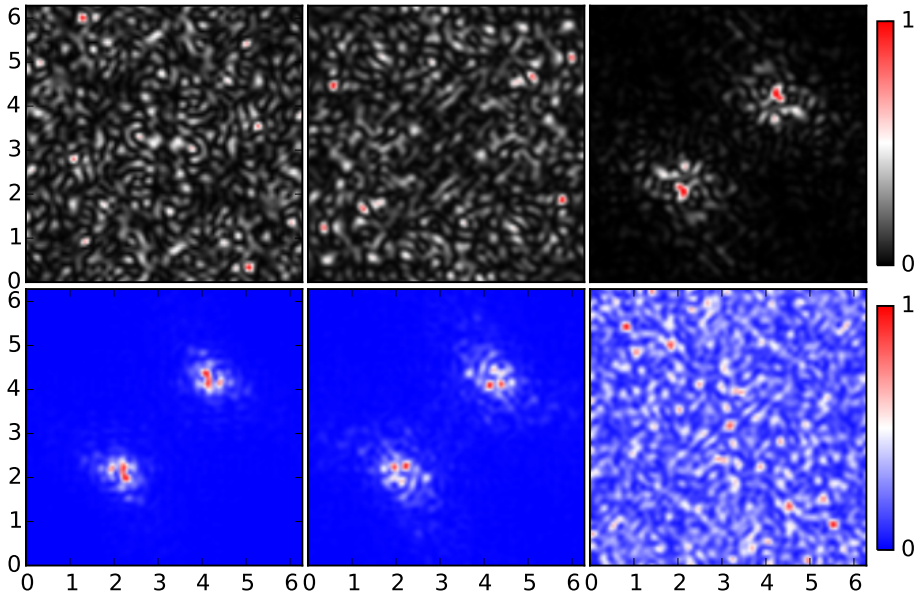

Figure 4.4: Charge (top row) and spin (bottom row) structure factor at lowest temperature $T = 0.001$ for a constant $U(= 8.0)$ and different values of V. Left column for $V = 1.0$ and middle and right column for $V = 3.0, 6.0$ respectively.

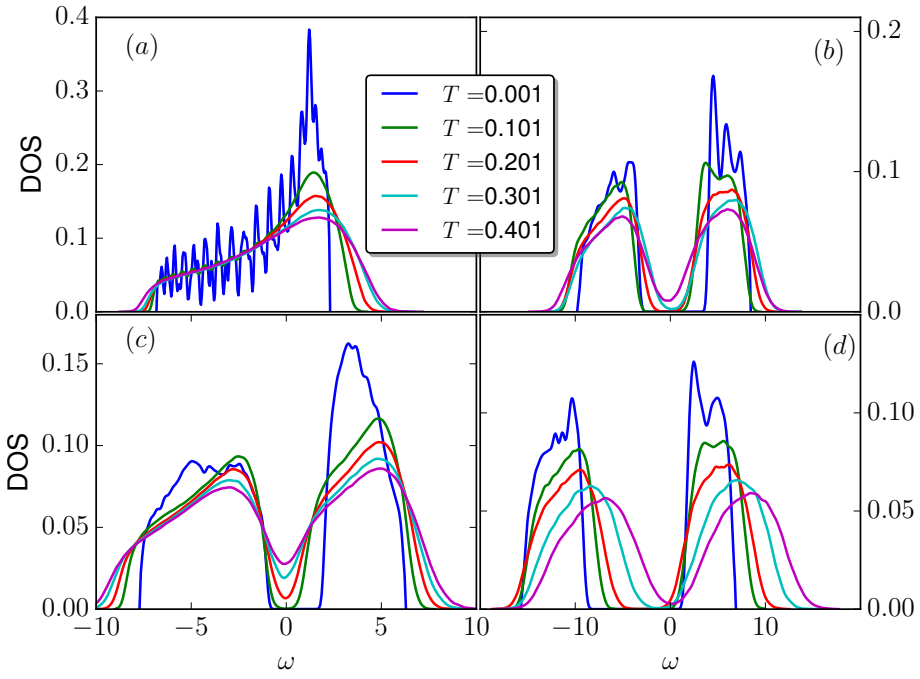

Figure 4.5: Single particle density of state for different temperature, U and V. $U = 3.0$ and $V = 2.0(a), 6.0(b)$. $U = 8.0, V = 2.0(c), 8.0(d)$ and $U = 8.0$ for $V = 2.0(c), 8.0(d)$

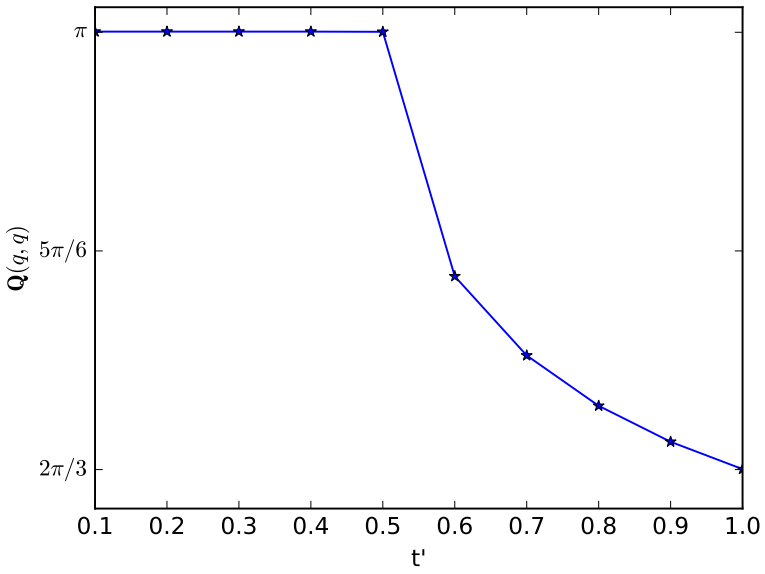

Figure 4.6: Ordering wave vector as a function of t'.

Fig[4.4] shows the charge and spin structure factor for a constant U with different V at the lowest temperature $T = 0.001$. In the small V region system that sustains magnetically ordered state, spin structure factor shows two peak at $2\pi/3, 2\pi/3$ and $4\pi/3, 4\pi/3$. But for larger values of V charge ordered state sets in and charge structure factor shows two peak structure. The contrasting evolutions match with the phase diagram obtained above.

The ordering wave vector seen above is very different from that of the square lattice and evolves smoothly as the anisotropy of the triangular lattice is changed. In Fig[4.6], we plot the ordering wave vector as a function of t' (in units of t). For small t' we retrieve the ordering vector $\mathbf{Q} = (\pi, \pi)$ for the square lattice case and persists till about $t' = t/2$. However, above that value $\mathbf{Q}$ changes smoothly moving over to $(2\pi/3, 2\pi/3)$. We expect that the momentum dependence of the electronic spectral functions will also follow this trend.

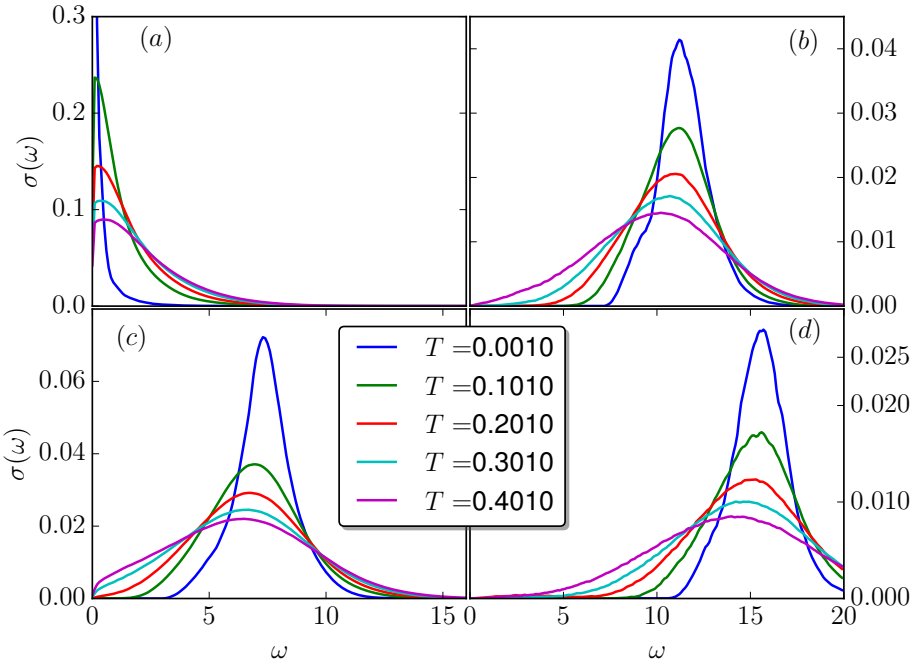

Figure 4.7: Optical conductivity as a function of energy ω for different values of U, V and T. $U = 3.0$ for $V = 2.0(a), 6.0(b)$ and $U = 8.0$ for $V = 2.0(c), 8.0(d)$

4.3 Spectrum

In the Fig[4.5] we present the single particle density of states for different values of U and V. As mentioned earlier, in the weak coupling region due to lack of any ordering system shows metallic behavior and density of states is finite at the Fermi energy($\omega = 0$). With increasing U or V system overcomes frustration and becomes charge or spin ordered at low temperatures. Fig[4.5](b,c) shows the density of states for parameters when the low temperature phase has charge and/or spin order. There is a range of temperatures for which the density of states show pseudogap features and it become gapless at very high temperature. The temperature at which the gap vanishes scales rapidly with U and V. Fig[4.5](d) shows that the density of states remains gapped even at highest temperature we have simulated for large values of the coupling.

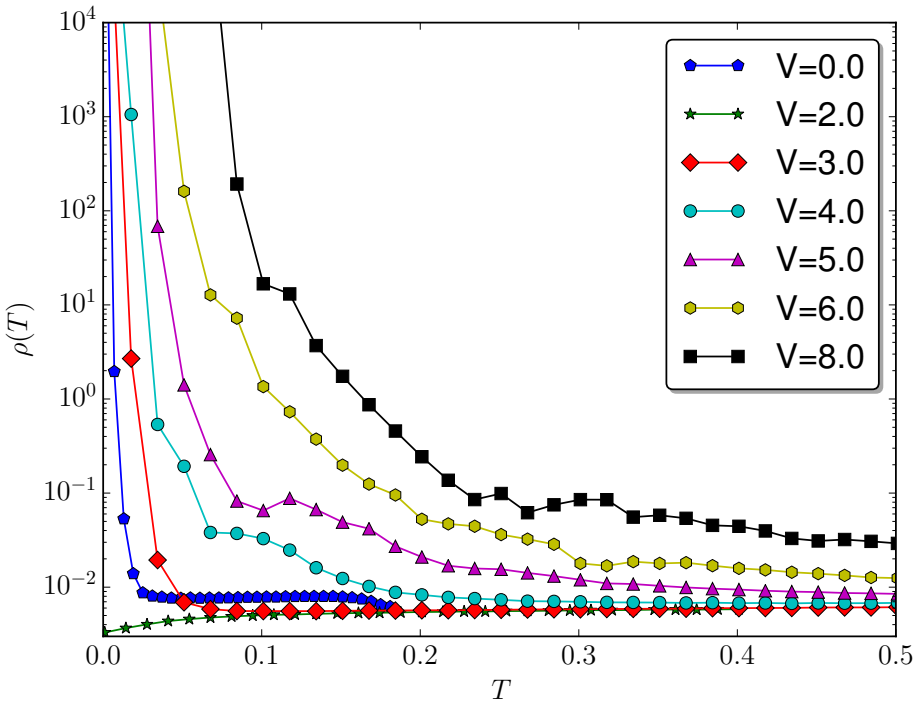

Figure 4.8: Resistivity as function of temperature for $U = 6.0$.MIT

4.4 Transport

We have calculated the optical conductivity using the Kubo formula. Fig[4.7] presents the real part of the optical conductivity. Fig[4.7](a) shows the temperature evolution of optical conductivity for metallic region. At low temperatures optical conductivity shows the Drude peak at $\omega = 0$ With increasing temperature the peak value ($\sigma(\omega \to 0)$) decreases. This is quite expected because at high temperatures there will be very strong fluctuations of the fields(Q_i, m_i) and that will increase scattering rate for the electron moving in this background. There is also a spectral weight transfer from lower energy to higher energy at higher temperatures. This picture changes completely in the strongly interacting region where one of ordered phases of charge or spin sets in. In this phases low temperature has a gap in the single particle density of states. To have a charge transport in the system one needs to excite an electron with energy larger than the gap. Optical conductivity reflects this gap which is clearly seen in the Fig[4.7](b,c,d). The gap increases with increasing U, V.

Single particle density of states has large spectral weight near the gap and smaller weight for energies far away from the gap. This behavior of the low temperature density of states gets reflected in the conductivity. At higher temperatures spectral weight get transferred from higher to lower energies within the gap. This transfer of spectral weight continues as temperature increases and $\sigma(\omega \to 0)$ is nonzero at sufficiently high temperatures. The temperature scale at which $\sigma(\omega \to 0)$ becomes nonzero also increases rapidly with U and V. We can see in the Fig[4.7](d) that the gap persists even at the highest temperatures explored.

We have calculated the resistivity of the system, which is inverse of the zero energy limit of the optical conductivity for a particular temperature. Fig[4.8] shows the behavior of resistivity as the system undergoes an insulator-metal-insulator transition at low temperatures for a constant $U(= 6.0)$. At small values V it shows a insulating behavior with resistivity increasing with decreasing temperature. However, for $V = 2.0$ the system shows metallic behavior with $d\rho/dT < 0$. This is because with increasing V both charge and magnetic order compete with each other and in the intermediate region neither of them is able to order at even very low temperatures. With further increasing V system goes back to an insulating phase with $d\rho/dT > 0$ since charge order is promoted.

4.5 Conclusions

In this chapter, we studied the competition between electron-electron and electron-phonon interactions on a triangular lattice. Geometry of the lattice has two effects. Absence of nesting makes the weak coupling phase metallic. Frustration leads to an order different from the conventional Neel order. We still obtain an order for both charge and spin since the auxiliary field are treated classically. It is possible that quantum effects could be significant and may eventually lead to spin liquid like states or polaronic glassy phase, which is beyond the scope of the present work.

Chapter 5

Effect of site dilution in the two-dimensional attractive Hubbard model

5.1 Introduction

The interplay between superconductivity (SC) and disorder is a long standing problem [137–140]. For weak disorder the two are not expected to be inimical to each other since pairing takes place between time-reversed states [3] that are present when only potential impurities disorder the system [141]. In this limit the superconducting state is not expected to be much different from the mean field BCS state. In particular, it remains homogeneous in the low-disorder regime. However, when the disorder is strong, it dramatically alters the superconducting phase [142]. Large phase fluctuations can reduce the superconducting transition temperature from its mean field value and in a temperature window between T_c and T_{BCS}, where T_c is the transition temperature and T_{BCS} is the mean field value expected from the BCS theory, a pseudogap phase is expected [139]. This is a regime where preformed pairs exist, but global coherence is absent. Strong disorder also makes the phase highly inhomogeneous. Theoretical studies at strong disorder [103, 143–152] reveal the inhomogeneous nature of the SC state, formation of superconducting puddles and presence of a ”pseudogap phase” where long-range SC order diminishes

although the quasiparticle gap remains open. While Josephson effect between these puddles can give rise to a globally SC ground state[153], strong phase fluctuations among them may lead to an insulating state[146, 154]. Recent experimental studies have probed this behavior [155–164]. They reveal fragmentation of the superconducting state into islands, pseudogap-like features in the normal state, and a change in the normal state resistivity suggestive of a metal-insulator transition (MIT).

Competition between superconductivity and disorder is expected to be more interesting in two dimensions since arbitrarily small disorder is capable of localizing electrons [165] while the superconducting transition itself is of Berezenskii-Kosterlitz-Thouless (BKT)-type [166] in nature. Superconductors and superfluids in two dimension goes through a phase transition at finite temperature known as Berezinskii-Kosterlitz-Thouless (BKT) transition. This phase transition is not a true phase transition. Correlation length diverges algebrically instead of exponentially at the transition point. This is driven by the vortex excitations at low temperature and it develops quasi-long-range order due . At low temperature vortices with opposite velocity attract each other while at high temperature large number of free vortices appear and the system goes into a disorder phase. The signature of the BKT transition in superconductors is not clear due to various reasons. One of them is the presence of the quasiparticle excitation limit the temperature range from T_{BKT} to BCS mean field T_C where specific feature of BKT transition emerge. Also to observe BKT features interaction between vortices needs to be logarithmic but screening modifies this. One way to reduce the screening effect is by reducing the thickness of the superconducting film but this introduces disorder in the system. In our theoretical studies we have introduced disorder in form of absence of the attractive sites in the lattice. Increasing disorder means there is less no of attractive sites to make phase coherence over the whole sample. System creates isolated region where superconducting phase is coherent but phase between these regions are incoherent and system goes into non-superconducting phase. Similar picture

also emerge form the potential disordered systems.

Experimental studies show a superconductor-insulator (SI) transition in many two dimensional systems[167–170], a theoretical understanding of which is still not very satisfactory. Another complication arises as one increases the strength of attractive interaction since, in absence of disorder, this is expected to lead to a BCS-BEC crossover [171–174]. The latter results from the Bose condensation of local pairs of electrons arising due to enhanced double occupancy for large local attractive interactions. The physics is remarkably different from the BCS limit; there is still a large, local pairing gap that is visible in the spectral function, but in contrast to the BCS limit, T_c is much reduced and does not scale with the pairing gap, though the zero temperature pairing gap continues to increase with interaction. Phase fluctuations play a dominant role here and is the cause of suppression of SC order even when there are strong local pairing tendencies. The effect of disorder in this limit has not been explored adequately.

Further, there are various systems in which a SC ground state is arrived at by doping an insulating host. For example, PbTe is a semiconductor, but when doped with Tl ($Pb_{(1-x)}Tl_xTe$) becomes superconducting beyond a critical $x_c \sim 0.3$ [175, 176]. T_c increases with x suggesting that Tl induces pairing. It is also known that T_c decreases when a superconducting material is doped with certain atoms. Examples include MgB_2 doped with carbon ($Mg_{(1-x)}C_xB_2$) [177] or aluminium ($Mg_{(1-x)}Al_xB_2$) [178]. A simple way of modeling such systems is to assume that a host metal/insulator is doped with inhomogeneous attractive centers which promote local pairing[179]. As the number of such attractive centers increases, superconducting islands start to form. However, onset of superconductivity requires percolation of these puddles, thereby establishing global phase coherence. This problem has several interesting features. Disorder and superconductivity contribute on an equal footing and the superconducting state is expected to be intrinsically inhomogeneous, except at low dilution. In absence of attractive centers, the host could be metallic or nonconducting, though we study only the former in this paper. One

could also explore the BCS-BEC crossover in the context of dilution of attractive centers if one is able to handle the regime of large attractive interactions. Thus, the study requires an inherently real-space-based exploration that goes beyond mean field approaches to capture strong correlations.

Theoretical studies based on the above picture have been carried out previously using mean field theory [180–182] or quantum Monte Carlo (QMC)[183]. The former does not have the prospect of studying large interaction strengths. The latter can handle the entire range, but is numerically expensive with obvious system size limitations; transport is harder to evaluate. Recently, dynamical mean field theory (DMFT) [115] was employed supplemented with coherent potential approximation (CPA) to treat disorder[184, 185]. However, neglect of spatial correlations lead to unphysical results, especially, at strong interactions. To this end, we use a numerically less expensive method that captures the entire parameter regime while retaining thermal fluctuations of the pairing field and is able to shed light on the physics in real space. We employ the random attractive Hubbard model [186] where the number of attractive centers is determined by the dilution on an average. We use a real-space Hubbard-Stratanovich (HS) [144, 187, 188] transformation by introducing auxiliary fields in the pairing and charge channels that couple to electrons. For simplicity, we assume the auxiliary fields to be classical; while we allow spatial fluctuations of amplitude and phase of the pairing field, we neglect their dynamics. This results in studying the self-consistent quantum dynamics of electrons coupled to thermally fluctuating, classical pairing fields which is treated numerically using Monte Carlo method[189].

The details of the model and numerical procedure are given in Section II. We discuss the critical temperature of the superconducting transition and its variation with dilution and strength of interaction in Section III. Afterwards, we present spectral and transport properties of this

model. Being a real-space method, this gives us a direct image of the physics in real space, while allowing to access the BCS-BEC crossover regime. We conclude by pointing out certain limitations of the present approach and possible extensions.

5.2 The Static Auxiliary Field Method

To study the nature of percolative superconductivity due to variation in the density of attractive centers, we employ a minimal model, which is the attractive Hubbard model with site dilution, that captures the essential features of the problem. The Hamiltonian reads:

$$H = -t \sum_{\langle ij \rangle, \sigma} c^{\dagger}_{i\sigma} c_{j\sigma} - \sum_{i} U_i n_{i\uparrow} n_{i\downarrow} - \mu \sum_{i} n_i. \tag{5.1}$$

Here, t is the nearest-neighbor hopping integral (which we take to be unity to set the energy scales), U_i is the strength of attractive interaction that is site-dependent, μ is the chemical potential which fixes the mean electron density. In this paper, we fix the electron density to be $n = 0.875$. However, the physics is not very sensitive to changes in average electron density, except at half filling. The case of half filling is special, which we discuss in the last section. Site dilution is introduced *via* site-dependent U_i that follows a bimodal probability distribution such that $U_i = U$ with probability $P(U) = \delta$ and $U_i = 0$ with probability $P(U) = 1 - \delta$ [190], where δ is the average number of sites having attractive centers (e.g., $\delta = 1$ when all sites have attractive centers, which is the clean limit). We employ the Hubbard-Stratanovich transformation to reduce the interacting, quartic Hamiltonian to a quadratic fermionic Hamiltonian coupled to a pairing field Δ_i, which is a complex variable and a real, scalar-valued charge (or, equivalently density) field ϕ_i. The resulting Hamiltonian is given by

$$H_{eff} = - t \sum_{\langle ij \rangle, \sigma} c^{\dagger}_{i\sigma} c_{j\sigma} - \mu \sum_{i} n_i + \sum_{i} \left(\Delta_i c^{\dagger}_{i\uparrow} c^{\dagger}_{i\downarrow} + h.c. \right)$$

$$+ \sum_i \frac{|\Delta_i|^2}{U_i} + \sum_i \phi_i n_i + \sum_i \frac{\phi_i^2}{U_i}, \tag{5.2}$$

where $\Delta_i = \langle c_{i\uparrow} c_{i\downarrow} \rangle$ and $n_i = \sum_\sigma c_{i\sigma}^\dagger c_{i\sigma}$. The partition function can be evaluated in terms of the effective Hamiltonian as

$$\mathcal{Z} = \int \mathcal{D}\Delta \mathcal{D}\Delta^* \mathcal{D}\phi \mathcal{D}\left[c^\dagger, c\right] e^{-\beta H_{eff}}, \tag{5.3}$$

so that the probability of occurrence of a particular configuration of Δ_i at inverse temperature $\beta = 1/(k_B T)$ is obtained from

$$P(\Delta_i) = \frac{1}{\mathcal{Z}} \int \mathcal{D}\phi \mathcal{D}\left[c^\dagger, c\right] e^{-\beta H_{eff}}. \tag{5.4}$$

We note that the saddle-point solutions of the action corresponding to the effective Hamiltonian give Bogoliubov-de Gennes (BdG) equations for the pairing field Δ_i and the charge field ϕ_i.

While at this level the action is exact, to make progress, we assume that the pairing fields are static (i.e., we neglect quantum fluctuations), but their amplitudes and phases are site-dependent and thermally fluctuating [148, 174, 189]. Charge field is also assumed to be classical. At finite temperatures, this necessitates thermally averaging over their most probable configurations, which we carry out using a Monte Carlo (MC) estimation of their weights based on Metropolis algorithm. This essentially means that for a given electron density, temperature, and strength of interaction, we start with a random configuration of attractive centers by fixing the amount of site dilution, and a judicious choice of the pairing and charge fields at every site. This leaves us with a problem of electrons moving in random (classical) fields that requires an exact diagonalization of the fermion problem. A thermal sampling of the configurations of the auxiliary fields

is performed by Monte Carlo updating of the (classical) fields. A disorder average has been performed by choosing different random configurations of attractive centers for a given value of dilution. Thermodynamic properties of the system as well as spectral features of electrons and transport are obtained by averaging over configurations thus obtained. This method, which requires exact diagonalization of the electron system at every Monte Carlo step, obviously restricts the system size and to circumvent it we use a traveling cluster algorithm (TCA)[191]. Here, the fermion problem is diagonalized on a smaller cluster around the chosen MC update site, embedded in a much larger lattice. The cluster moves during every MC update, thereby restoring ergodicity. A similar approach was recently used successfully for the case of repulsive Holstein-Hubbard model in two dimensions [192].

Before presenting our results, we review the previous works based on the above model. These include mean field calculations based on BdG equations[180–182] with disorder treated using CPA, quantum Monte Carlo[183], and the dynamical mean field theory with iterated perturbation theory (IPT) as an impurity solver in conjunction with CPA to handle disorder[184, 185]. In general, scaling analysis suggests that a critical concentration of attractive centers, δ_c, is required to get superconducting ground state; however, such arguments cannot be relied upon to get the variation of δ_c with U. The system undergoes a first order metal-SC transition at δ_c. While δ_c increases with U in mean field calculations, it is seen to decrease and then saturate with U in QMC. DMFT studies reveal that δ_c decreases sharply with increasing U. For all $U \geqslant 2.7$, $\delta_c \sim 0$. This is obviously an artifact of the infinite coordination number employed in DMFT, thus neglecting spatial correlations. In general, δ_c displays a strong dependence on U, which suggests that the transition from the metallic to SC state cannot be thought of entirely in terms of percolation alone. In the next section, we provide results on the metal-SC transition in this model based on our study focusing on the variation of structure factor with temperature

which determines T_c.

5.3 Order Parameter and Critical Temperature

Once the system reaches equilibrium, we use the thermal, and disorder averaged structure factor for the pairing field $\Delta_i = \langle c_{i\uparrow} c_{i\downarrow} \rangle$, to track the onset of superconductivity as a function of dilution and temperature:

$$S(\mathbf{q}) = \frac{1}{N^2} \sum_{ij} \langle \Delta_i \Delta_j^* \rangle \, e^{i\mathbf{q}\cdot(\mathbf{r}_i - \mathbf{r}_j)}. \tag{5.5}$$

For a uniform superconducting solution, we look at the wave vector $\mathbf{q} = (0,0)$ and the corresponding structure factor $S(\mathbf{0})$. For a given dilution, $S(\mathbf{0})$ is vanishingly small at high temperatures and starts picking up at a characteristic temperature, which we identify with the superconducting transition temperature T_c. A typical result is plotted in Fig. (5.1) corresponding to $U = 8$. We note that there is a critical concentration of attractive centers, δ_c, needed to have "globally phase-coherent " superconductivity, which for this case happens to be roughly $\delta_c = 0.6$. Further, the low-temperature saturation value of $S(\mathbf{0})$ as well as T_c increases with δ. For most of our discussions, we have used a system size of 32×32 with the size of the traveling cluster being 8×8. There is a marginal decrease in T_c as system size increases which is to be expected in a two-dimensional system. However, we expect that in a three-dimensional system, even with a small hopping between layers (or, in other words a large anisotropy between them), transition temperatures would stabilize. Of course, we do not take up this task since it is computationally expensive and more importantly, we are interested in the generic features of the problem, demonstrating the usefulness of the procedure. Results for other values of U show similar behavior. We will now discuss in detail the variation of T_c with U and δ.

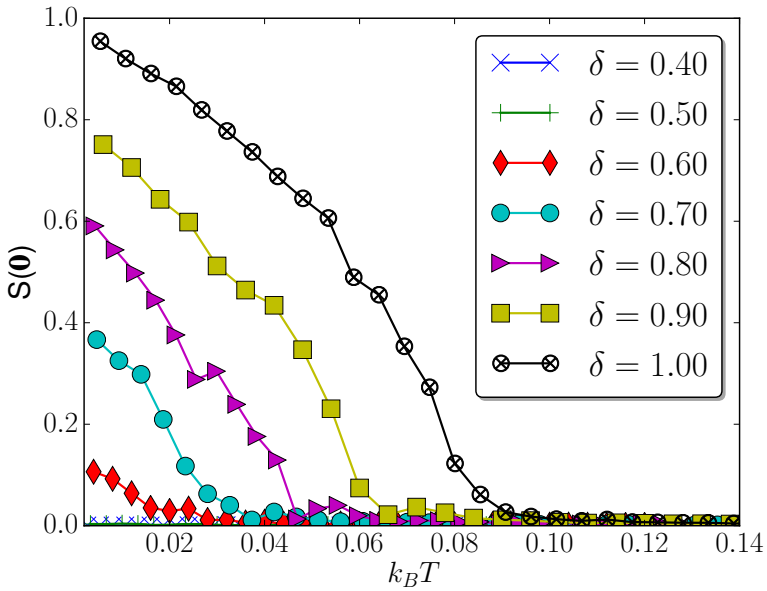

Figure 5.1: Structure factor $S(\mathbf{0})$ for the pairing field as a function of temperature for $U = 8$ and for different values of dilution δ.

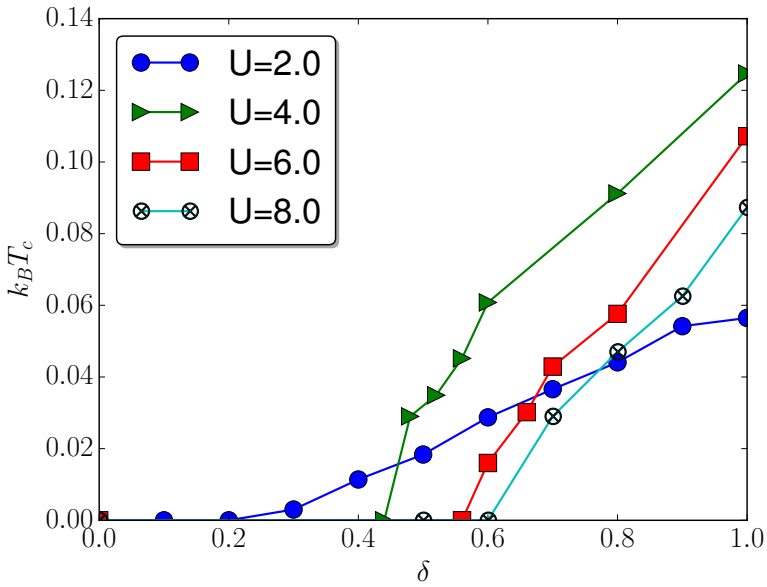

Figure 5.2: Transition temperature T_c as a function of dilution δ for different values of interaction strength U.

Fig. (5.2) shows the variation of T_c as a function of δ for different values of U as extracted from $S(\mathbf{0})$. For a given value of U, T_c increases with δ beyond δ_c. From our results, it appears that δ_c needed for the onset of superconductivity increases with U and more or less saturates around $U = 6$ with a saturation value of about $\delta_c = 0.6$. The saturation of δ_c at larger U, consistent with previous QMC study [183], brings out the advantage our method has over BdG mean field theories, where δ_c seemingly increases with U. Our results also differ from the DMFT that obtains a sharply decreasing δ_c with U, and $\delta_c = 0$ beyond a critical value of U (~ 2.7), an unphysical result arising due to the local approximation made in the latter. One would expect that the onset of superconductivity is brought about by percolation of locally superconducting islands and having larger number of attractive centers helps in enhancing the superconducting correlations, and hence the transition temperature itself that would scale with U. While this is indeed true at smaller interaction strengths, the physics is governed by other factors at larger U. The very perceptible non-monotonic variation of T_c as a function of U (see Fig. 5.2), which we discuss next, is indicative of this.

To get some perspective of the energy scales in the problem and how they affect the transition, we turn to the the clean limit first. For small values of U, T_c is controlled by the pairing scale below which the amplitude of the Cooper pair becomes non-zero. This is the BCS limit where phase fluctuations hardly play any role and the pairing scale is determined by the zero-temperature gap $\Delta(T = 0)$. Correspondingly, the transition occurs at a temperature $k_B T_c \sim te^{-t/U}$ for small U, beyond which the spectral gap vanishes. However, as U increases, the pair size (or equivalently, the coherence length) comes down and the onset of superconductivity is determined by the phase coherence temperature, instead of the pairing scale. In fact, at large U, the pairing amplitude remains almost constant across the transition at the sites where there is an attractive center. Thermal fluctuations are capable of closing the gap only

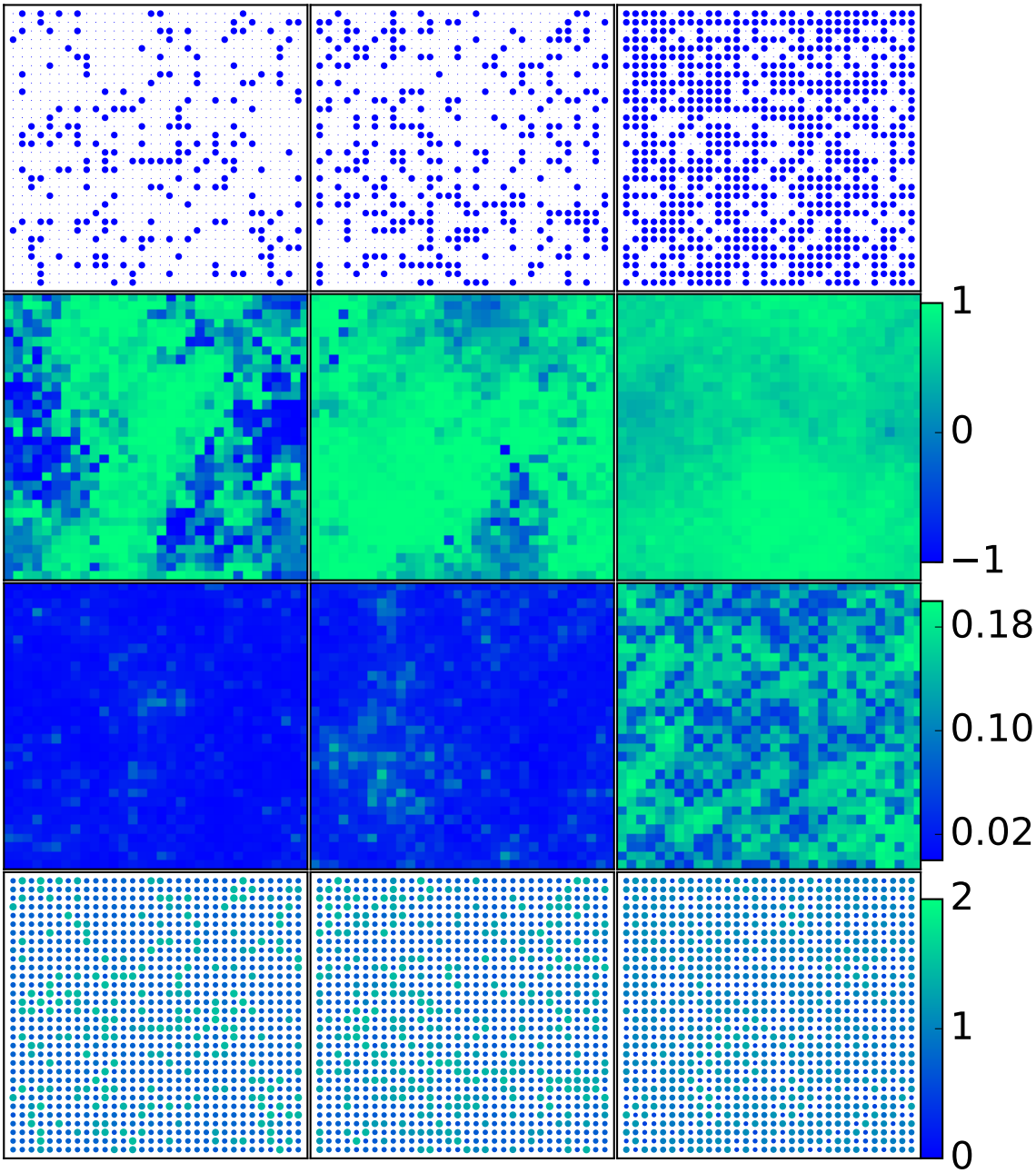

Figure 5.3: Real-space configurations of the distribution of attractive centers and various auxiliary fields at $U = 2$ at the lowest temperature ($T = 0.001$ in units of t . The three columns correspond to different dilution : $\delta = 0.2$ (first), $\delta = 0.3$ (second) and $\delta = 0.7$ (third). The first row gives the distribution of attractive centers with blue circles denoting sites with $U_i = U$. The other rows depict the phase $\cos(\arg(\Delta_i))$ (second) and the amplitude $|\Delta_i|$ (third) of the pairing fields, and the charge field n_i (fourth). The system size is 32×32.

at temperatures $k_B T \sim U$ [193]. However, the relative phases among the sites fluctuate wildly and global coherence is established only at a much lower temperature (as compared to the BCS mean field value) determined by the phase fluctuation scale, and goes as $\sim f(n)t^2/U$, where $f(n)$ is a function of carrier density n. This results in a nonmonotonic variation of T_c with U arising due to the BCS-BEC crossover and is most clearly seen in Fig. (5.2) for $\delta = 1$ (the clean limit). However, such a behavior sets in roughly at $U = 6$ and for $\delta \geqslant 0.6$, establishing this crossover in an inherently disordered system. Thus a separation of relevant energy scales that determine the transition occurs as U increases. The zero-temperature pairing gap in the quasiparticle spectrum continues to increase with U, though it determines the superconducting T_c only in the weak-coupling limit. This also results in a nontrivial behavior of the normal phase, wherein it changes from a Fermi liquid to a gapped phase at large interaction strengths. There is a smooth crossover between these two regimes with an intervening high-temperature normal phase in the crossover region with anomalous properties, which we will discuss in the next section.

Our method incorporates spatial fluctuations of the pairing field, both its amplitude and phase, in an unbiased way and in fact, this is a crucial ingredient to **access** the BCS-BEC crossover. The latter arises due to site-dependent phase fluctuations, which cannot be captured in the conventional BCS framework as was discussed earlier. Further, unique to this problem is the local charge fluctuations that can be quite large due to site dilution. Next, we discuss the role of each of these, the charge and the amplitude and phase of pairing field fluctuations and their role in nucleating/stabilizing superconductivity as a function of temperature and dilution. In the clean limit with $\delta = 1$, all sites have uniform charge distribution and fluctuations are negligible. However, as sites are being diluted, there is a strong tendency to have average charge density to be larger near attractive centers and this can be seen most clearly in the lowest rows of Fig. (5.4) corresponding to $U = 8$.

On the contrary, the local amplitude of the pairing field $|\Delta_i|$, where $\Delta_i = |\Delta_i| e^{i\theta_i}$, is almost vanishing at every site for large enough dilution, except in small islands where it is nonzero, grows in size as dilution decreases. This in fact, is the origin of the percolative nature of the transition as a function of δ for a fixed U. There are puddles where amplitude is nonzero, but there are large intervening regions where it is vanishingly small. There is phase coherence within a given puddle, but that cannot stabilise a global superconducting state. Beyond a percolation threshold δ_c, which happens mostly in the BCS-BEC crossover region, there is sufficient pairing amplitude at most sites since the dilution is less. However, physics in this strong-coupling region is determined entirely by phase fluctuations. To bring out this feature more clearly, we present the same physical quantities in Fig. (5.4) for $U = 8$. The behaviour of $\langle n_i \rangle$ and $|\Delta_i|$ are qualitatively different at larger values of U. The site-to-site charge fluctuations increase enormously, with attractive centers having localised pair of electrons with opposite spins. As δ varies from 0.4 to 0.8, charge-rich sites increases in number. The charge density at the charge-rich sites reaches close to 2 for systems with large U. Amplitude of the order takes zero almost everywhere in the lattice for $\delta = 0.40$ or smaller than that. It starts to take non-zero values from $\delta = 0.50$ onwards. However, there is a strong fluctuation of these amplitudes compared to $U = 2$ (see Fig. (5.3). Average value of this amplitude on sites with $U_i = U$ increases with δ for $\delta > 0.50$ whereas $|\Delta|$ does not change much on the sites with $U_i = 0$.

Naturally, the picture that emerges is that, as expected, fluctuations of the phase degrees of freedom do not play a major role for small values of U. The transition is entirely BCS-like. Variation of δ affects the percolative nature of the transition since, the otherwise locally phase coherent islands have to overlap to give rise to a globally superconducting state. However, as can be seen from the second rows of Figs. 3 and 4, the phase of the order parameter changes

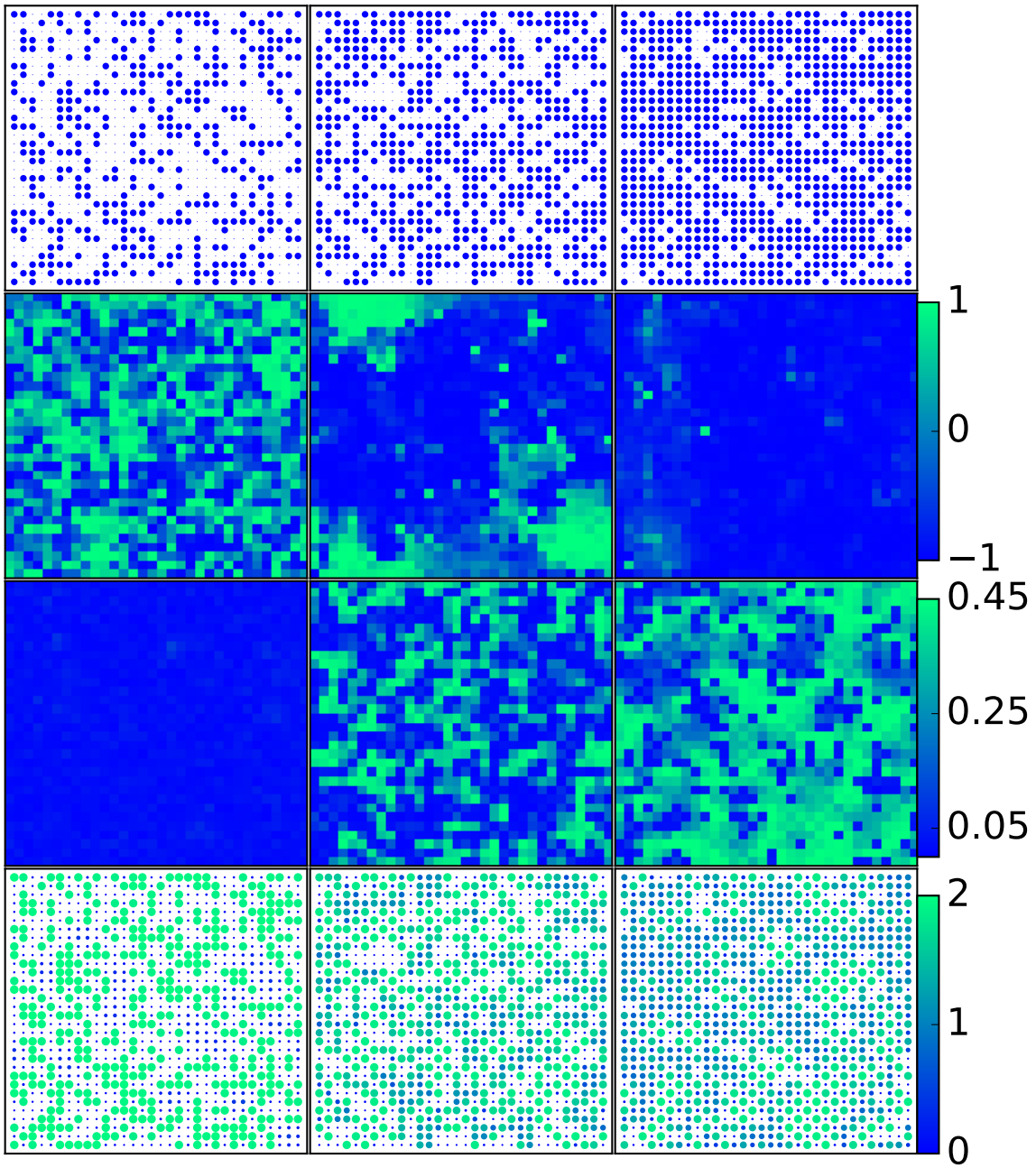

Figure 5.4: Real-space configurations of the distribution of attractive centers and various auxiliary fields at $U = 8$ at the lowest temperature ($T = 0.001$ in units of t.The three columns correspond to different dilution : $\delta = 0.4$ (first), $\delta = 0.6$ (second) and $\delta = 0.8$ (third). The first row gives the distribution of attractive centers with blue circles denoting sites with $U_i = U$. The other rows depict the phase $\cos(\arg(\Delta_i))$ (second) and the amplitude $|\Delta_i|$ (third) of the pairing fields, and the charge field n_i (fourth). The system size is 32×32.

dramatically as we change U. At large U, even though the amplitudes have acquired reasonably large values at every site, their phases become uncorrelated due to thermal fluctuations of these soft degrees of freedom. This reduces T_c as U increases. The nonmonotonic variation of δ_c and T_c as a function of U suggests that the transition from a metallic to a superconducting ground state cannot be thought of as entirely due to percolation of amplitude puddles, as noted in an earlier work[183] . The contrast between the two extreme ends of weak and strong coupling is striking: There are phase-coherent patches of relatively small amplitudes at small U and leads to a percolative transition as the number of attractive centers increases; however, strong phase fluctuations suppress the T_c at large U even though the pairing amplitude is quite strong enough at most of the sites.

5.4 Electronic Spectral Functions

In this section we look at the spectral properties of the system, in particular, concentrating on the single particle density of states (DOS). Once the system reaches equilibrium for a given set of parameters and temperature, we evaluate the DOS as

$$N(\omega) = \left\langle \sum_{i,n} \left(\left|u_n^i\right|^2 \delta(\omega - \varepsilon_n) + \left|v_n^i\right|^2 \delta(\omega + \varepsilon_n) \right) \right\rangle, \tag{5.6}$$

where $\langle \ldots \rangle$ denotes thermal and disorder average. Here ε_n and $\{u_n^i, v_n^i\}$ are the positive eigenvalues and eigenvectors respectively of the Bogoliubov quasiparticles states, obtained from the BdG Hamiltonian, in a given equilibrium configuration used in the averaging. This is expected to show a bulk superconducting gap and coherence peaks when the system turns superconducting. Fig. (5.5a) shows its variation as a function of δ at the lowest temperature we have accessed in the weak-coupling regime with $U = 2.$. There is no gap until about $\delta \sim 0.3$ and a gap appears

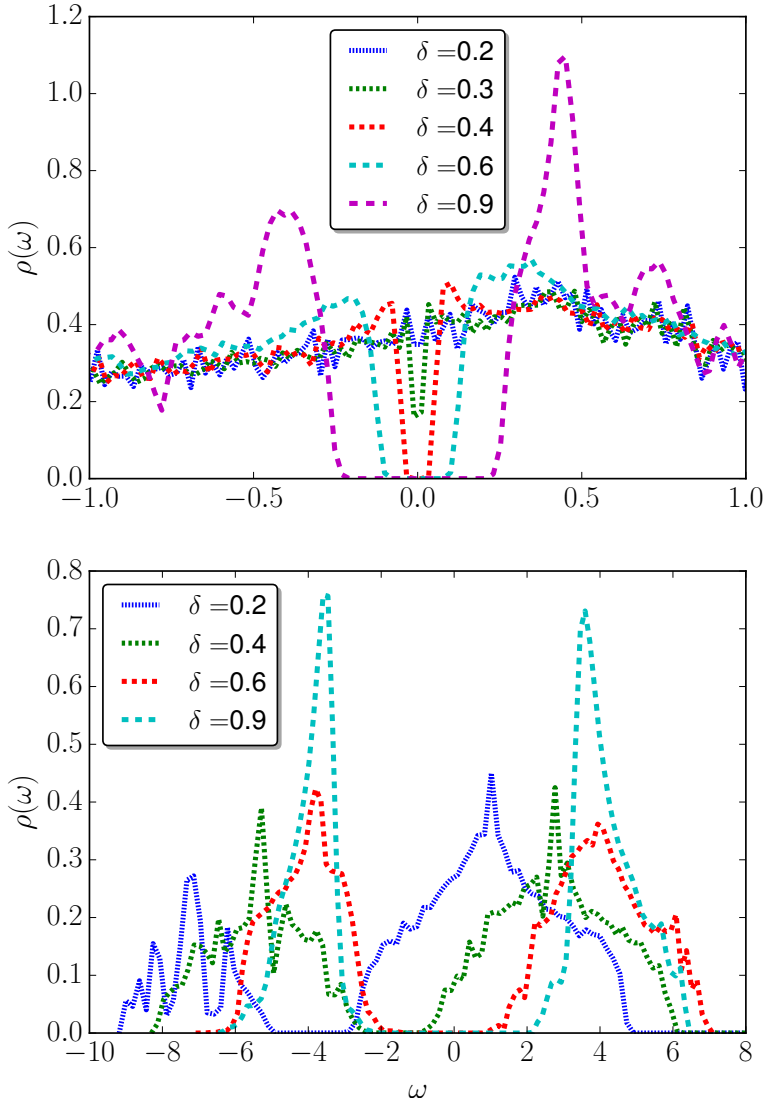

Figure 5.5: Single-particle density of states at the lowest temperature ($T = 0.001$ in units of t) as a function of dilution for (a) $U = 2$ and (b) $U = 8$.

as δ approaches 0.4. A clear spectral gap is seen at larger values of δ, which increases with increase in δ. Also visible are the coherence peaks on either side of the gap. These results match very well with those obtained from the structure factor in Fig. (5.1). In fact, this gap vanishes as we increase the temperature across T_c in this region of parameter space (for small U). However, the temperature variation of the spectral gap changes dramatically as we increase U. The temperature at which the gap vanishes increases very rapidly with U even though as mentioned in the previous section, the T_c comes down drastically. This shows a clear separation the pairing scale determined from the spectral gap and superconducting scale that determines T_c. Note that the thermal fluctuations can destroy the pairing gap only when $T \sim \Delta_0$, which scales with U. However, due to the loss of phase coherence, T_c is much reduced. This leads to a nontrivial phase at intermediate temperatures and moderate-to-large values of U, where the gap persists in the spectral function, but the superfluid stiffness is zero. When $T \sim U$, there is a spectral weight transfer leading to gradual filling up of the hard gap before the coherence features are completely lost. This region with its own characteristic optics is referred to as the pseudogap phase.

We also find that the gap in the density of states is larger at larger values of U, as expected. However, the effect of δ is more subtle. While the gap decreases with δ, it exists even when superconductivity is not present in the system. We show typical results for a representative value of $U = 8$ in Fig. (5.5b). Even when very few sites have attractive centers, when U is large enough, local pairing tendencies are stronger. Thus centers which have large U become doubly occupied and gain an energy of the order of $-U$. In the large U limit this states with energy $-U$ will be isolated from the kinetic energy band. If the average no of particle is nearly half then one has to fill up higher energy states above the gap. Density at state at the Fermi energy($\omega = 0$) will be non-zero; the ground state of the system would be a metal as can be seen for $\delta = 0.2$ and

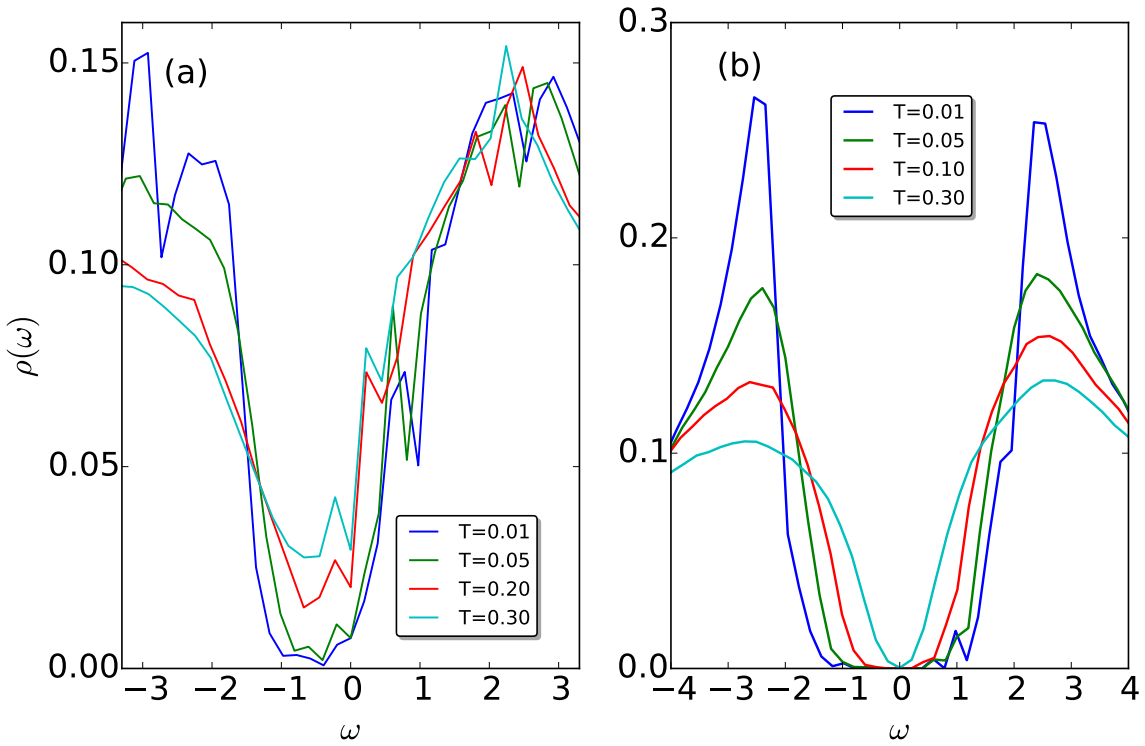

Figure 5.6: Single-particle density of states for $U = 6$ with $\delta = 0.5$ (a) and 0.8 (b) at different temperatures.

0.4. Fig. (5.6) shows the behavior of single particle density of states for two different dilution $\delta = 0.5$ (Fig. (5.6a) and 0.8 (Fig. 5.6b) at two representative temperatures. As expected, sharp coherence peaks are not seen in the spectral function. What is striking is that at larger δ, the spectral gap, even though diminished in size, persists at high temperatures

5.5 Optical Transport

Optical conductivity is expected to be directly correlated to the spectral features discussed previously and we explore it in this section. In the superconducting state, $\sigma(\omega)$ has two contributions; there is a zero frequency diamagnetic response that is proportional to the superfluid stiffness. In addition, there is a ω-dependent regular part arising due to various effects such as pair breaking, quasiparticle scattering etc. We concentrate on the latter in this section. In the superconducting ground state and in the clean, BCS limit, the latter contributes only at fre-

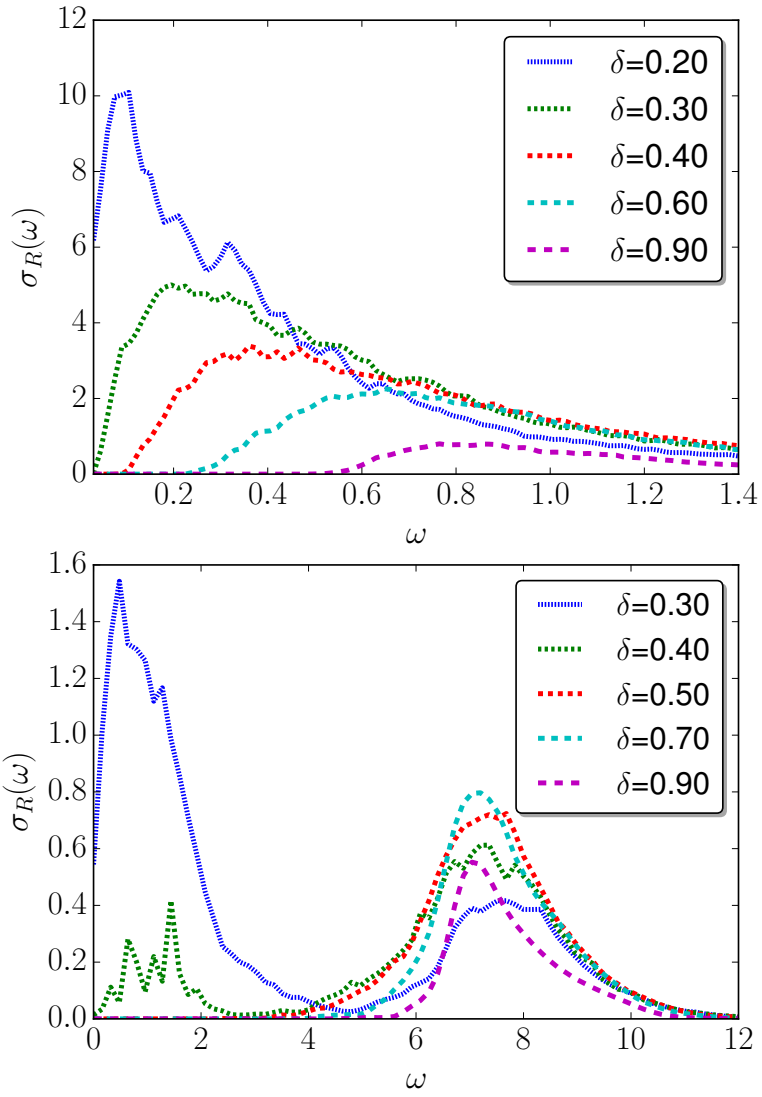

Figure 5.7: The real part of the optical conductivity $\sigma_R(\omega)$ as a function of frequency ω at the lowest temperature ($T = 0.001$ in units of t) for different values of site dilution and interaction strengths $U = 2$ (upper panel) and $U = 8$ (lower panel).

quencies larger than twice the superconducting gap. At nonzero temperatures, there is finite contribution even inside this frequency window, but exponentially suppressed. We find that the site-diluted system has its own characteristic features, especially in the low frequency regime, giving rise to a richer structure.

Optical conductivity, $\sigma(\omega)$, is computed using the Kubo formula as follows [148]. Formally, $\sigma(\omega) = -\omega^{-1}\Im(\Lambda_{xx}(\mathbf{q}=0,\omega))$, where $\Lambda_{xx}(\mathbf{q}=0,\omega)$ is the current-current correlation function:

$$\Lambda_{xx}(\mathbf{q}=0,\omega) = \frac{1}{\mathcal{Z}}\sum_{a,b}|\langle a|j_{xx}|b\rangle|^2\frac{e^{-\beta E_a}-e^{-\beta E_b}}{\omega+E_a-E_b+i\delta}, \tag{5.7}$$

with $\delta \to 0^+$. Here, $|a\rangle$, $|b\rangle$ are the many-particles eigenstates of the system with eigenvalues E_a, E_b respectively and $j_{xx} = (-it)\sum_{i,\sigma}\left(c^{\dagger}_{i+x,\sigma}c_{i,\sigma} - h.c.\right)$ is the current operator in the x-direction. Evaluating this expression in terms of the Bogoliubov quasiparticle operators, we obtain the regular part of the optical conductivity as

$$\begin{aligned}\sigma_{reg}(\omega) &= \sum_{n,m}F_1(n,m)\frac{(f(\varepsilon_n)+f(\varepsilon_m)-1)}{\varepsilon_n+\varepsilon_m}\delta(\omega-\varepsilon_n-\varepsilon_m)\\ &+ \sum_{n,m}F_2(n,m)\frac{(f(\varepsilon_n)-f(\varepsilon_m))}{\varepsilon_n-\varepsilon_m}\delta(\omega-\varepsilon_n+\varepsilon_m),\end{aligned} \tag{5.8}$$

where $f(\varepsilon_n)$, $f(\varepsilon_m)$ are the Fermi functions corresponding to the positive single-particle eigenvalues ε_n, ε_m of the BdG Hamiltonian as mentioned in the previous section, and $F_1(n,m)$, $F_2(n,m)$ are the current-matrix elements computed from the BdG eigenstates. The latter are given by $F_1(n,m) = \left|\sum_i g_1^i(n,m)\right|^2 + \left|\sum_i g_2^i(m,n)\right|^2$ and $F_2(n,m) = \left|\sum_i g_3^i(n,m)\right|^2$, with

$$\begin{aligned}g_1^i(n,m) &= v_n^{i+x}u_m^i - v_n^i u_m^{i+x} + v_m^{i+x}u_n^i - v_m^i u_n^{i+x}\\ g_2^i(n,m) &= u_n^{*i+x}u_m^i - u_n^{*i}u_m^{i+x} - v_m^{i+x}v_n^{*i} + v_m^i v_n^{*i+x}\end{aligned}$$

$$g_3^i(n,m) = v_n^{i+x} v_m^{*i} - v_n^i v_m^{*i+x} - u_m^{*i+x} u_n^i + u_m^{*i} u_n^{i+x}. \quad (5.9)$$

For small values of U, the above features appear to be generic and a representative behavior is shown in Fig. (5.7a) for U =2. The gapped spectrum results in the vanishing of the optical conductivity for $\delta \geqslant 0.4$. At small δ, the system remains a metal. However, there is intrinsic disorder present due to small number of attractive centers which give rise to enhanced scattering even at low temperatures and results in a non-Drude behavior of $\sigma(\omega)$. In the large U limit optical conductivity behaves differently as a function δ. Strong optical response at larger ω arises due to excitations across the SC gap, while the excitations within the kinetic band, separated from the lower band at $-U$, give rise to low frequency non-Drude-like behavior. (See Fig. 5.7b.)

We summarise these findings in the next two figures. In Fig. (5.8), we give two representative phase diagrams of the site-diluted attractive Hubbard model as a function of T and U for two specific values of $\delta = 0.8$ (Fig. 5.8a) and $\delta = 0.5$ (Fig. 5.8b). At small values of U, the system turns from a BCS-like superconducting state to a normal metal above T_c, which scales with the pairing gap. However, at larger U even though the pairing gap continues to increase, T_c reduces from the mean field value due to strong phase fluctuations. The normal state above T_c has quasiparticle gap in the spectrum. However, there is an intervening region, where, a hard gap does not appear in the spectrum, but there is significant reduction of spectral weight at low frequencies. We call this the pseudogap phase.

For smaller δ, SC ground state vanishes above a critical value of U since there is a critical dilution δ_c that increases with U. Finally, Fig. (5.9) shows the three dimensional phase diagram of the model as a function of T, δ, and U, clearly brining out the variation of δ_c with U and the nonmonotonic behavior of T_c as the strength of interaction changes.

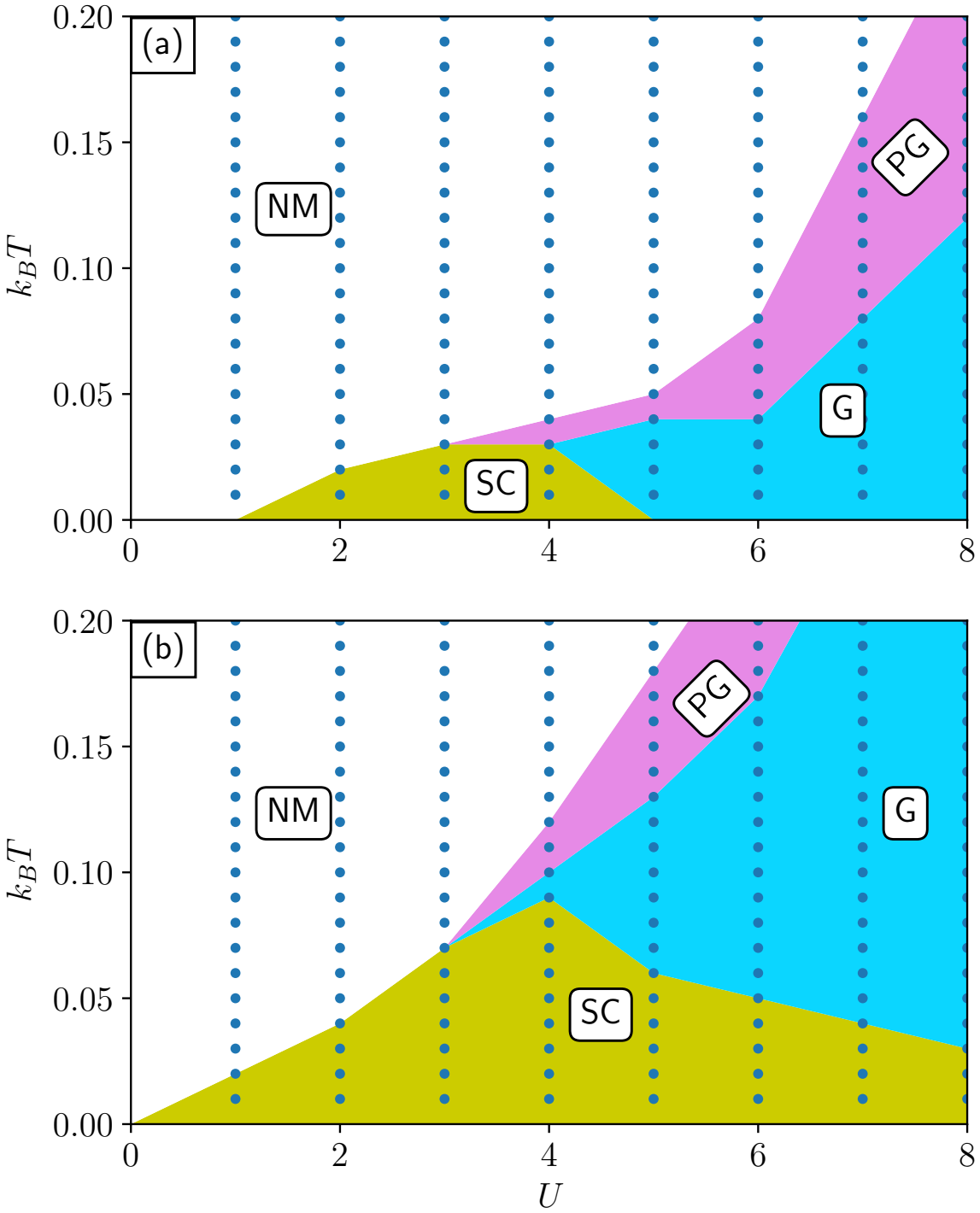

Figure 5.8: Two representative phase diagrams of the site-diluted attractive Hubbard model as a function of temperature T and strength of the attractive interaction U for (a) $\delta = 0.8$ and for (b) $\delta = 0.5$. SC, NM, PG, and G represent superconducting, normal metal, pseudogap phase, and gapped phases.

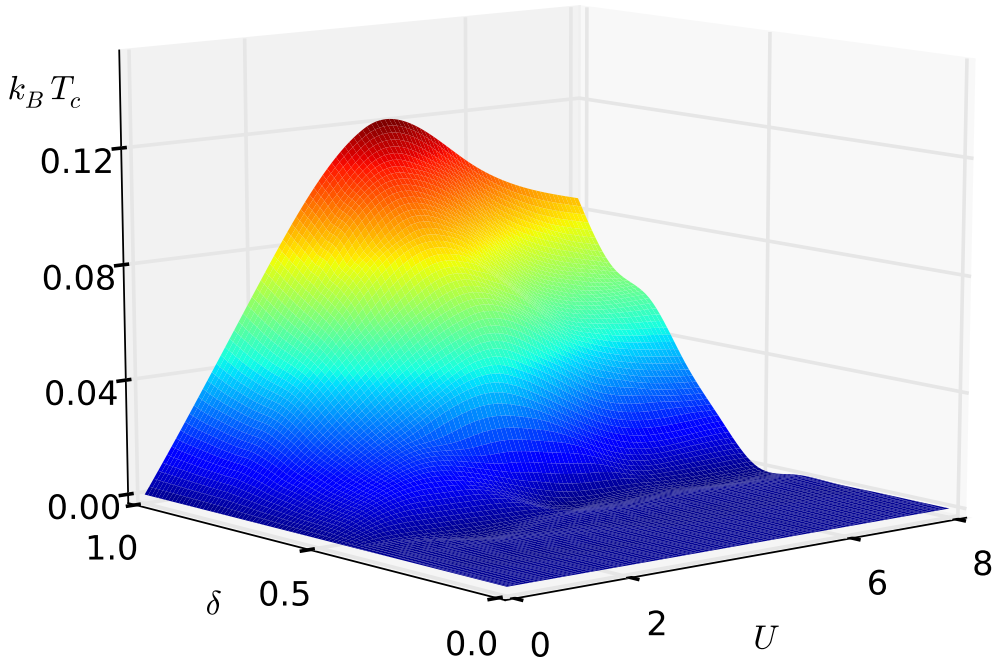

Figure 5.9: Phase diagram of the site-diluted attractive Hubbard model as a function of the superconducting transition temperature T_c, attractive interaction U, and the average density of attractive centers δ.

5.6 Conclusions

In this chapter, we studied random, local attraction driven metal-superconductor transition in two dimensions using the attractive Hubbard model. A real-space Monte Carlo method was employed after introducing pairing and density fields *via* Hubbard-Stratanovich transformation. Needless to say, it has many advantages over BdG mean field theory and the DMFT, both of which utilize coherent potential and local approximations. The present method is capable of capturing the physics from weak-to-strong coupling regimes and gives a real-space depiction of the transition, which are crucial to the problem at hand. In particular, the effect of intrinsic disorder on the BCS-BEC crossover has been studied. We can calculate the self-energy of the free electron due to introduction of the attractive sites. Imaginary part of this self-energy will

give a finite lifetime to the single particle states of the free electrons. This will give a measure of disorderness in our site diluted context .

The main results are as follows. As observed in previous studies, we find that there is a critical concentration of attractive centers needed for the onset of globally phase-coherent superconductivity. The critical density increases with U and appears to saturate beyond $U \sim 6$. For small values of U the transition is percolative in nature and the physics is akin to that of a BCS superconductor. In this regime the metal-superconductor transition is driven by percolation of internally phase-coherent superconducting islands at the critical density of randomly placed negative-U centers. However, the scenario is different at larger strengths of interaction. In this regime, the zero-temperature pairing gap continues to increase with U, but no longer determines T_c. Local pairing tendencies persist even above the transition temperature resulting in either a pseudogap or a robust gap in the quasiparticle spectral functions, but a dominant role is played by the strong spatial phase fluctuations leading to a BCS-BEC crossover. Transition temperatures are suppressed and T_c exhibits a nonmonotonic behavior as U is varied. The high-temperature normal state transforms from a metal to a gapped phase as U increases and has pseudogap features in the intermediate region due to the existence of short-range order of the amplitude of the order parameter. Spectral functions and transport properties corroborate these findings. We believe that this is, perhaps, the first study that probes the nature of the BCS-BEC crossover, an inherently strong-coupling problem, in an intrinsically disordered superconductor from a real-space perspective.

Next, we comment on a few shortcomings of our study. First, we have allowed for numerically exact treatment of thermal fluctuations of the order parameter (and also, of the charge field), but neglected their dynamics. Thus the inherent quantum fluctuations of these auxiliary fields are not taken into account. This may affect the low temperature properties, especially

near the critical concentration of impurities. Second, it is expected that T_c will reduce to zero in the clean limit as one moves towards half filling and the system will transform to a charge density wave (CDW) phase. However,, while our approach works very well away from half filling, it is not expected to capture the CDW instability that competes with superconductivity. The present method allows for large charge fluctuations at sites as U_i varies. This calls for caution. In real systems, there are long-ranged Coulomb interactions among electrons that, albeit screened, would still deter charge inhomogeneities appearing over large length scales as it costs Coulomb energy. We wish to address this problem in future. In real two-dimensional systems there cannot be finite temperature phase transitions, in contrast to what is seen here, since thermal fluctuations prohibit any order at nonzero temperatures. However, T_c obtained in this work should be thought of as a crossover scale below which correlation length increases rapidly. If so, even a weak coupling to a third dimension will stabilize the SC phase at nonzero temperatures.

The present work could be extended in many ways. One could include the dynamics of the order parameter field at a semiclassical level after obtaining the equilibrium configurations. This would allow us to extract some interesting physical properties of the normal phase having preformed pairs at moderate-to-large coupling, reminiscent of the Nernst effect in cuprates [194], and its persistence in the BEC regime. One could study the competition between disorder arising due to site dilution with those of alternate origin, for example, the presence of magnetic impurities. The latter is expected to have a detrimental effect on the conventional BCS state [195]. The effect of site dilution in an insulating host is an interesting problem where an insulating gap and SC gap compete with each other [196]; the application of the present method shows a further suppression of T_c as one moves towards the clean limit and a transition to a charge-modulated insulating phase[131]. A further extension would be to study the role

of site dilution in SC systems with order parameter symmetry different from the *s*-wave considered here as well as in imbalanced lattice fermion system that could support breached pair and Fulde-Ferrel-Larkin-Ovchinnikov (FFLO) [197] states. We present some results of these studies in the next chapter

Chapter 6

Site dilution in an Insulator

In the previous chapter we studied the effect of site dilution on the superconducting state when the host is metallic. One could very well ask the behavior of the randomly site diluted attractive Hubbard model on an insulating host. This, of course, is related to the general question of whether pairing of electrons and the existence of BCS-like (or for that matter BEC-like) state is possible in absence of Fermi surface. This was first discussed by Kohn and coworkers [198] in the context of pairing in semiconductors. Quite obviously, the existence of an insulating state necessarily requires multiple (at least two well separated) band appearing explicitly or arising due to some other effects such as a CDW formation in an otherwise single band model of electrons. Due to electron-phonon coupling, attractive interaction could exist between intra band or inter band electrons. In general, both could contribute. Kohn reasoned that the gain in energy due to pair formation has to exceed the energy cost of formation of electron-hole pair (an exciton) across the semiconductor gap for the superconducting state to stabilise. Otherwise, excitons formed would move across the material independently and incoherently. Based on this phenomenology, a couple of models were proposed to study the nature of superconductivity in an otherwise insulating system. Kohmoto and Takada [199] used an inter band pairing model while Nozieres and Pistolesi [196] employed a pseudogap model. These studies revealed that not only superconductivity is possible starting from a state that has no Fermi surface, but its

nature could show nontrivial features. However, the above studies were carried out in the mean field spirit. A couple of questions arise naturally. What is the effect of disorder on such phases? Is it possible to have a BEC state close to the insulator? Does the normal state close to the insulator exhibit anomalous features in thermodynamics or transport? These questions also appear to be relevant in the context of cuprates since a superconducting state appears due to doping of a Mott insulator. In this chapter, we apply the methods developed earlier to address a simple problem of the effect of site dilution on the superconducting state having an insulating host.

6.1 Effective model for an insulating host

We consider the attractive Hubbard Model with site dilation.

$$H = \sum_{\langle ij\rangle\sigma} t c^{\dagger}_{i\sigma} c_{j\sigma} - \sum_i U_i n_{i\uparrow} n_{i\downarrow} - \sum_i (\mu + \varepsilon_i) n_i \tag{6.1}$$

Here $c_i^{\dagger}(c_i)$ is the fermion creation(annihilation) operator. The first term is the kinetic energy of electrons with t being the nearest neighbor hopping integral which we set equal to unity. Third term is the chemical potential term which fixes the average number of particles in the system. We have carried out all calculations with total number of particle kept fixed at $n = 1.0$. We have introduced ε_i to make the noninteracting system a insulator. A square lattice is a bipartite lattice composed of two sublattices, A and B, and the local potential ε_i is defined as

$$\varepsilon_i = \begin{cases} V & \text{for } i \in A, \\ -V & \text{for } i \in B. \end{cases} \tag{6.2}$$

U_i is the strength of the two-particle attraction which is site dependent. U_i takes the value

according to the probability distribution $P(U)$ which defined as

$$U_i = \begin{cases} U, & P(U) = \delta \\ 0, & P(U) = 1-\delta \end{cases} \tag{6.3}$$

We have taken $U > 0$ for the attractive Hubbard Model. We also specialise to the case when $V = 0.20$. This gives rise to a CDW state at half filling in absence of interactions. δ can take value from 0 to 1 and $\delta = 1$ is the homogeneous(undiluted) attractive Hubbard Model. After employing the standard Hubbard-Stratanovich transformation, the effective Hamiltonian in terms of these time independent HS fields becomes

$$\begin{aligned} H = & \sum_{\{ij\}\sigma} (t_{ij} - \mu\delta_{ij}) c^{\dagger}_{i\sigma} c_{j\sigma} + \sum (\Delta_i c^{\dagger}_{i\uparrow} c^{\dagger}_{i\downarrow} + h.c.) \\ & + \sum_i (\varepsilon_i - \phi_i) n_i + \sum_i \left(\frac{|\Delta_i|^2}{U_i} + \frac{|\phi_i|^2}{U_i} \right) \end{aligned} \tag{6.4}$$

6.2 Order parameter and the critical temperature

We have used the structure factor $S(\mathbf{q})$ of the auxiliary pairing field Δ_i to track the superconducting transition.

$$S(\mathbf{q}) = \frac{1}{N^2} \sum_{ij} \Delta_i \Delta^*_j e^{i\mathbf{q}.(\mathbf{r_i}-\mathbf{r_j})} \tag{6.5}$$

where Δ_i defined as

$$\Delta_i = \langle c^{\dagger}_{i\uparrow} c^{\dagger}_{i\downarrow} \rangle. \tag{6.6}$$

We have considered only $S(\mathbf{0})$ since the attractive Hubbard model produces only a $s-$wave symmetric superconductiing state. $S(\mathbf{0})$ acts as a order parameter for the superconducting transition. We define T_c to be the temperature at which $S(\mathbf{0})$ takes a finite, nonzero value as we lower the temperature.

The transition temperature (T_c) depends on various parameter. Fig[6.1] shows T_c as a func-

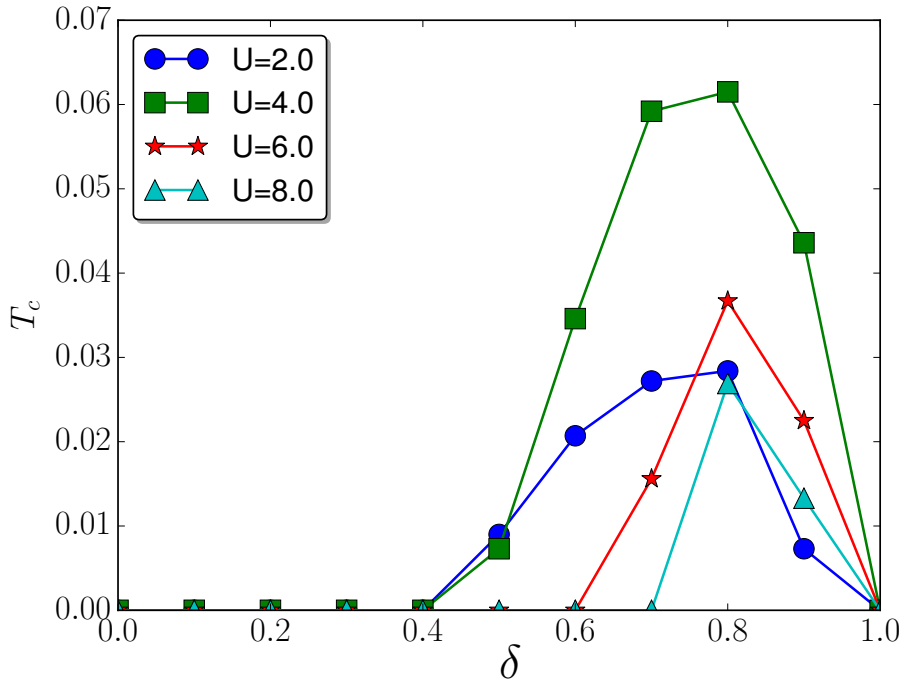

Figure 6.1: Superconducting transition temperature T_c versus δ for various values of U.

tion of δ for various values of U. Transitions temperature shows a nonmonotonic behaviour as δ increases from 0 to 1. At half filling, *i.e.,* $n = 1$ and $V = 0$, the charge density wave (CDW) and superconducting state are degenerate resulting in neither of them winning over the other at finite temperatures. In presence of a sublattice dependent potential, the CDW state is promoted and the superconducting state is less favored. There is an overall decrease in the transition temperature compared to the situation when $V = 0$. At $\delta = 1$ transition temperature goes to zero at all values of U. T_c increases as δ decreases from $\delta = 1$. This is because away from $\delta = 1$, a finite amount of dilution helps to promote superconductivity. There is also a clear indication of BCS-BEC crossover; specifically T_c first increases with increase in U and in the strong coupling it decreases with U. Transition temperature also shows a maximum as δ varies from 1 to 0. A critical δ_c is required for the onset of superconductivity which increases with increasing U. This is due to the percolateve nature f the transition. At small U, the coherence length is large and even if there are very few attractive centres, coherence gets established. However, at larger U, the pair strength reduces and a dense embedding of attractive centers is needed for a globally

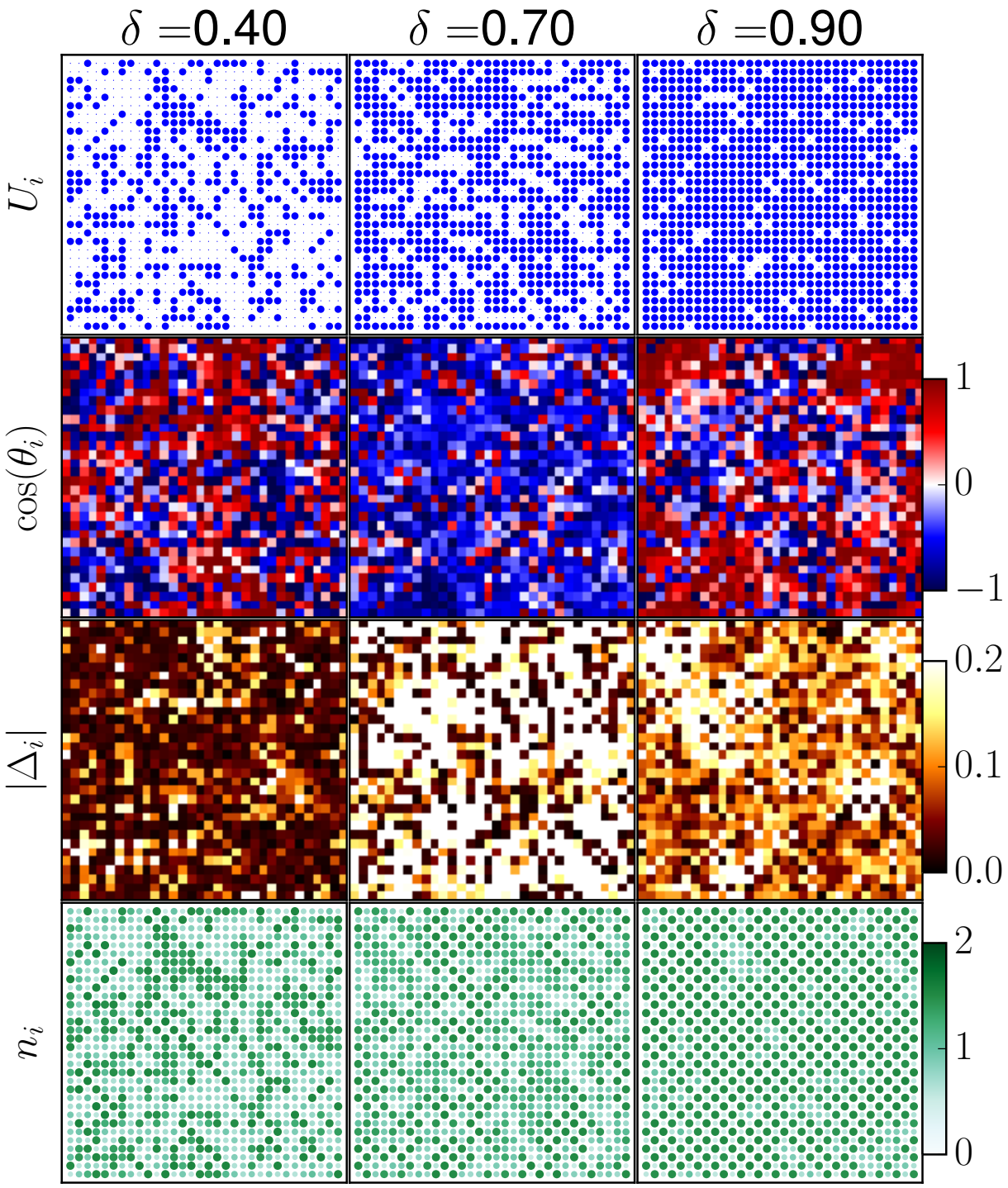

Figure 6.2: Real space configuration of U_i, phase $(\cos(\theta_i))$, $|\Delta_i|$ and charge (n_i) for different values of δ at $U = 2.0$ and $T = 0.001$.

phase coherent superconducting state to develop.

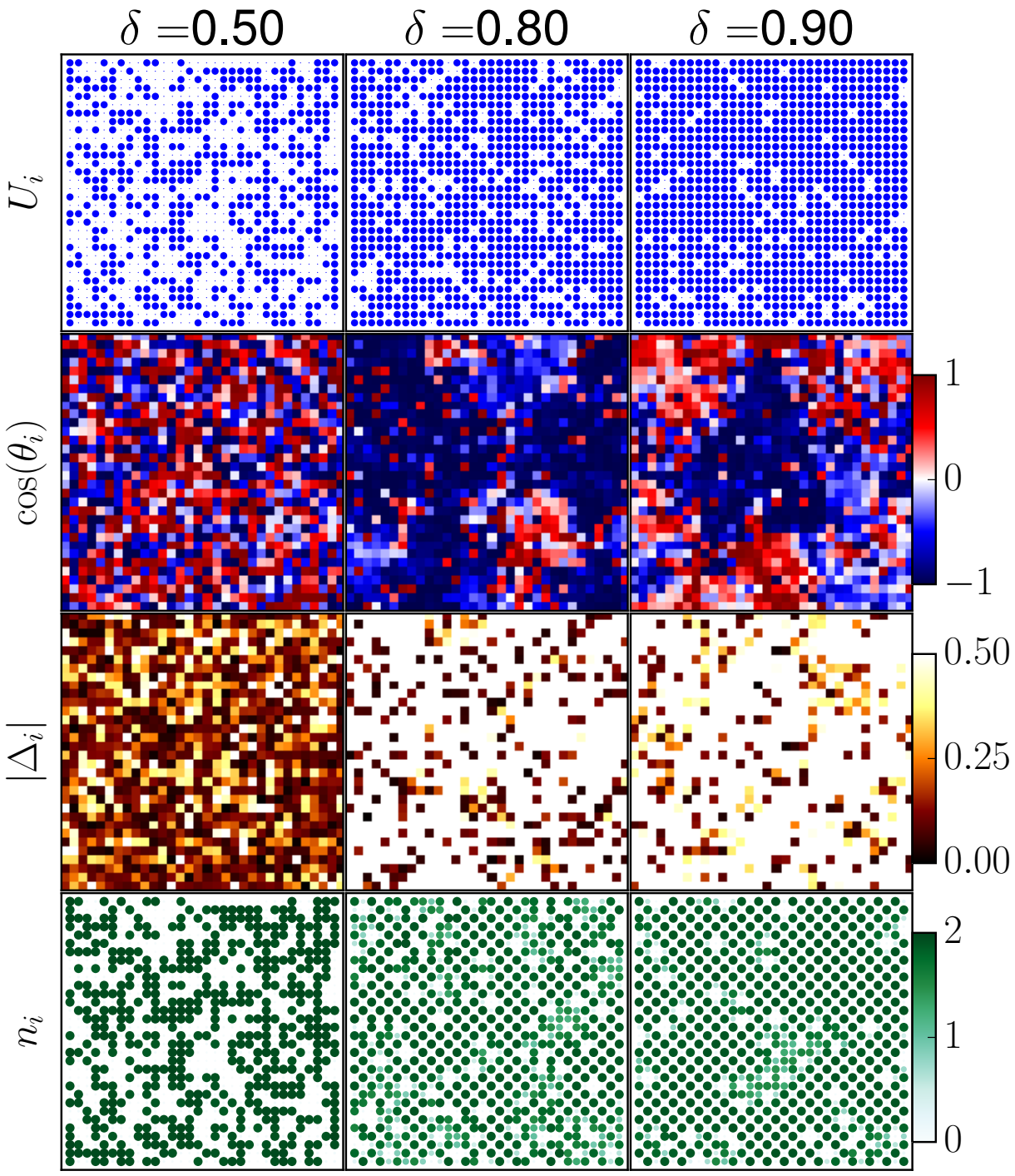

Figure 6.3: Real space configuration of U_i, phase $(\cos(\theta_i))$, $|\Delta_i|$ and charge (n_i) for different values of δ at $U = 8.0$ and $T = 0.001$.

6.3 Real space analysis

Fig[6.2] shows the spacial map of different physical quantities for $U = 2.0$ at low temperature. We see that for $\delta = 0.40$, n_i has very strong fluctuations from site to site and follow the distribution of U_i. n_i takes binary values which are near 0 and 2 depending $U_i = 0, U$ respectively. This correspondence between n_i and U_i becomes less prominent with increasing δ and the CDW becomes much more noticeable as δ approaches unity. There are short ranged CDW correlations even at $\delta = 0.70$ and the size of these regions grows with δ. For $\delta = 0.90$ large CDW regions are clearly visible.

Pairing gap shows very distinct behavior as δ changes. Though there is very strong fluctuation of the amplitude of Δ_i, for $\delta = 0.40$ it takes very low values. The average value of $|\Delta_i|$ increases at $\delta = 0.70$ and again decreases at $\delta = 0.90$. Global phase coherence of the condensate wavefunction sets superconductivity in the system. The attractive Hubbard model exhibits a phase coherent superconducting ground state in the absence of any site dilution. There is a fluctuation of this phase even at zero temperature in presence of site dilution. At $\delta = 0.40$ phase fluctuation dominates and there is no global superconductivity even at the lowest temperatures studied. These phase fluctuations decrease with increasing δ. At $\delta = 0.70$ though there is some amount of phase fluctuation we can still find large coherent regions with finite nonzero transition temperature. With further increase of δ, the CDW dominates and superconductivity weakens. There is degeneracy between CDW and superconductivity in the absence of the sublattice dependent potential (V) and at $\delta = 1$. This degeneracy is lifted by the nonzero V and the CDW phase appears at $\delta = 1$.

If a site has very large attractive U, it is energetically favourable to doubly occupy it. This

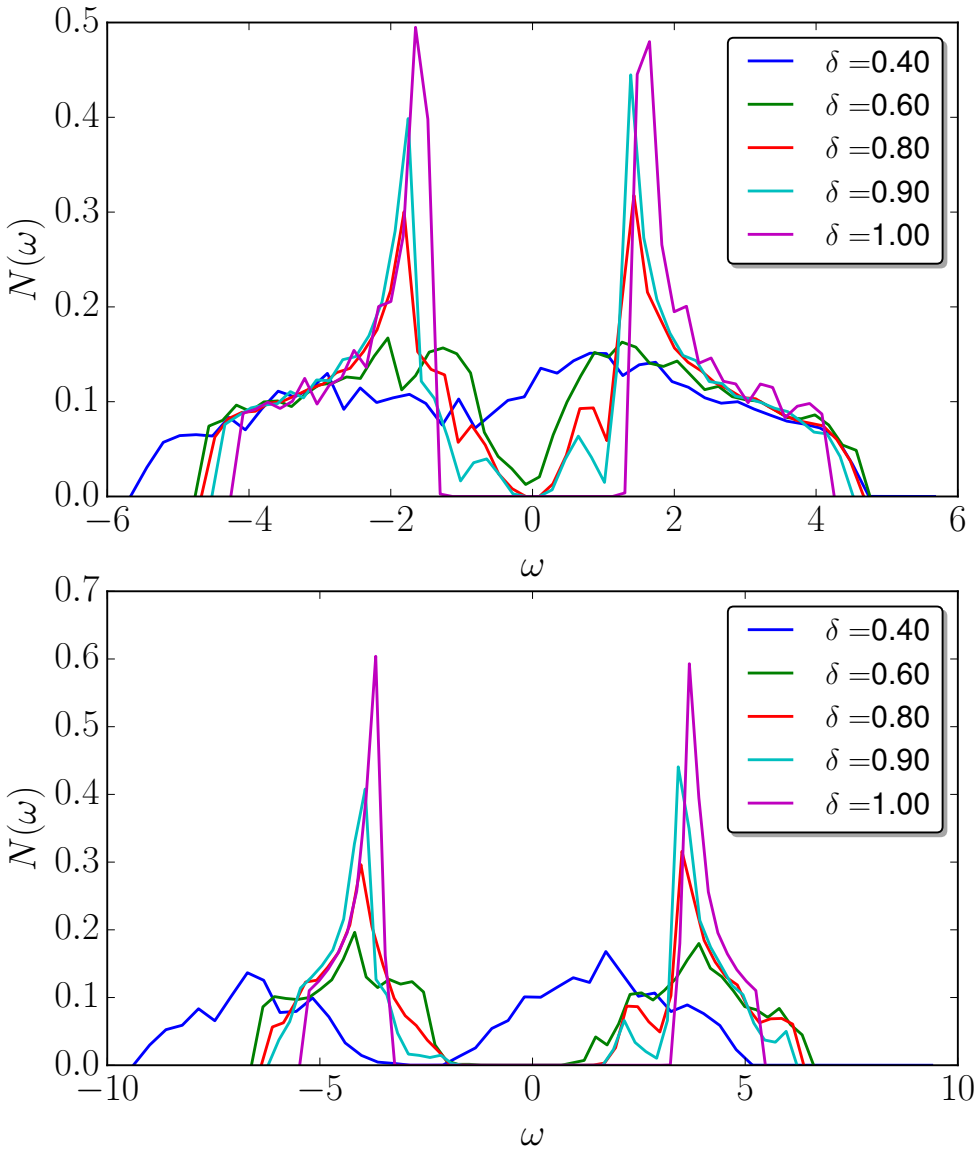

Figure 6.4: Single particle density of state for different values of δ at $U = 4.0$ and $T = 0.0010$.

doubly occupied site will, in general, follow the distribution of U_i in real space, namely n_i takes 2,0 at those site where $U_i = U, 0$ respectively. In the Fig[6.3], for $\delta = 0.5$ we find this kind of behavior of n_i and on the average $|\Delta_i|$ takes very small inhomogeneous values. Phases of Δ_i become non-uniform giving zero structure factor. At $\delta = 0.80$ superconducting and charge density wave phases compete with each other. Spacial pattern of n_i shows small regions of charge density wave. $|\Delta_i|$ takes larger value with very less fluctuation. Phase of Δ_i shows large coherent regions giving rise to a finite, nonzero transition temperature. At $\delta = 0.90$ charge

density wave state becomes much more prominent while phases become less coherent resulting in lower transition temperatures.

6.4 Density of states

Fig[6.4(a)] shows the single particle density of states (DOS at low temperature ($T = 0.0010$) and for $U = 4.0$ and 8.0.

There are state that appear within the gap as dilution increases, but the DOS remains gaped in the superconducting region. The DOS become gapless when superconductivity disappears. In the strong coupling region DOS show a nontrivial two band structure which are the two Hubbard bands. The lower and upper Hubbard band have weights δ and $1-\delta$ respectively. These two bands are well separated when the ratio t/U becomes very small. However, since we have fixed the average number of particle to unity, the Fermi energy remains pinned in the upper Hubbard band and the system shows a metallic behavior. Fig[6.4(b)] shows the DOS in the strong coupling region for $U = 8.0$.

6.5 Optical Conductivity

As discussed in the previous chapter, the optical conductivity has two contributions in the superconducting state. The first part (a diamagnetic contribution) is a Delta function at $\omega = 0$ responsible for the supercurrent in the system and weight(D) of this Delta function is proportional to the superfluid density. The total optical conductivity can be written as

$$\sigma(\omega) = D\delta(\omega) + \sigma_R(\omega) \tag{6.7}$$

$\sigma_R(\omega)$ is the regular part of the optical conductivity. In our study we will discuss only the regular part of the optical conductivity. Fig[6.5] shows the optical conductivity for weak and strong

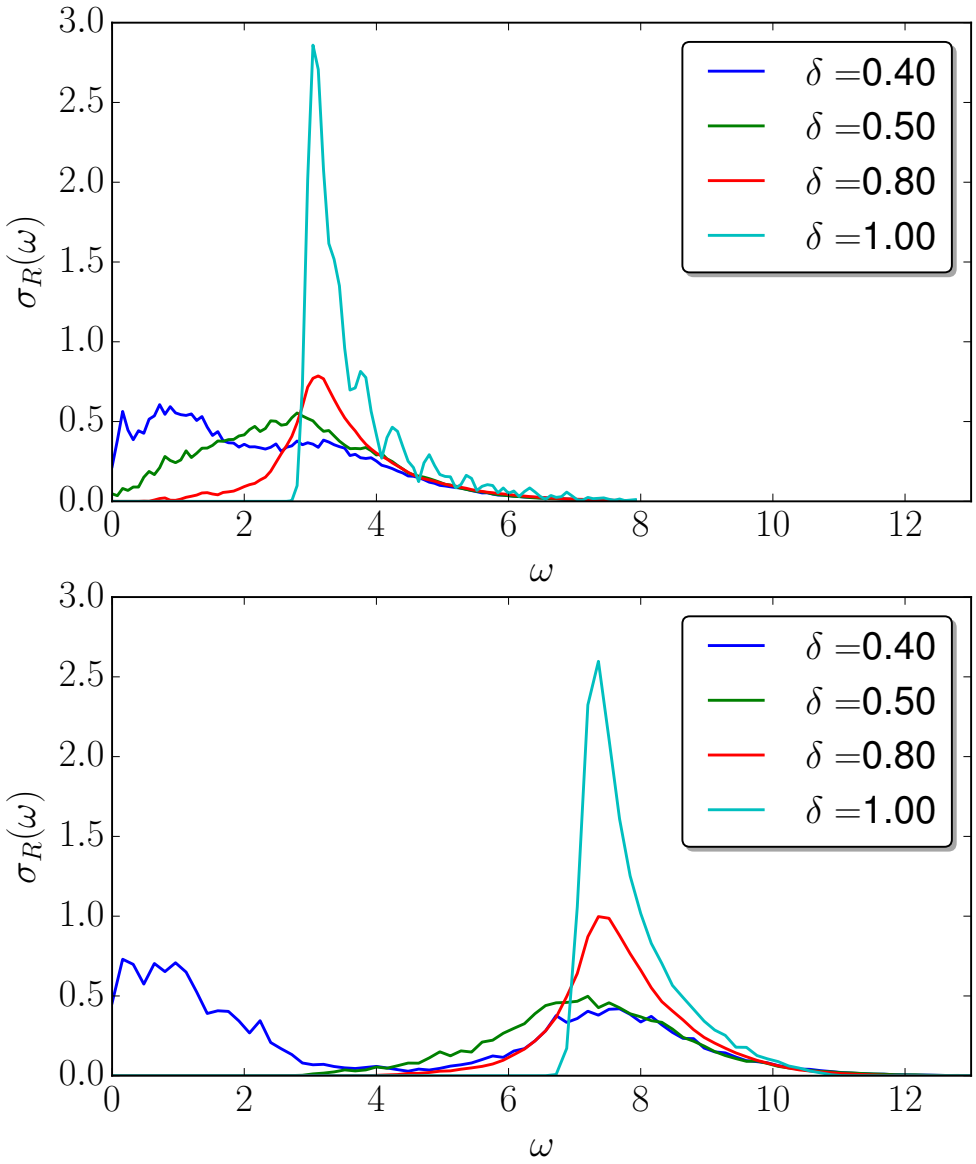

Figure 6.5: Lowest temperature ($T = 0.001$) optical conductivity for different values of δ for $U = 4.0$(upper panel) and $U = 8.0$(lower panel).

coupling regimes in the low temperature limit. BCS like behaviour appears in the undiluted case (δ 1). In this limit $\sigma_R(\omega)$ has a gap as single particle spectrum is also gapped. There is also the signature of a strong coherence peak appearing just after the gap. The coherence peak gets suppressed with site dilution and disappears in the non-superconducting state. In the intermediate coupling ($U = 4$) region, a finite spectral weight shows up in the gap. With further site dilution gap vanishes and the conductivity becomes Drude like. The gap in the $\sigma_R(\omega)$ also

decreases with dilution, but a two peak structure is visible. The lower energy peak in the metallic region is due to electronic transitions within the upper Hubbard band (see Fig[6.4]). There is a gap between upper and lower Hubbard bands. Fermi energy lies in the upper Hubbard band. The second peak in $\sigma_R(\omega)$ is due to transition from lower Hubbard band to the upper Hubbard band.

6.6 Conclusions

We have studied the effect of site dilution on the nature of superconducting state in an insulating host. This is perhaps the first study which explores the entire coupling regime of this problem and gives a real space description of the goings on. It is possible that T_c does not continuously vanish as $\delta \rightarrow 1$ due to quantum fluctuations which are neglected here. It will be worthwhile to study models having specific inter and intra band couplings to shed more light on this problem.

Chapter 7

Conclusions

This thesis explores some problems in strongly correlated electron systems, which is an active area of quantum condensed matter physics. Two classes of problems were investigated. The first one pertains to the interplay between electron-electron interactions and electron-lattice coupling. The second study dwells on the effect of randomly placed attractive centres on a lattice leading to electron pairing and a superconducting ground state While the effective models used in both the studies are rather simple, they encode a rich physics, most of which cannot be rationalised using the conventional framework of mean field or variational states and/or perturbative approaches. Nontrivial effect of competing interactions lead to transitions among several phases. Thermal fluctuations and spatial inhomogeneities bring in novel features to electronic properties. To deal with the multitude of these issues, we adopted a static auxiliary field approach to deal with correlations. This converts an interacting, quantum electron problem to one in which electrons interact with spatially and thermally fluctuating classical fields. This is much more amenable to a numerical treatment using exact diagonalisation and statistical sampling and a reasonably large number of degrees of freedom can be incorporated. The method smoothly interpolates from weak-to-strong coupling, handles spatial and thermal fluctuations, and being a real space based approach, helps us visualise the phases and transitions among them. A large number of physical quantities can be evaluated including thermodynamic, spectral, and trans-

port properties. It was benchmarked by applying to a few limiting cases first, where the general features are already well known.

We first studied the Holstein-Hubbard model at half filling on a square lattice. The salient results include the appearance of a nonmagnetic metallic phase at low values of coupling parameters in addition to the ordered phases, including antiferromagnetic and charge-modulated ones. However, the finite-temperature phase diagram shows rich features and includes a pseudogap phase at intermediate coupling. This arises due to the persistence of local order in charge and spin degrees. Characteristic changes in spectral features get reflected in other physical properties and example being a non-Drude like behavior in optical conductivity. To explore the effect of geometrical frustration, we change the lattice geometry to triangular and find that a critical interaction is needed to get ordered insulating phases. Spatial ordering also changes due to geometry. In the second part of the thesis, we investigated the effect of randomly placed attractive centers on electron pairing leading to superconductivity. Phase fluctuations play an important role in determining the percolative nature of the transition as well as the BCS-BEC crossover that occurs as interaction strength increases. The host in which the attractive centers reside could be a metal or insulator. The latter allows us to study superconducting instability in a system with no Fermi surface.

We outline some of the shortcomings of the present approach and discuss ways to overcome them. While rewriting the interaction in terms of auxiliary fields is exact, we neglect the quantum fluctuations of the fields during the numerical implementation by assuming them to be static. This has several drawbacks. Quantum fluctuations become more relevant in lower dimensions and at low temperatures and our results may not be reliable in those regimes. Further, phenomena such as Kondo effect and more exotic phases such as spin liquid states cannot be captured since quantum correlations are at the heart of these behaviors. A glaring problem with

this approach is that d-wave superconducting state that may possibly exist in two dimensional repulsive Hubbard model cannot even be anticipated using the present approach. Neglect of phonon dynamics in the Holstein means that we are working in a very limited range of the parameters of the model and phenomena arising due to retarded effects such as superconductivity within Holstein model cannot be addressed. The present method may be thought of in the same spirit as spin wave theory applied to spin systems, whereby one starts with a classical ground state configuration for the spins and builds up quantum corrections perturbatively in some small parameter. The present method is a step towards implementing such a procedure for many constituents interacting among themselves. However, it goes beyond the analogy of spin wave theory in several aspects. We do not need to assume a classical ground state; the Monte Carlo procedure selects it naturally. The latter also incorporates thermal fluctuations. An obvious way of including corrections is to retain fluctuations at the Gaussian level and study the stability of the phases and how these fluctuations affect the low-temperature thermal, spectral, and transport properties. Equivalently, one can think of Fourier transforming the auxiliary fields into bosonic Matsubara frequencies and the static approach corresponds to retaining only the $\omega_n = 0$ mode. In this language, corrections could be added by progressively adding small frequency modes to it. A further approximation is made while handling g the repulsive interaction by treating the charge fields at the saddle-point level. The charge fields turn out to be purely imaginary and their contribution to the classical action does not have a lower bound. This makes the classical Monte Carlo sampling of these fields very unstable and necessitates the saddle-point approximation which we have resorted to. The results obtained this way, for the pure Hubbard and Holstein models, respectively suggest that the saddle-point approximation does not affect the results severely. However, this limits its applicability to half filled case for the repulsive model. Note that the attractive interaction does not suffer from this limitation. We have restricted ourselves to two dimensions in the present study. This is not a handicap and can easily be extended to three dimensions at the expense of more computational resources. However, questions could

be raised as to validity of our results since we obtain finite temperature transitions in two dimensions. However, it is expected that there would be a coherence temperature roughly mimicking the above transition temperatures even in two dimensions below which the correlation lengths increase rapidly. In other words, the system enters the renormalized classical regime. If so, even a weak coupling to a third dimension will stabilize the ordered phases. There could be some qualitative changes such as disappearance of insulating phases at weak couplings since nesting is no longer possible, but we expect gross features to remain the same.

Our approach has several advantages. It is computationally inexpensive unlike numerically exact methods such as quantum Monte Carlo and exact diagonalization and large system sizes can be accessed. It is also easy to calculate several physical properties including transport. It retains spatial correlations and fluctuations unlike dynamical mean field theory which is essential to understand features such as pseudogap, phase coherence driven phenomena, and localisation. Thermal fluctuations are fully retained and there are no low temperature constraints since the statistical sampling involves only a classical Monte Carlo procedure. Most importantly, it covers the entire coupling range from weak to strong. in a unified way. Comparison of our results with previous studies capturing dynamics suggests that neglect of quantum dynamics may not severely affect the physics in many strongly correlated phenomena. However, as suggested above, we hope that corrections can be systematically added and make this a well controlled approximation.

There are many applications/extensions of the present study. One could use multi band, multi phonon models that are more appropriate for realistic systems. It could be extended to study interfaces or heterostructures of correlated systems. One could incorporate more order parameter symmetries while dealing with attractive interactions. Exploring three dimensional models is very natural and is currently restricted only by the adequate availability of computational re-

sources. Finally, it could be applied to more exotic system such as those showing topological phenomena where the effect of interactions is not well understood.

Bibliography

[1] Sommerfeld. A, Zeitschrift fr Physik **47**: 13 (1928).

[2] Drude, Paul ., Annalen der Physik **306**(3): 566 (1889).

[3] Anderson, P. W., Phys. Rev. **109**, 1492 (1958).

[4] Abrahams, E., P. W. Anderson, D. C. Licciardello, and T. V. Ramakrishnan, Phys. Rev. Lett. **42**, 673 (1979).

[5] D. J. Thouless, Phys. Rep. **13**, 93 (1974).

[6] Imada M, Fujimori A and Tokura Y, Rev. Mod. Phys. **70**, 1039 (1998).

[7] Limelette P, Wzietek P, Florens S, Georges A, Costi T A, Pasquier C, Jerome D, Meziere C and Batail P , Phys. Rev. Lett. **91**, 016401 (2003).

[8] Paalanen M A and Bhatt R N, Physica B **169**, 231 (1991).

[9] Sarachik M P, Metal-Insulator Transitions Revisited ed P Edwards and C N R Rao (London: Taylor and Francis) 1995.

[10] Rosenbaum T F, Andres K, Thomas G A and Bhatt R N, Phys. Rev. Lett. **45**, 1423 (1980).

[11] G. Keller, K. Held, V. Eyert, D. Vollhardt, V.I. Anisimov, Phys. Rev. B **70**, 205116 (2004).

[12] J. Hubbard, Proc. R. Soc. A **276**, 238 (1963).

[13] M. C. Gutzwiller, Phys. Rev. Lett. **10**, 159 (1963).

[14] J. Kanamori, Prog. Theor. Phys. **30**, 257 (1963).

[15] Patrick Fazekas, Lecture Notes on Electron Correlation and Magnetism, World Scientific, (1999).

[16] P. Fulde, Electron correlations in molecules and solids, Springer, Berlin (1995).

[17] E. Lieb and F. Y. Wu, Phys. Rev. Lett. **20**, 1445 (1967).

[18] A. Georges, G. Kotliar, W. Krauth and M. J. Rozenberg, Rev. Mod. Phys. **68**, 13 (1996).

[19] M. C. Gutzwiller, Phys. Rev. Lett. **10**, 159 (1963); J. Kanamori, Prog. Theor. Phys. **30**, 275 (1963).

[20] W. F. Brinkman and T. M. Rice, Phys. Rev. B **2**, 4302 (1970).

[21] Moessner R and Ramirez P, Physics Today **59** 24 (2006).

[22] Takehiko Ishiguro, Kunihiko Yamaji and Gunzi Saito, Organic Superconductors, Springer, 2012.

[23] John Singleton, Rep. Prog. Phys. **63** 1111 (2000).

[24] Miyagawa, K., Kawamoto, A., Nakazawa, Y., and Kanoda, K., Phys. Rev Lett. **75**, 1174(1995).

[25] Shimizu, Y., Miyagawa, K., Kanoda, K., et al., Phys. Rev Lett. **91**, 107001 (2003).

[26] Kurosaki, Y., Shimizu, Y., Miyagawa, K., et al., Phys. Rev Lett. **95**, 177001 (2005).

[27] R. Coldea, D.A. Tennant, A.M. Tsvelik and Z. Tylczynski, Phys. Rev. Lett. **86**, 1335 (2001).

[28] J.S. Helton, K. Matan, M.P. Shores, E.A. Nytko, B.M. Bartlett, Y. Yoshida, Y. Takano, A. Suslov, Y. Qiu, J.-H. Chung, D.G.Nocera and Y.S. Lee, Phys. Rev. Lett. **98**, 107204 (2007).

[29] L. D. Landau, Phys. Z. Sowjetunion **3**, 664 [English translation (1965), Collected Papers, New York: Gordon and Breach, pp. 67-68].

[30] Holstein T, Ann. Phys. (Leipzig) **8**, 325 (1959).

[31] T. Holstein, Ann. Phys. (N.Y.) **8**, 343 (1959).

[32] Wi1son, J. A. , F. J. DiSalvo, and S. Mahajan, Adv. Phys. **24**, 117. (1975).

[33] I. G. Lang and Y. A. Firsov, Sov. Phys. JETP **16**, 1301 (1963).

[34] F. Marsiglio, Physica C **21**, 224 (1995).

[35] Kamerlingh-Onnes, H., Comm. Phys. Lab. Univ. Leiden, Nos. 122 and 124, (1911).

[36] W. Meissner and R. Ochsenfeld. *Naturwissenchaften*, **21**, 787 (1933).

[37] Leon N. Cooper, Phys. Rev., **104**, 1189(1956).

[38] P. G. de Gennes, Superconductivity in Metals and Alloys Benjamin, New York, 1966 .

[39] Micnas R., S. Robaszkiewicz, Cond. Mat. Phys Vol. **1**, No 1(13), 89 (1998).

[40] P. Fulde and R. A. Ferrell: Phys. Rev. **135** (1964) A550.

[41] A. I. Larkin and Yu. N. Ovchinnikov: Zh. Eksp. Teor. Fiz. **47**, 1136(1964). [translation: Sov. Phys. JETP **20** (1965) 762].

[42] R. Casalbuoni and G. Narduli: Rev. Mod. Phys. **76**, 263(2004).

[43] K. Gloos, R. Modler, H. Schimanski, C. D. Bredl, C. Geibel, F. Steglich, A. I. Buzdin, N. Sato, and T. Komatsubara, Phys. Rev. Lett. **70**, 501(1993).

[44] G. Yin and K. Maki: Phys. Rev. B **48** 650 (1993).

[45] H. Burkhardt and D. Rainer: Ann. Physik **3** 181 (1994).

[46] H. Shimahara: Phys. Rev. B **50**, 12760 (1994).

[47] M. Tachiki, S. Takahashi, P. Gegenwart, M. Weiden, M. Lang, C. Geibel, F. Steglich, R. Modler, C. Paulsen, and Y. Onuki: Z. Phys. B **100**, 369 (1996).

[48] P. W. Anderson, J. Phys. Chem. Solids **11**, 26 (1959).

[49] A. A. Abrikosov, L. P. Gorkov, Sov. Phys. JETP **9**, 220 (1959).

[50] D. J. Bishop, E. G. Spencer, and R. C. Dynes, The Metal-Insulator Transition in Amorphous Nb:Si, Solid St. Electron **28**, 73 (1985).

[51] D. B. Haviland, Y. Liu, and A. M. Goldman, Phys. Rev. Lett. **62**, 2180 (1989).

[52] T. I. Baturina, A. Y. Mironov, V. M. Vinokur, M. R. Baklanov, and C. Strunk, Phys. Rev. Lett. **99**, 257003 (2007).

[53] J. Bonca and S. A. Trugman, Phys. Rev. B, **64**, 094507 (2001).

[54] J. P. Hague and P. E. Kornilovitch, Phys. Rev. B, **80**, 054301 (2009).

[55] A. S. Alexandrov and P. E. Kornilovitch, Phys. Rev. B, **82**, 807 (1999).

[56] J. P. Hague, P. E. Kornilovitch, J. H. Samson, and A. S. Alexandrov, Journal of Physics Condensed Matter, **19**, 255214 (2007).

[57] T. M. Hardy, J. P. Hague, J. H. Samson, and A. S. Alexandrov, Phys. Rev. B. **79**, 212501, (2009).

[58] A B Migdal , Sov. Phys. JETP **7**, 996 (1958).

[59] Eliashberg G M, Sov. Phys. JETP **11** 696 (1960).

[60] Bickers N E and Scalapino D J., Ann. Phys., NY **193** 206 (1989).

[61] Freericks J K, Zlatic V, Chung W and Jarrell M., Phys. Rev. B, **58** 11613 (1998).

[62] Millis A J, Mueller R and Shraiman B I., Phys. Rev. B, **54** 5389 (1996).

[63] P. Sahebsara and D. Senechal, Phys. Rev. Lett. **100**, 136402 (2008).

[64] H. Y. Yang, A. M. Lauchli, F. Mila and K. P. Schmidt, Phys. Rev. Lett. **105**, 267204 (2010).

[65] Nicholas Metropolis, Arianna W. Rosenbluth, Marshall N. Rosenbluth, Augusta H. Teller, and Edward Teller. The Journal of Chemical Physics, **21**, 1087 (1953).

[66] S. Kumar and P. Majumdar, Eur. Phys. J. B, **50**, 571 (2006).

[67] The effect of geometric frustration on some correlated electron systems, Thesis by Rajarshi Tiwari.

[68] Borejsza K and Dupuis N, Phys. Rev. B **69**, 085119 (2004).

[69] Bartosch L and Kopietz P, Phys. Rev. B **62** R16223 (2002).

[70] Dupuis N, Phys. Rev. B **65**, 245118 (2002).

[71] Emery V J, Correlated Electron Systems, edited, World Scientific, Singapore, (1993).

[72] Lee P A, Nagaosa N and Wen X G, Rev. Mod. Phys. **78**, 17(2006).

[73] Freericks J K and Zlatić V , Rev. Mod. Phys. **75**, 1333 (2003).

[74] Lanzara A, Bogdanov P V, Zhou X J, Kellar S A, Feng D L, Lu E D, Yoshida T, Eisaki H, Fujimori A, Kishio K, Shimoyama J I, Noda T , Uchida S, Hussain Z, and Shen Z X, Nature (London) **412**, 510 (2001).

[75] Dagotto E, Rev. Mod. Phys. **66**, 763 (1994).

[76] Danmascelli A, Shen Z X, and Hussain Z, Rev. Mod. Phys. **75**, 473 (2003).

[77] Bar-Yam Y, Egami T, Leon J M, and Bishop A R , Lattice Effects in High-T_c Superconductors, World Scientific, Singapore, (1992)

[78] Dagotto E, Rev. Mod. Phys. **66**, 763 (1994).

[79] Takabayashi Y, Ganin A Y, Jeglic P, Arcon D, Takano T, Iwasa Y, Ohishi Y, Takata M, Takeshita N, Prassides K, and Rosseinsky M J, Science **323**, 1585 (2009).

[80] Capone M, Fabrizio M, Castellani C, and Tosatti E, Rev. Mod. Phys. **81**, 943 (2009).

[81] Gunnarsson O, Rev. Mod. Phys. **69**, 575 (1997).

[82] Taraphder A, Pandit R, Krishnamurthy H R, Ramakrishnan T V, Int. J. Mod. Phys. B **10**, 863 (1996).

[83] Cava R J, Batlogg B, Krajewski J J, Farrow R, Rupp Jr L W, White A E, Short K, Peck W F, and Kometani T, Nature **332**, 814 (1988).

[84] Ramakrishnan T V, J. Phys.: Condens. Matter **19**, 125211 (2007).

[85] Dagotto E, Nanoscale Phase Separation and Colossal Magnetoresistance: The Physics of Manganites and Related Compounds, Springer Science, (2013)

[86] Mishchenko A S and Nagaosa N, Phys. Rev. Lett. **93**, 036402 (2004).

[87] Gr*ü*ner G, Density Waves in Solids , Westview Press (2000) .

[88] Dagotto E , Hotta T and Moreo A, Phys. Rep. **344**, 1 (2001).

[89] Millis A J, Littlewood P B, and Shraiman B I, Phys. Rev. Lett. **74**, 5144 (1995).

[90] Millis A J, Mueller R, and Shraiman B I, Phys. Rev. B **54**, 5389 (1996).

[91] Cataudella V, Filippis G D, Mishchenko A S, Nagaosa N, Phys. Rev. Lett. **99**, 226402 (2007).

[92] Murakami Y, Werner P, Tsuji N, and Aoki H, Phys. Rev. B **88**, 125126 (2013).

[93] Fehske H, Hager G and Jeckelmann E, Europhys. Lett **84**, 57001 (2008).

[94] Berger E, Val*á*šek P, and Linden W, Phys. Rev. B **52**, 4806 (1995).

[95] Bauer J and Hewson A C, Phys. Rev. B **81**, 235113 (2010).

[96] Johnston S, Nowadnick E A, Kung Y F, Moritz B, Scalettar R T and Devereaux T P, Phys. Rev. B **87**, 235133 (2013).

[97] Freericks J K, Phys. Rev. B **48**, 3881 (1993).

[98] Freericks J K and Jarrell M, Phys. Rev. Lett. **75**, 2570 (1995).

[99] Khatami E, Macridin A, and Jarrell M, Phys. Rev. B **78**, R060502 (2008).

[100] Macridin A, Moritz B, Jarrell M, and Maier T, Phys. Rev. Lett. **97**, 056402 (2006).

[101] Marsiglio F, Physica C **162**, 1453 (1989).

[102] Nowadnick E A, Johnston S, Moritz B, Scalettar R T, and Devereaux T P, Phys. Rev. Lett. **109**, 246404 (2012).

[103] Scalettar R T, Bickers N E, and Scalapino D J, Phys. Rev. B **40**, 197 (1989).

[104] Vekič M and White S R, Phys. Rev. B **48**, 7643 (1993).

[105] Goodenough J B, Phys. Rev. **100**, 564 (1955).

[106] Borejsza K and Dupuis N, Europhys. Lett. **63**, 722 (2003).

[107] Huang Z B, Hanke W, Arrigoni E, and Scalapino D J , Phys. Rev. B **68**, 220507(R) (2003).

[108] Dobry A, Greco A, Lorenzana J, and Riera J, Phys. Rev. B **49**, 505 (1994).

[109] Dobry A, Greco A, Lorenzana J, Riera J and Diep H T, Europhys. Lett. **27**, 617 (1994).

[110] Grilli M and Castellani C, Phys. Rev. B **50**, 16880 (1994).

[111] De Ciolo A , Lorenzana J, Grilli M and Seibold G, Phys. Rev. B **79**, 085101 (2009).

[112] Bauer J, Europhys. Lett. **90**, 27002 (2010).

[113] Bauer J and Hewson A C, Phys. Rev. B **81**, 235113 (2010).

[114] Werner P and Millis A. J, Phys. Rev. Lett. **99**, 146404 (2007).

[115] Georges A, Kotliar G, Krauth W and Rozenberg M, Rev. Mod. Phys. **68**, 13 (1996).

[116] Capone M, Sangiovanni G, Castellani C, Di Castro C, and Grilli M, Phys. Rev. Lett. **92**, 106401 (2004).

[117] Koller W, Meyer D, $\bar{O}$no Y and Hewson A C, Europhys. Lett. **66** 559 (2004).

[118] Koller W, Meyer D, and Hewson A C, Phys. Rev. B **70**, 155103 (2004).

[119] Wilson K, Rev. Mod. Phys. **47**, 773 (1975).

[120] Bulla R, Costi T and Pruschke T, Rev. Mod. Phys. **80**, 395 (2008).

[121] Schulz H J, Phys. Rev. Lett. **65**, 2462 (1990)

[122] Zaleski T A and Kopeć T K, Phys. Rev. B **77**, 125120 (2008).

[123] Ramakrishnan T V and Saha D, (private communication)

[124] Tiwari R and Majumdar P, Europhys. Lett. **108**, 27007 (2014).

[125] Slater J C, Phys. Rev. **82** , 538 (1951).

[126] Nakatsuji S, Machida Y, Maeno Y, Tayama T, Sakakibara T, Duijn J v, Balicas L, Millican J N, Macaluso R T, and Chan J Y, Phys. Rev. Lett. **96**, 087204 (2006).

[127] Okamoto S and Millis A J, Nature **428**, 630 (2004).

[128] Bhattacharya A and May S J, Annu. Rev. Mater. Res. **44**, 65 (2014).

[129] Kanoda K. and Kato R, Annu. Rev. Condens. Matter Physics **2**, 167 (2011).

[130] Debauche M, Diep H T , Phys. Rev. B **46**, 8214 (1992).

[131] Pradhan S and Pai G V, (In preparation)

[132] K. Miyagawa, A. Kawamoto, and K. Kanoda, Phys. Rev. B **61**, R7679 (2000).

[133] K. Yamamoto, K. Yakushi, K. Miyagawa, K. Kanoda, and A. Kawamoto, Phys. Rev. B **65**, 085110 (2002).

[134] M. Watanabe, Y. Nogami, K. Oshima, H. Mori, and S. Tanaka, J. Phys. Soc. Jpn. **68**, 2354 (1999).

[135] M. Watanabe, Y. Noda, Y. Nogami, and H. Mori, J. Phys. Soc. Jpn. **73**, 116 (2004).

[136] M. Watanabe, Y. Noda, Y. Nogami, and H. Mori, J. Phys. Soc. Jpn. **74**, 2011 (2005).

[137] D. Belitz and T. R. Kirkpatrick, Rev. Mod. Phys. **66**, 261 (1994).

[138] V. F. Gantmakher and V. T. Dolgopolov, Phys. Usp. **53**, 3 (2010).

[139] M. Sadowskii, Phys. Rep. **202**, 225 (1997).

[140] V. Dobrosavljevic, N. Trivedi, and J. M. Valles , *Conductor-Insulator Quantum Phase Transitions* (Oxford University Press (2012)).

[141] A. A. Abrikosov and L. P. Gorkov, Sov. Phys. JETP **9**, 220 (1959).

[142] G. Deutscher, *New Superconductors: From Granulr to High* T_c (World Scientific (2006)).

[143] A. Ghosal, M. Randeria, and N. Trivedi, Phys. Rev. Lett. **81**, 3940 (1998); Phys. Rev. B **65**, 014501 (2001).

[144] Y. Dubi, Y. Meir, and Y. Avishai, Nature(London) **449**, 876 (2007).

[145] S. Ghosh and S. S. Mandal, Phys. Rev. Lett. **111**, 207004 (2013).

[146] K. Bouadim, Y. L. Loh, M. Randeria, and N. Trivedi, Nature Phys. **7**, 884 (2011).

[147] M. V. Feigel'man, L. B. Ioffe, V. E. Kravtsov, and E. A. Yuzbashyam, Phys. Rev. Lett. **98**, 027001 (2007).

[148] S. Tarat and P. Majumdar, Europhys. Lett. **105**, 67002 (2014).

[149] N. Trivedi, R. T. Scalettar, and M. Randeria, Phys. Rev. B **54**, R3756 (1996).

[150] C. Huscroft and R. T. Scalettar, Phys. Rev. Lett. **81**, 2775 (1998); R. T. Scalettar, N. Trivedi, and C. Huscroft, Phys. Rev. B **59**, 4364 (1999).

[151] Y. Dubi, Y. Meir, and Y. Avishai, Phys. Rev. B **78**, 024502 (2008).

[152] G. Seibold, L. Benfatto, C. Castellani, and J. Lorenzana, Phys. Rev. Lett. **108**, 207004 (2012).

[153] M. P. A. Fisher, Phys. Rev. Lett **65**, 923 (1990).

[154] T. V. Ramakrishnan, Phys. Scripta **T27**, 24 (1989).

[155] B. Sacépé *et al.*, Nature Comm. **1**, 140 (2010).

[156] B. Sacépé *et al.*, Nature Phys. **7**, 239 (2011).

[157] M. Chand *et al.*, Phys. Rev. B **85**, 014508 (2012).

[158] M. Mondal *et al.*, Phys. Rev. Lett. **106**, 047001 (2011).

[159] M. Mondal *et al.*, Sc. Rep. **3**, 1357 (2013).

[160] A. Kamlapure *et al.*, Sci. Rep. **3**, 2979 (2013).

[161] B. Sacépé *et al.*, Phys. Rev. Lett. **101**, 157006 (2008).

[162] Y. Noat *et al.*, Phys. Rev. B **88**, 014503 (2013).

[163] T. I. Baturina, C. Strunk, M. R. Baklanov, and A. Satta, Phys. Rev. Lett. **98**, 127003 (2007); T. I. Baturina, A. Yu. Mironov, V. M. Vinokur, M. R. Baklanov, and C. Strunk, Phys. Rev. Lett. **99**, 257003 (2007).

[164] M. A. Steiner, N. P. Breznay, and A. Kapitulnik, Phys. Rev. B **77**, 212501 (2008).

[165] P. A. Lee and T. V. Ramakrishnan, Rev. Mod. Phys. **57**, 287 (1985).

[166] V. Berezinskii, Sov. Phys. JETP **32**, 493 (1971); J. M. Kosterlitz and D. J. Thouless, J. Phys. C **5**, L124 (1972), *ibid.* **6**, 1181 (1973).

[167] D. B. Haviland, Y. Liu, and A. M. Goldman, Phys. Rev. Lett. **62**, 2180 (1989).

[168] A. F. Hebard and M. A. Paalanen, Phys. Rev. Lett. **65**, 927 (1990).

[169] R. Crane *et al.*, Phys. Rev. B **75**, 184530 (2007).

[170] K. H. S. B. Tan, K. A. Parendo, and A. M. Goldman, Phys. Rev. B **78**, 014506 (2008).

[171] A. J. Leggett, *Quantum Liquids* (Oxford University Press (2006)).

[172] P. Nozières and S. Schmitt-Rink, Jl. Low Temp. Phys. **59**, 195 (1985)

[173] Q. Chen, J. Stajic, S. Tan, K. Levin, Phys. Rep. **412**, 1 (2005).

[174] S. Tarat and P. Majumdar, Eur. Phys. Jl. B **88**, 68 (2015).

[175] Y. Matsushita, H. Bluhm, T. H. Geballe, and I. R. Fisher, Phys. Rev. Lett. **94**, 157002 (2005).

[176] Y. Matsushita, P. A. Wianecki, A. T. Sommer, T. H. Geballe, and I. R. Fisher, Phys. Rev. B **74**, 134512 (2006).

[177] S. M. Kazakov *et al.*, Phys. Rev. B **71**, 024533 (2005).

[178] J. Karpinski *et al.*, Phys. Rev. B **71** , 174506 (2005).

[179] In some cases doping may induce local structural changes in the insulating host, promoting pairing. Impurity band superconductivity is another possibility. The simplified model in Eq. (1) does not capture such refinements.

[180] G. Litak and B. L. Györffy, Phys. Rev. B **62**, 6629 (2000).

[181] K. Aryanpour, E. R. Dagotto, M. Mayr, T. Paiva, W. E. Pickett, and R. T. Scalettar, Phys. Rev. B **73**, 104518 (2006)

[182] K. Aryanpour, T. Paiva, W. E. Pickett, and R. T. Scalettar, Phys. Rev. B **76**, 184521 (2007)

[183] F. Mondaini, T. Paiva, R. R. dos Santos, and R. T. Scalettar, Phys. Rev. B **78**, 174519 (2008).

[184] V. B. Shenoy, Phys. Rev. B **78**, 134503 (2008).

[185] N. A. Kamar and N. S. Vidhyadhiraja, `arXiv:1404.0621`.

[186] R. Micnas, J. Ranninger, and S. Robaszkiewicz Rev. Mod. Phys. **62**, 113 (1990).

[187] A. Erez and Y. Meir, Europhys. Lett. **91**, 47003 (2010).

[188] N. Dupuis, Phys. Rev. A **72**, 013606 (2005).

[189] M. Mayr, G. Alvarez, C. Şen, and E. Dagotto, Phys. Rev. Lett. **94** 217001 (2005).

[190] In practice, we take U_i to be a negligibly small number $(\sim 10^{-5})$ with $P(U) = 1 - \delta$.

[191] S. Kumar and P. Majumdar Eur. Phys. J. B **50** 571 (2006).

[192] Saurabh Pradhan and G. Venketeswara Pai, Phys. Rev. B **92**, 165124 (2015).

[193] This, in fact, roughly determines the temperature scale at which the pseudogap to normal metal crossover occurs at large U as depicted in Fig. 8.

[194] N. P. Ong, Y. Wang, S. Ono, Y. Ando, and S. Uchida, Annal. der Physik **13**, 9 (2004).

[195] A. A. Abrikosov and L. P. Gorkov, Sov. Phys. JETP **12**, 1243 (1961); A. V. Balatsky, I. Vekhter, and J-X. Zhu, Rev. Mod. Phys. **78**, 373 (2006).

[196] P. Nozières and F. Pistolesi, Eur. Phys. Jl. B **10**, 649 (1999).

[197] P. Fulde and R. A. Ferrel, Phys. Rev. **135** A550 (1964); A. I. Larkin and Yu. N. Ovchinnikov, Sov. Phys. JETP **20**, 762 (1965).

[198] D. Jrome, T. M. Rice, and W. Kohn, Phys. Rev. **158**, 462475 (1967)

[199] Y. Kohmoto and Y. Takada, Jl. Phys. Soc. Jpn **59**, 1541 (1990)